

Fig.1

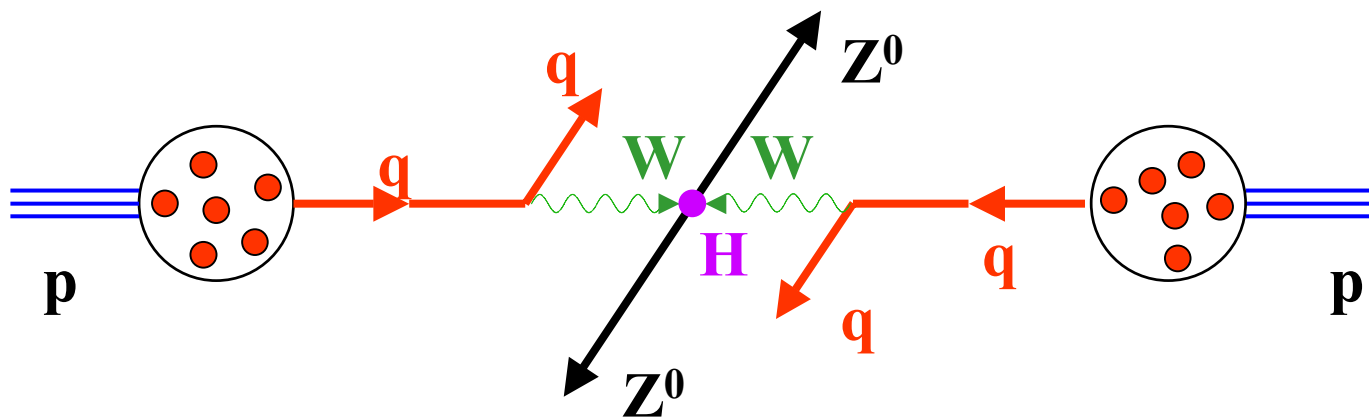
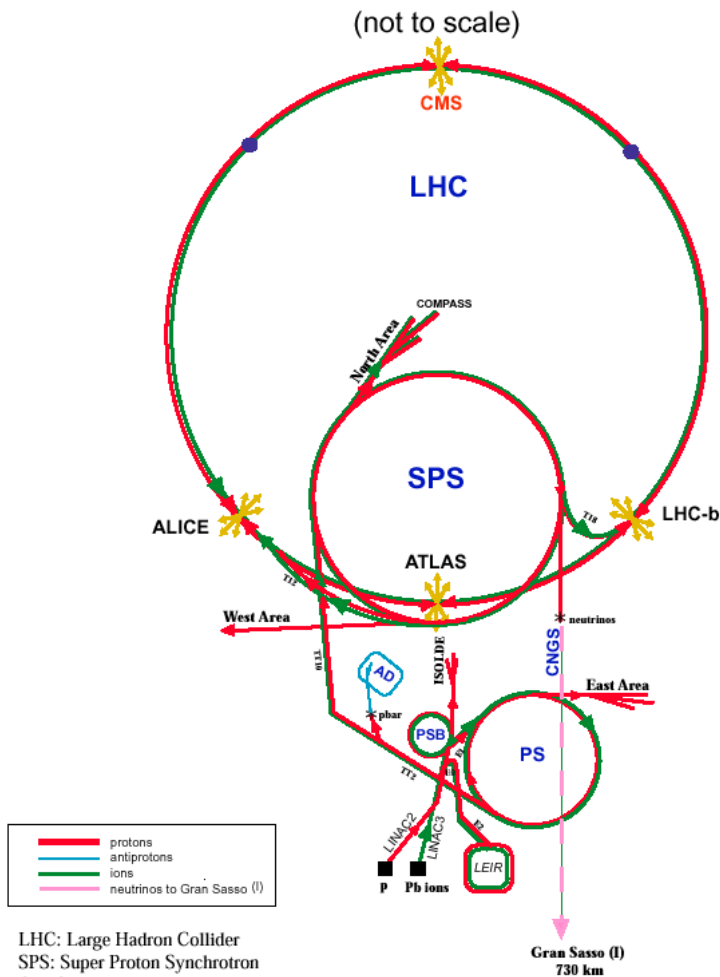
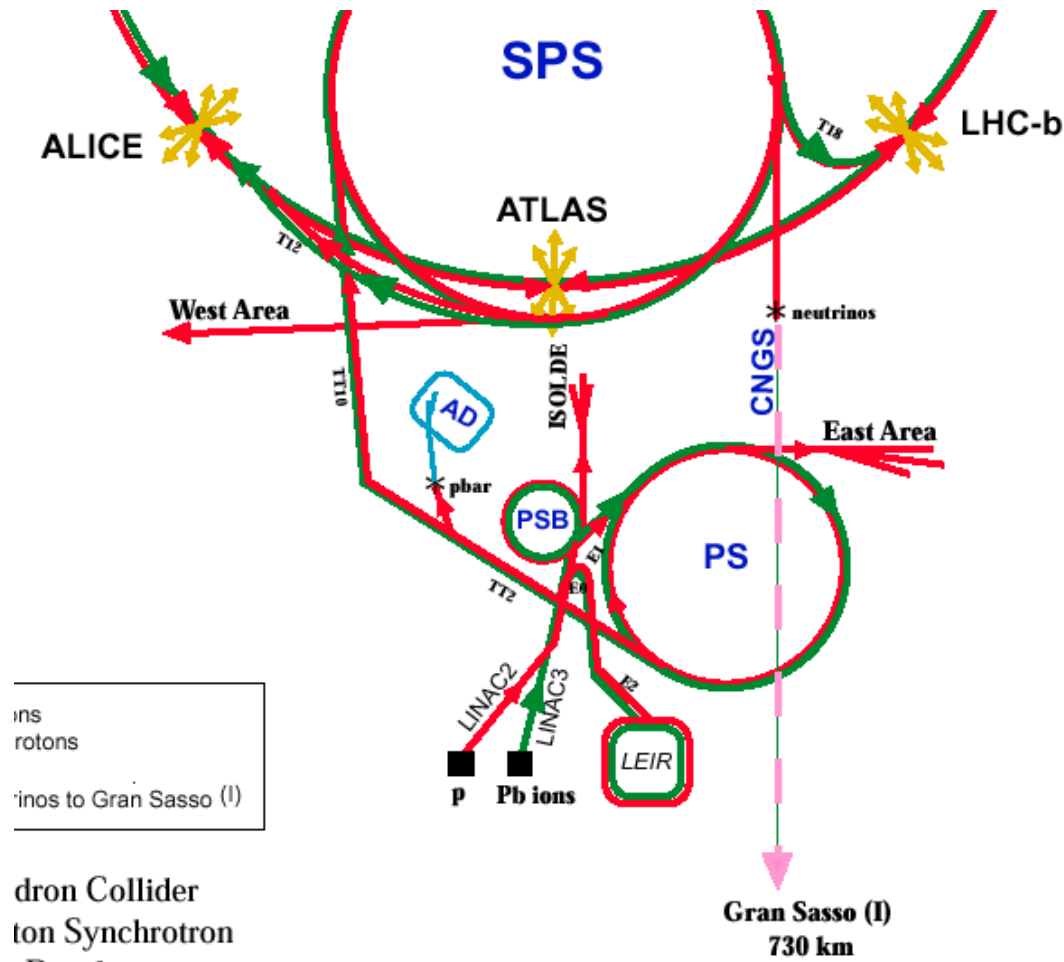


Fig.2



LHC: Large Hadron Collider
 SPS: Super Proton Synchrotron
 AD: Antiproton Decelerator
 ISOLDE: Isotope Separator OnLine DEvice
 PSB: Proton Synchrotron Booster
 PS: Proton Synchrotron
 LINAC: LINear ACcelerator
 LEIR: Low Energy Ion Ring
 CNGS: Cern Neutrinos to Gran Sasso

Rudolf LEY, PS Division, CERN, 02.09.96
 Revised and adapted by Antonella Del Rosso, ETI Div.,
 in collaboration with B. Desforges, SI Div., and
 D. Manghutti, PS Div. CERN, 23.05.01



Large Hadron Collider
 Super Proton Synchrotron

Fig.3

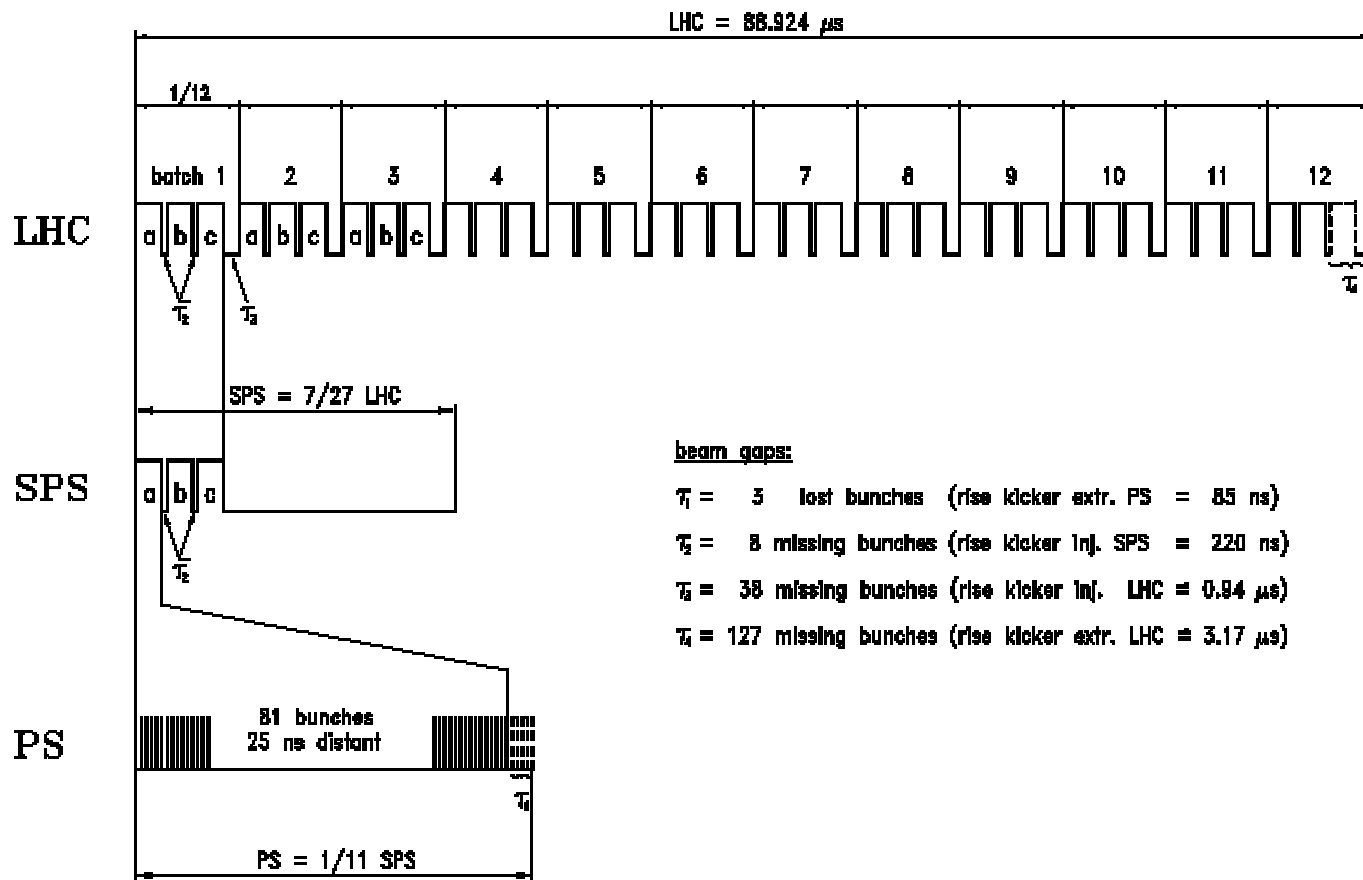


Fig.4

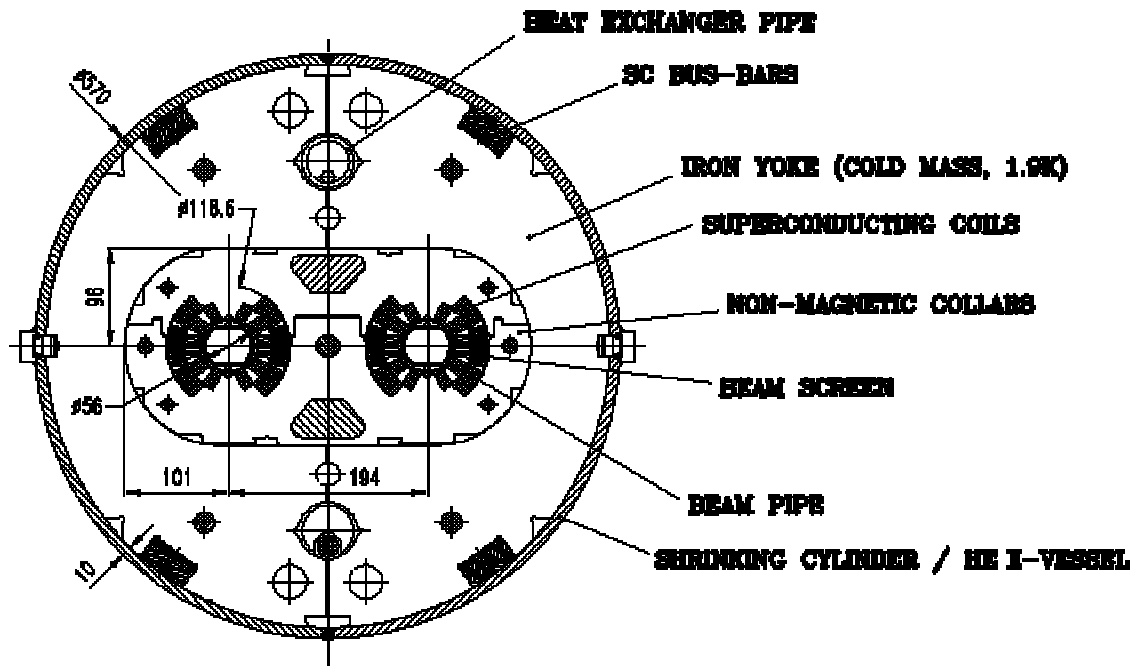


Fig.5

Training Quenches at 1.8K - first runs

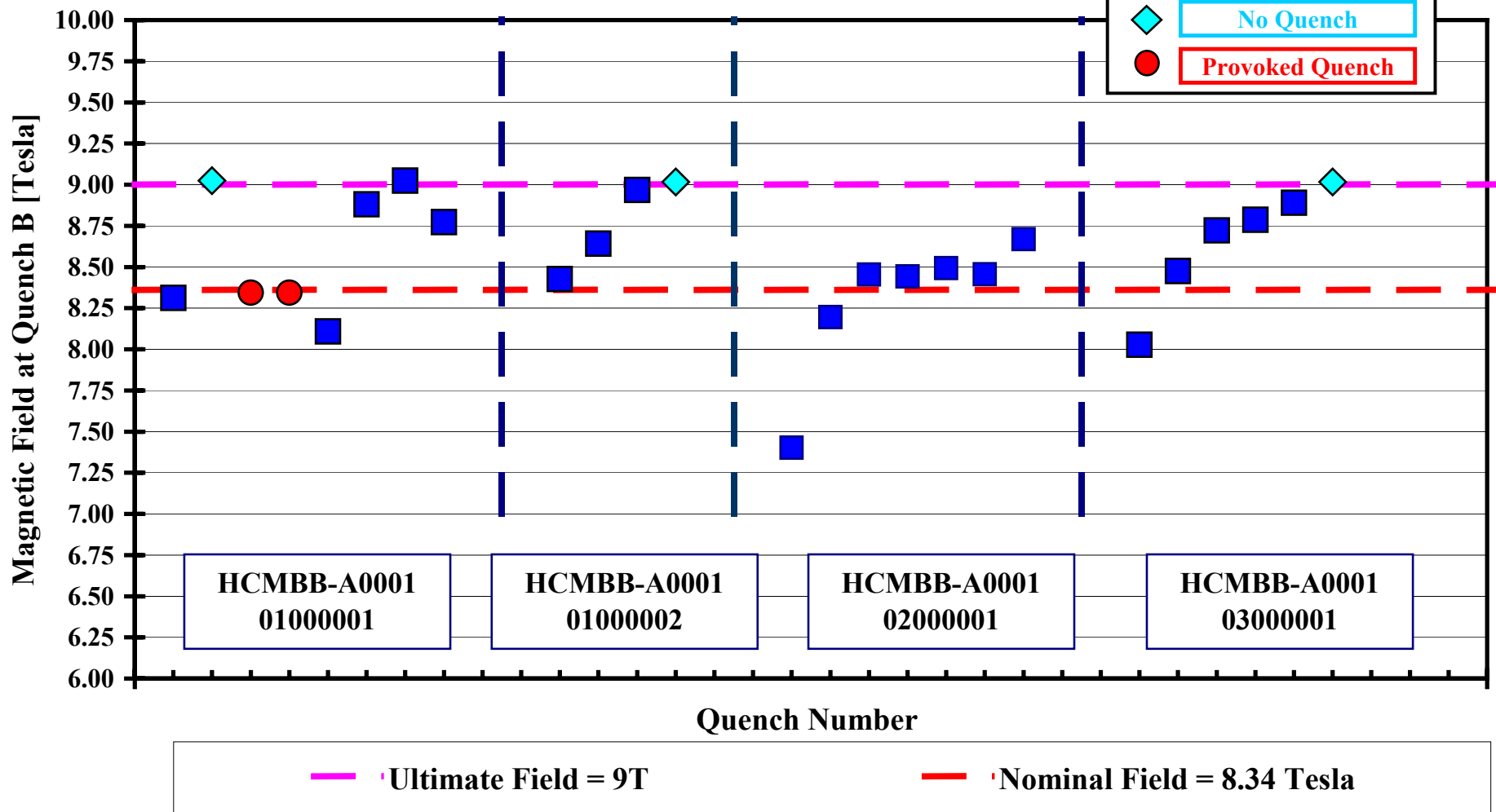


Fig.6

LHC PROJECT

UNDERGROUND WORKS

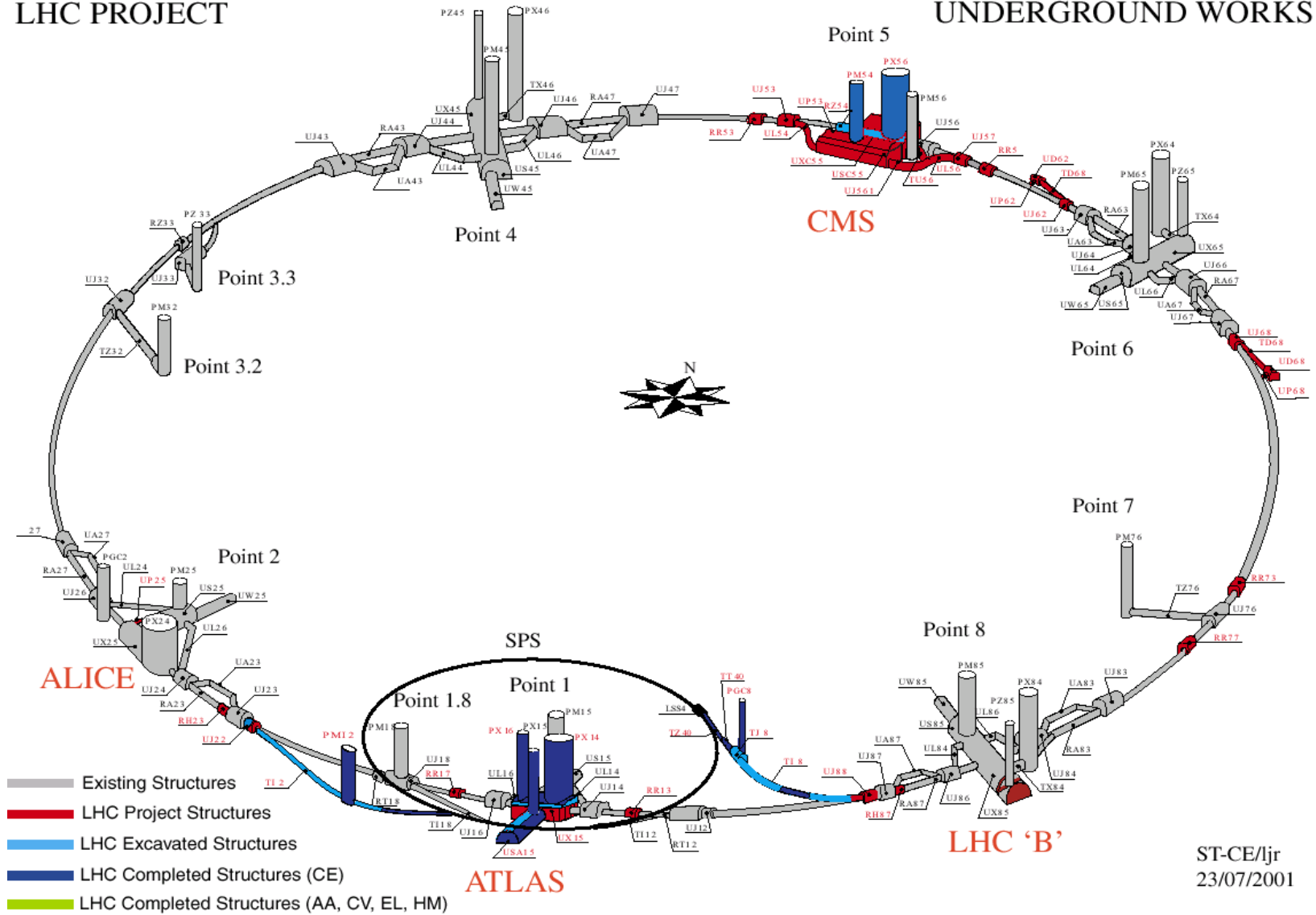
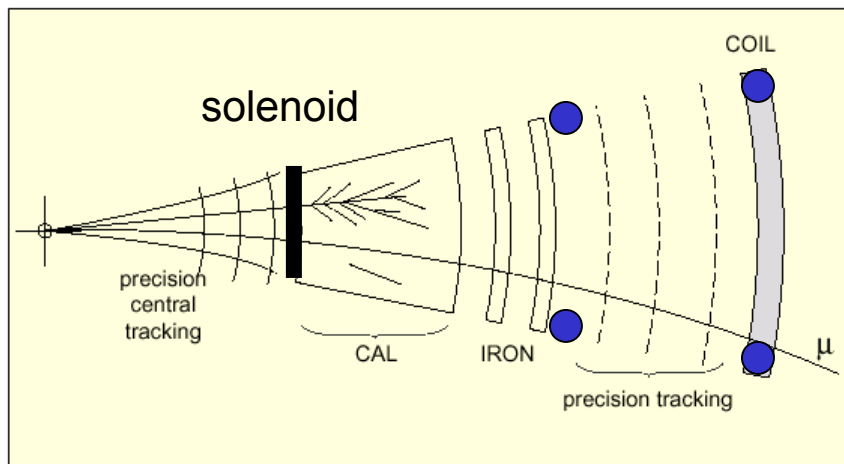
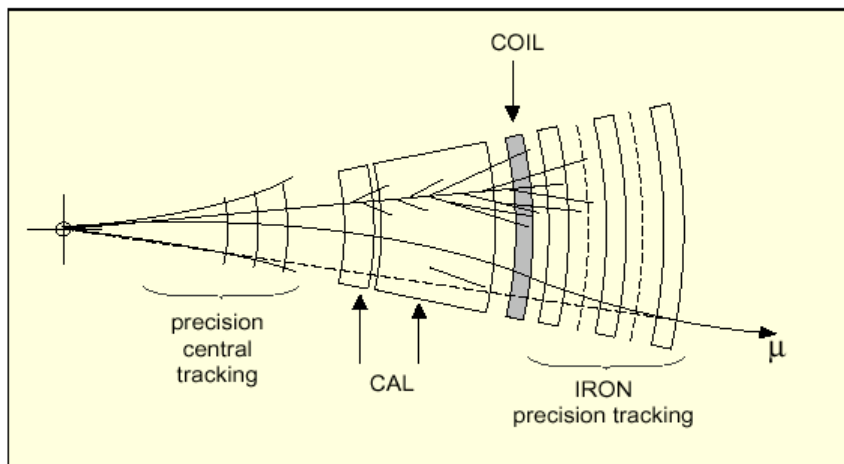


Fig.7



ATLAS



CMS

Fig.8

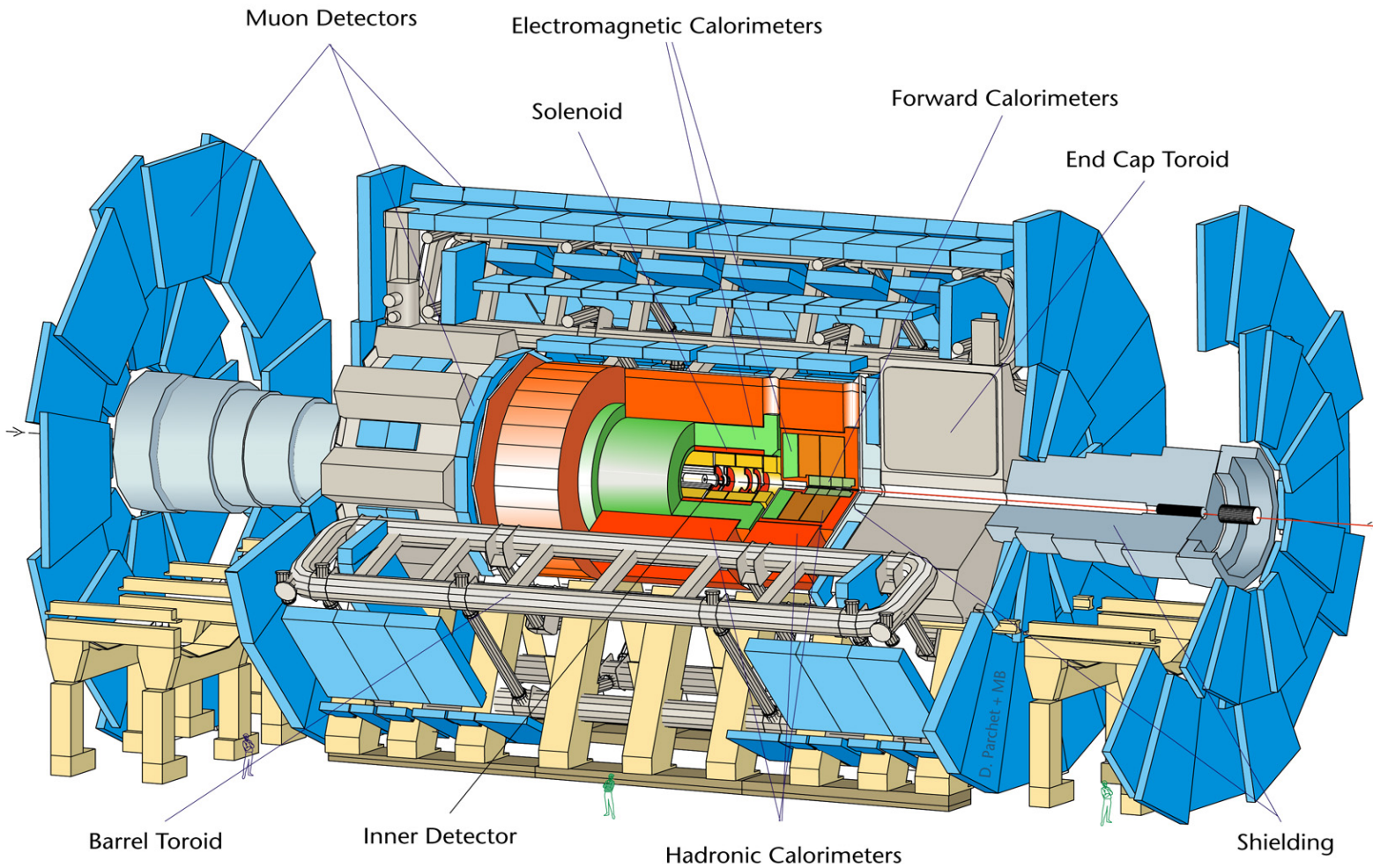


Fig.9

CMS

A Compact Solenoidal Detector for LHC

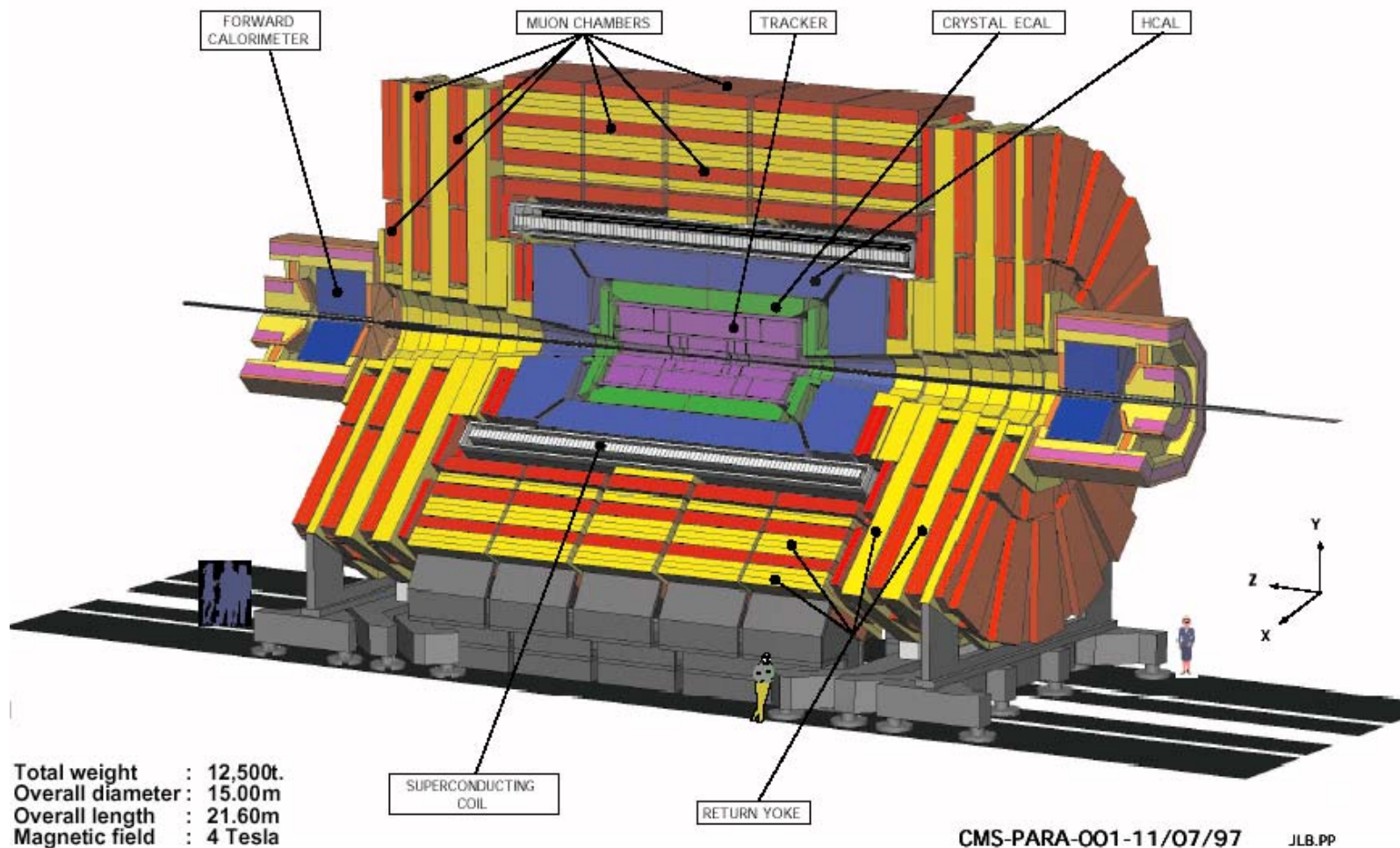


Fig.10

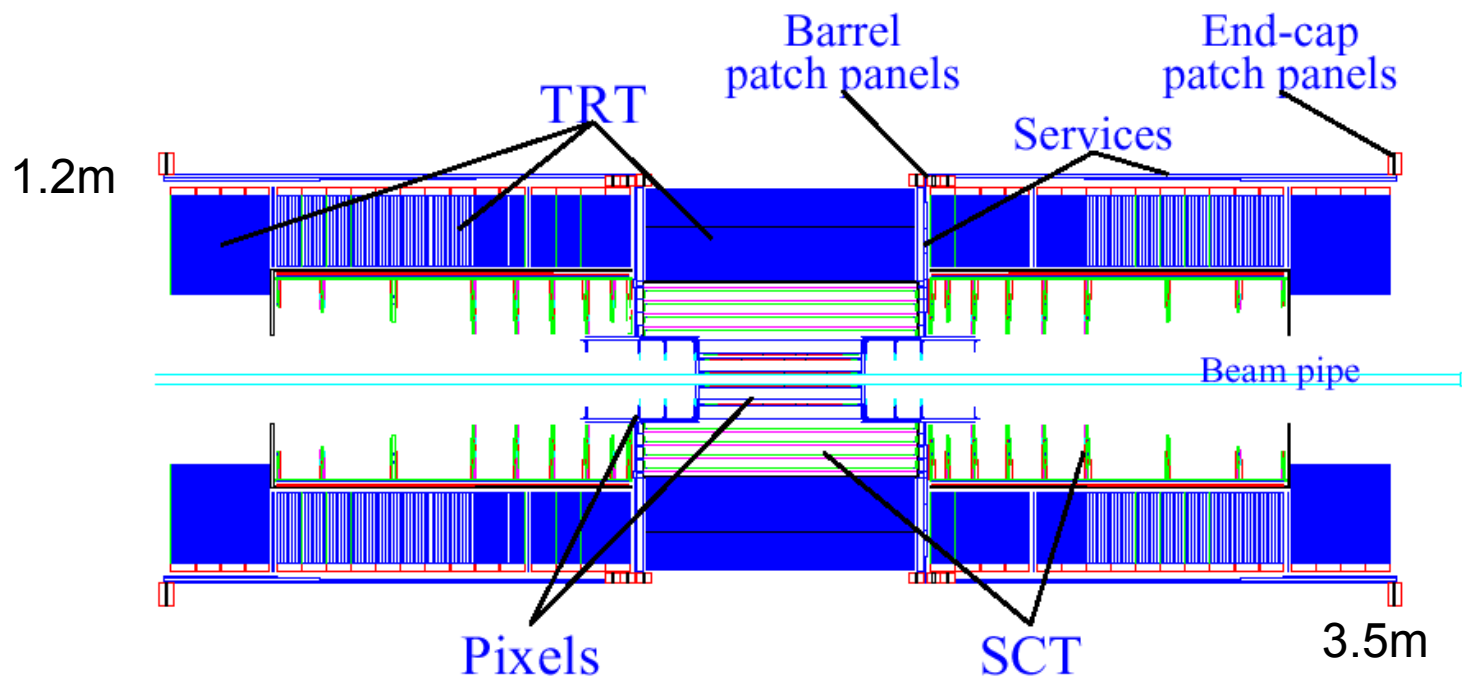


Fig.11

1 of the 128 channels

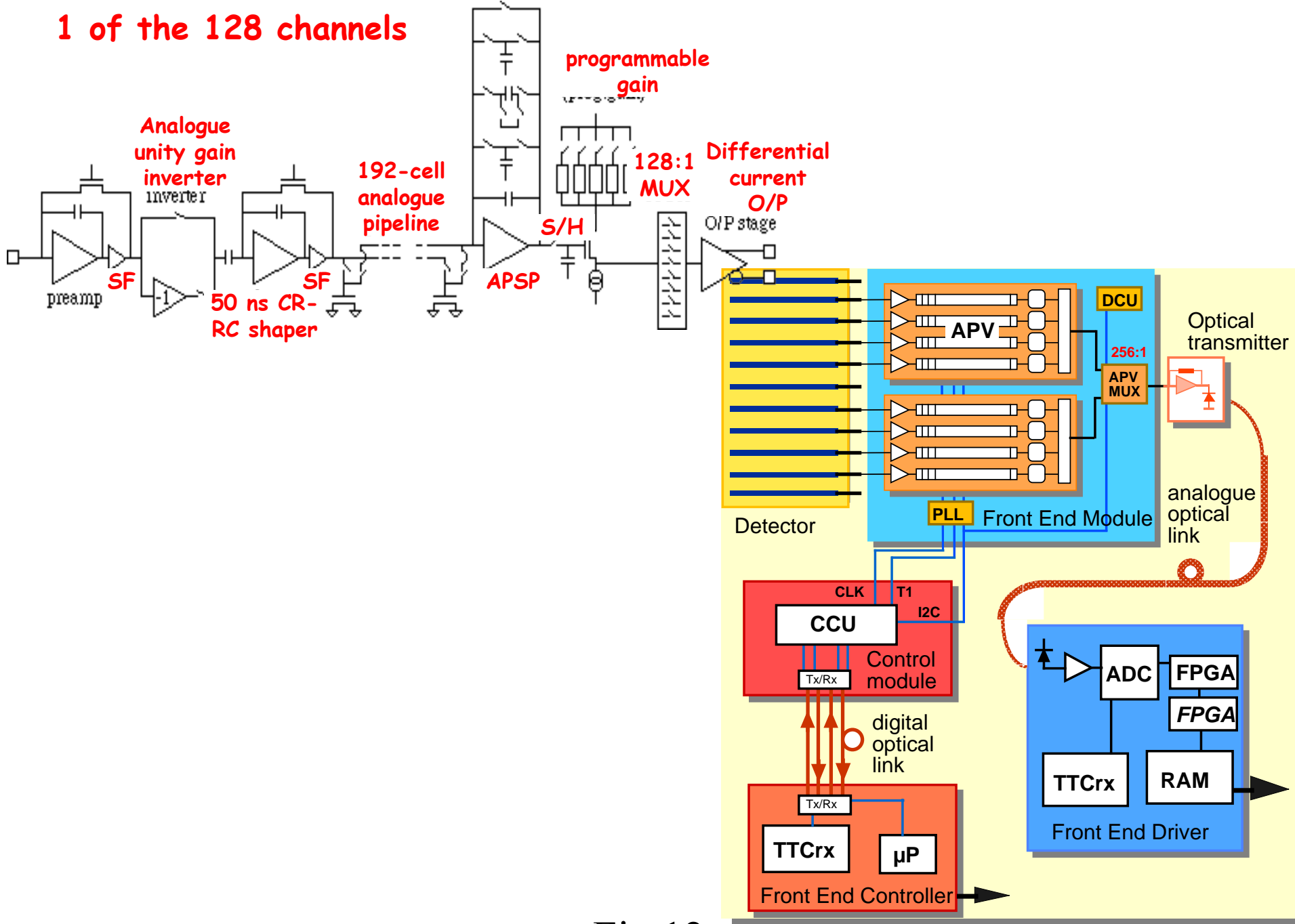


Fig.12

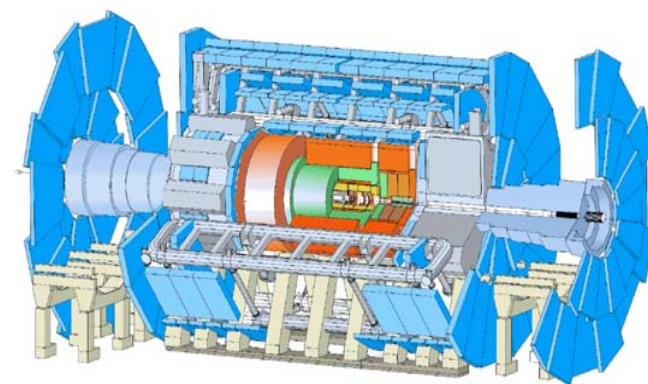
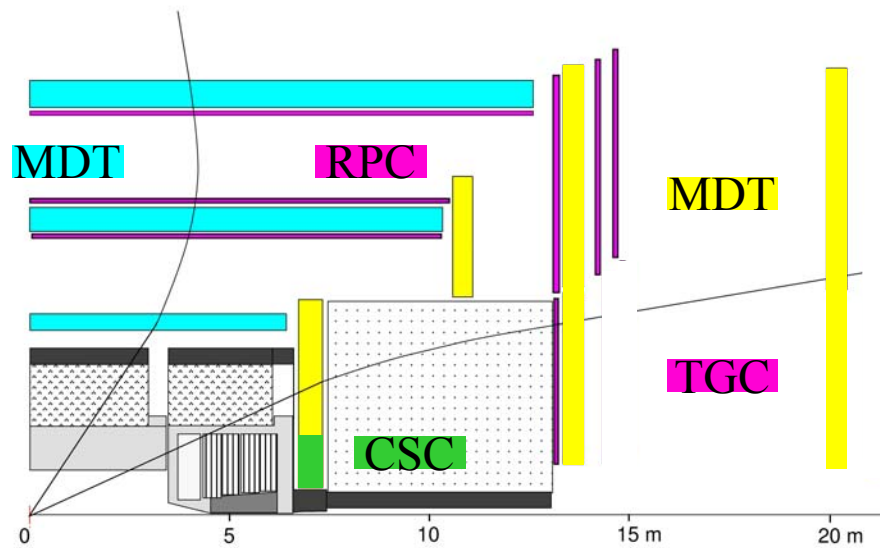
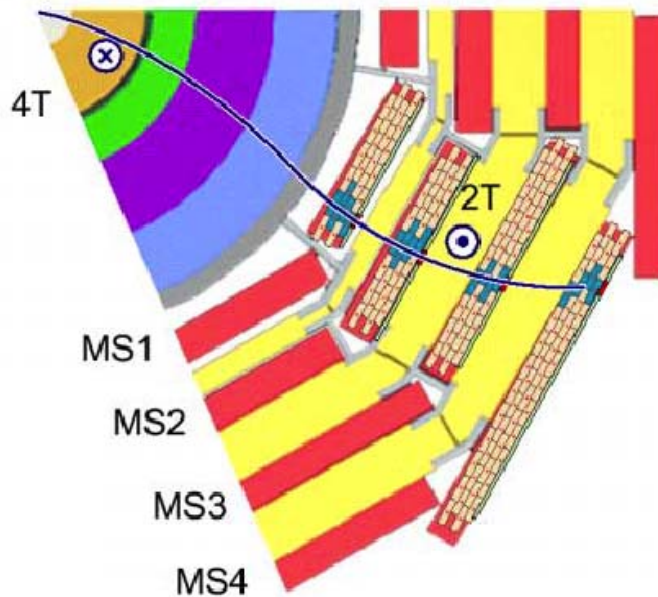
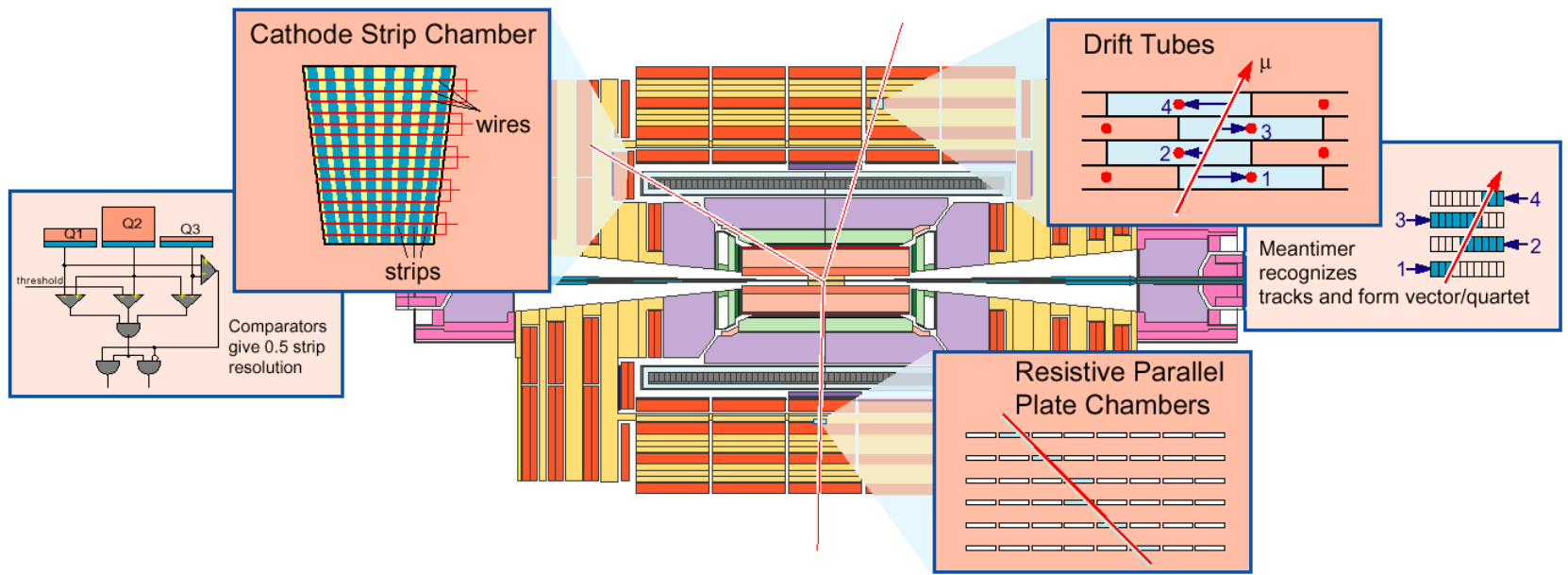


Fig.13



4 Muon Stations
 redundancy
 acceptance

Per Station
 barrel – 12 measuring planes
 endcap – 6 measuring planes

Measurement Accuracy
 position 70 – 100 μm /station
 direction ~ 1 mrad

Fig.14

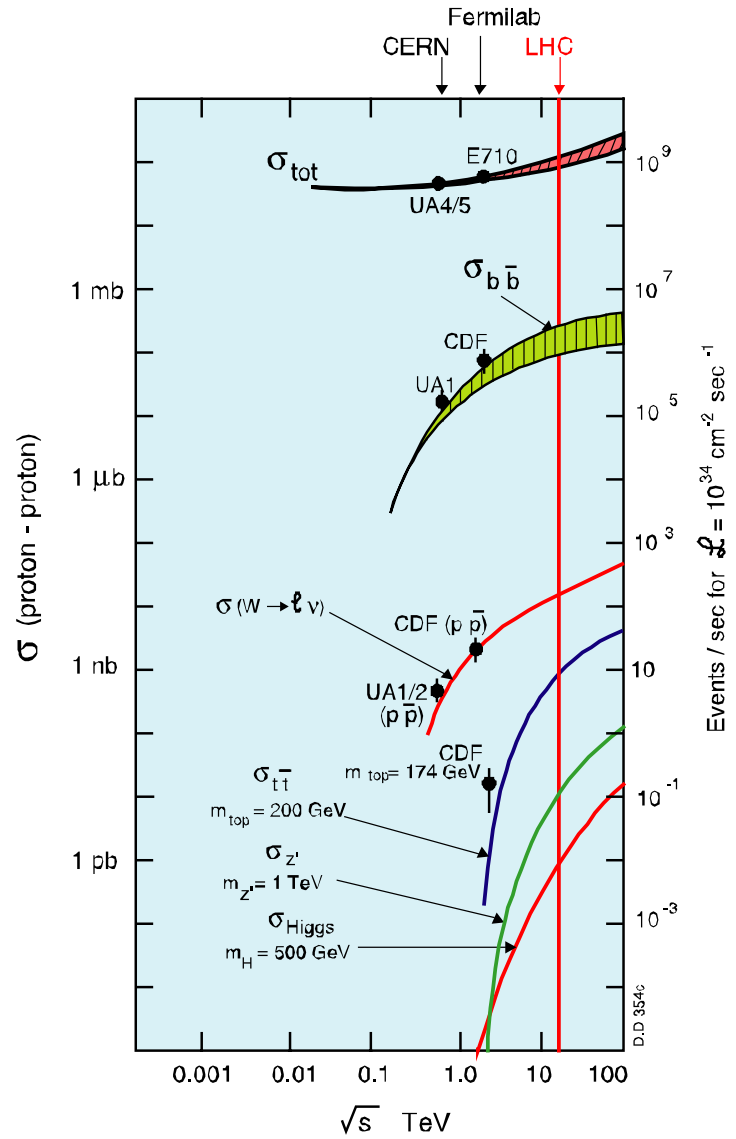


Fig.15

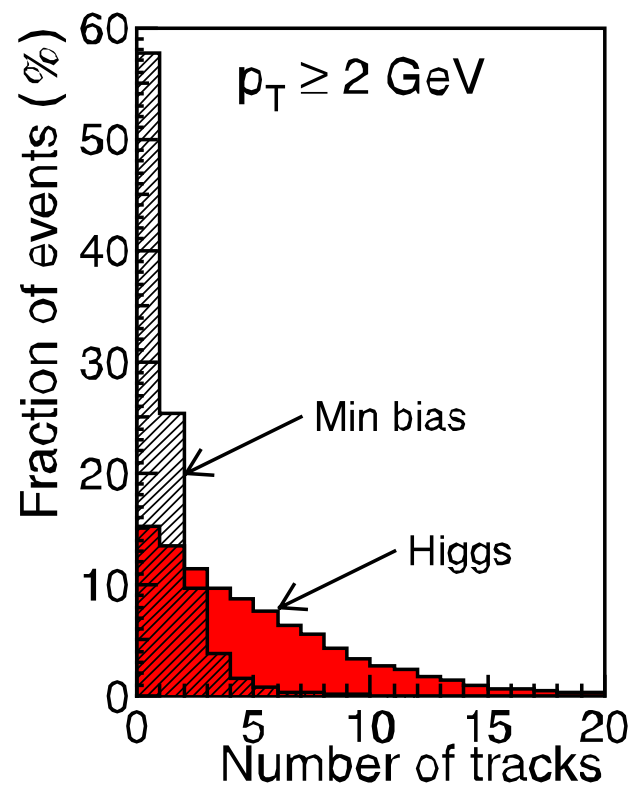
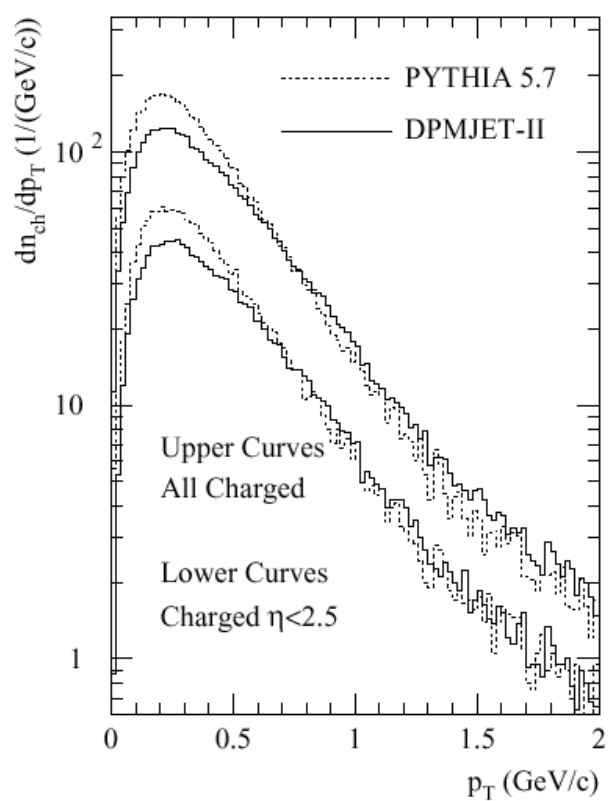
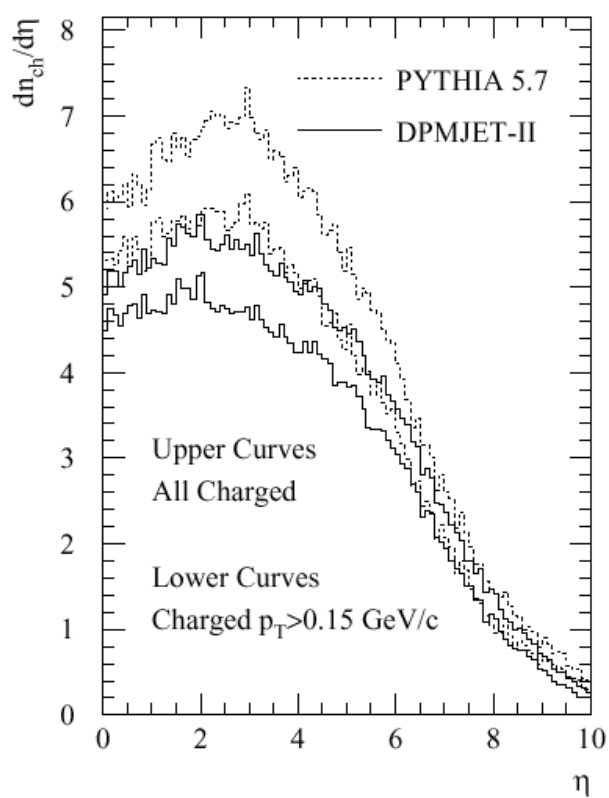


Fig.16

CMS: Transverse energy flow in $\Delta\eta\times\Delta\phi \sim 0.1\times 0.1$ at $L=10^{34} \text{ cm}^{-2}\text{s}^{-1}$

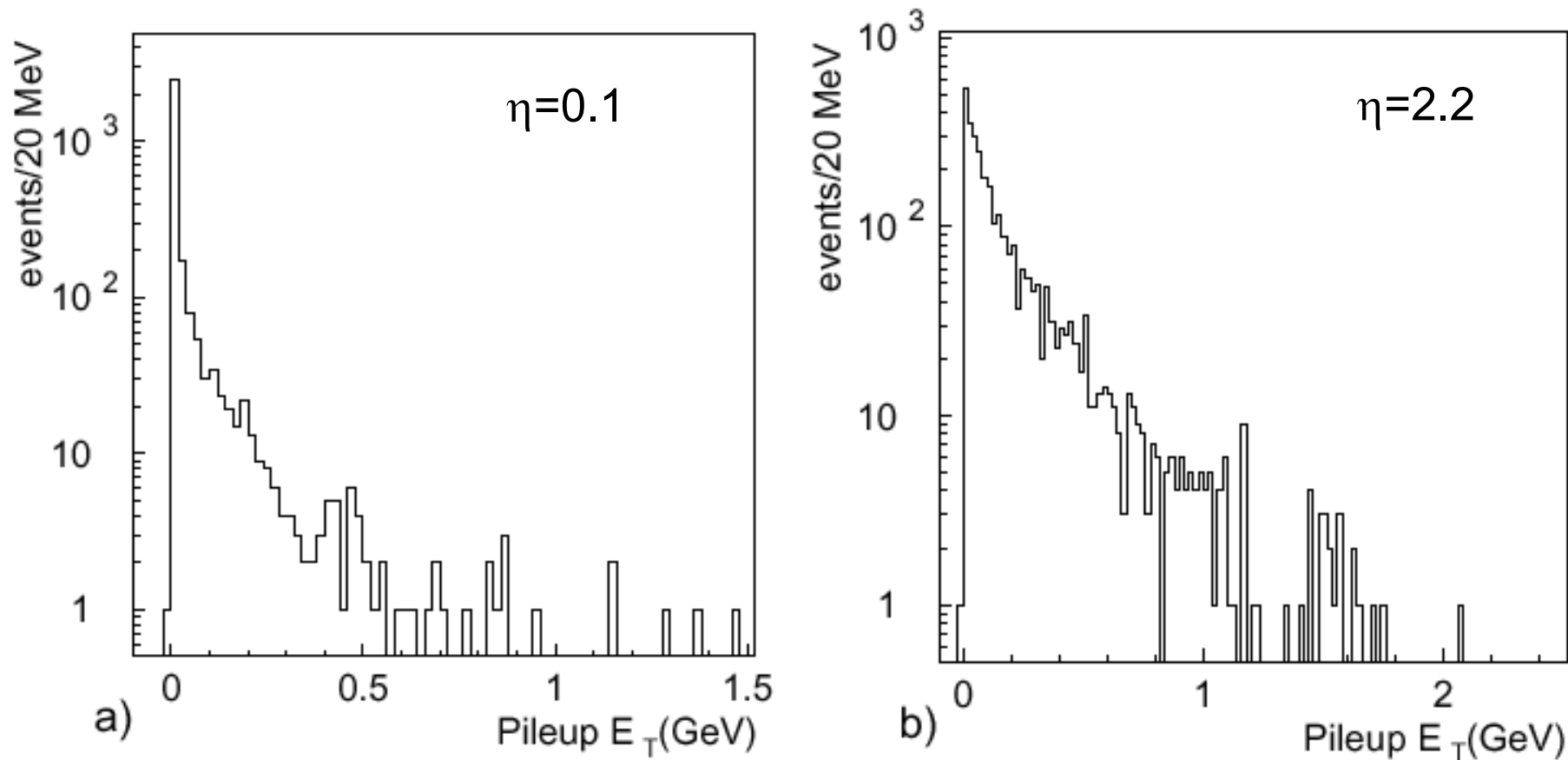
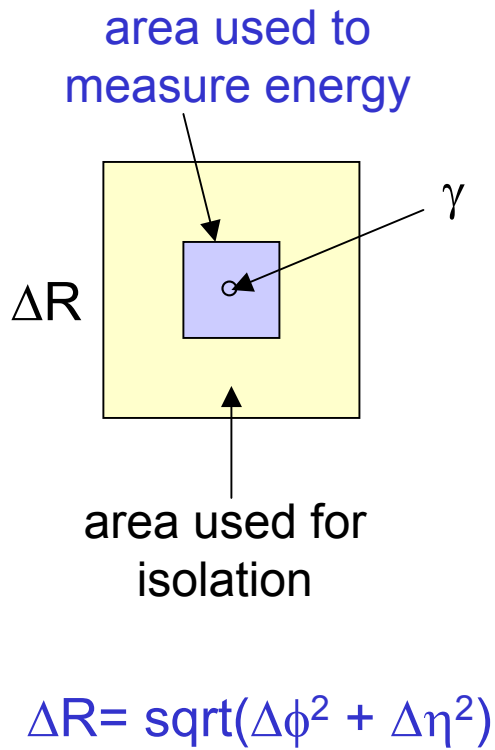
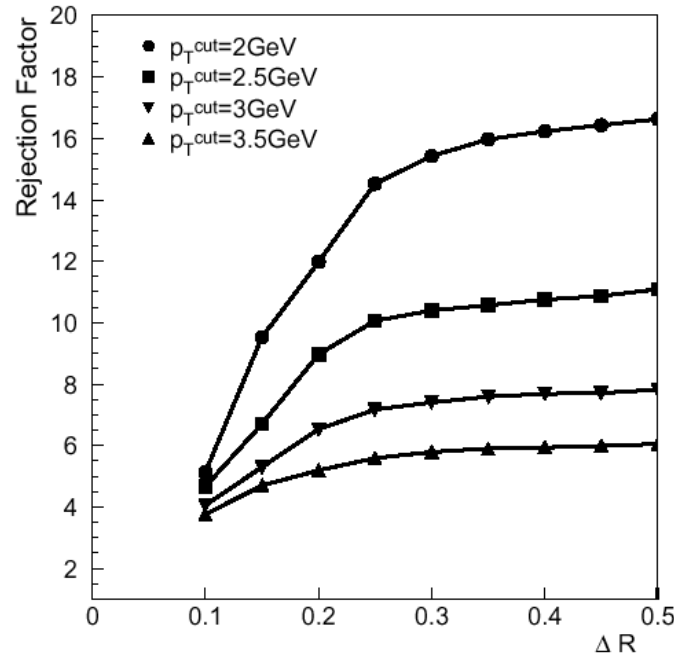


Fig.17



Rejection power against π^0 s in jets



Loss of efficiency at Hi L for $H \rightarrow \gamma\gamma$

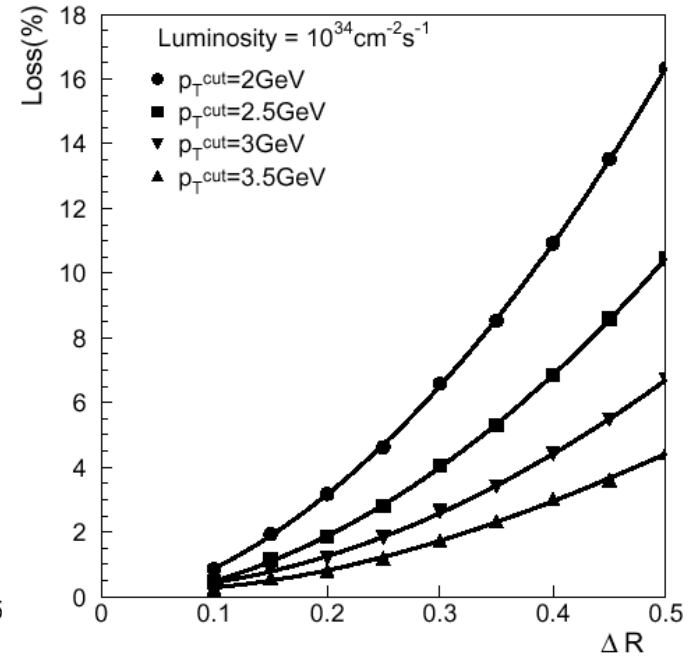
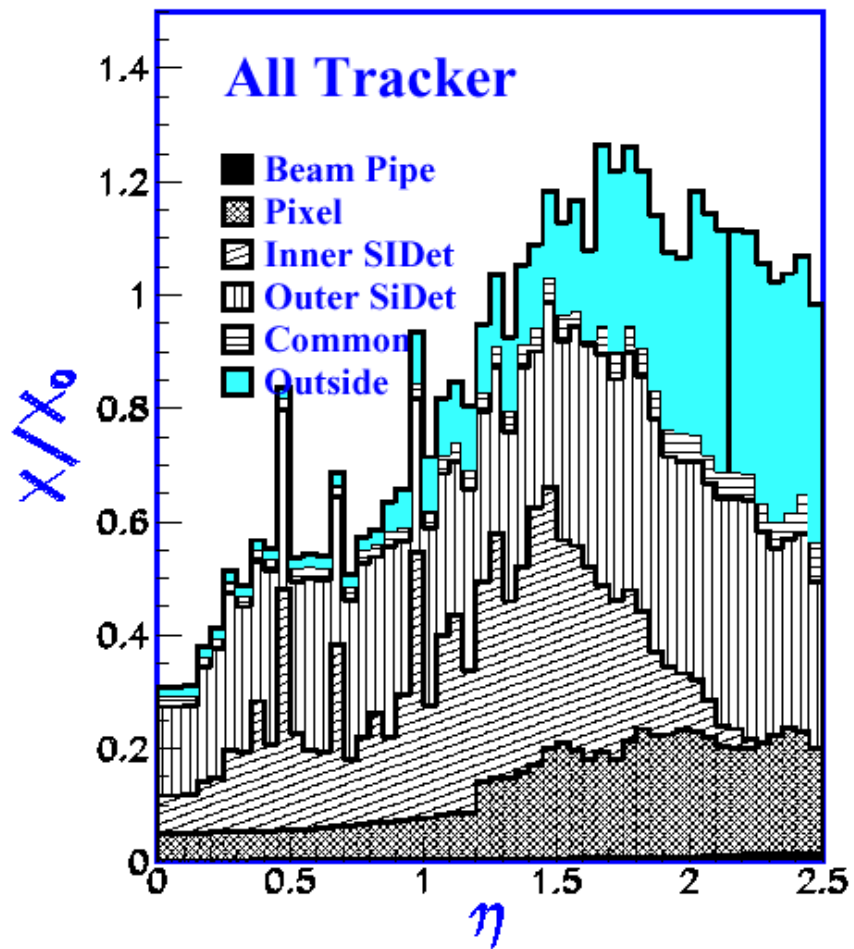


Fig.18

CMS



ATLAS

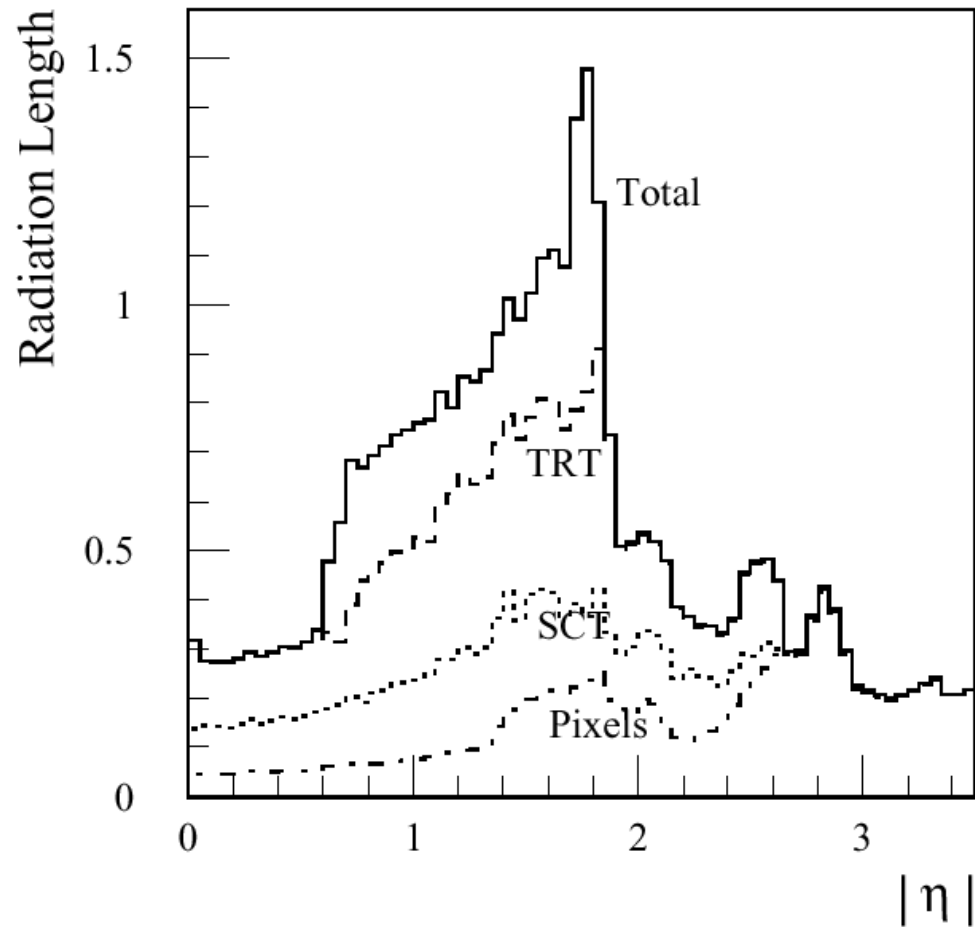


Fig.19

ATLAS
Pattern
Recognition
>9 precision hits
+ 2 pixel hits
+ $\sigma_d < 1\text{mm}$

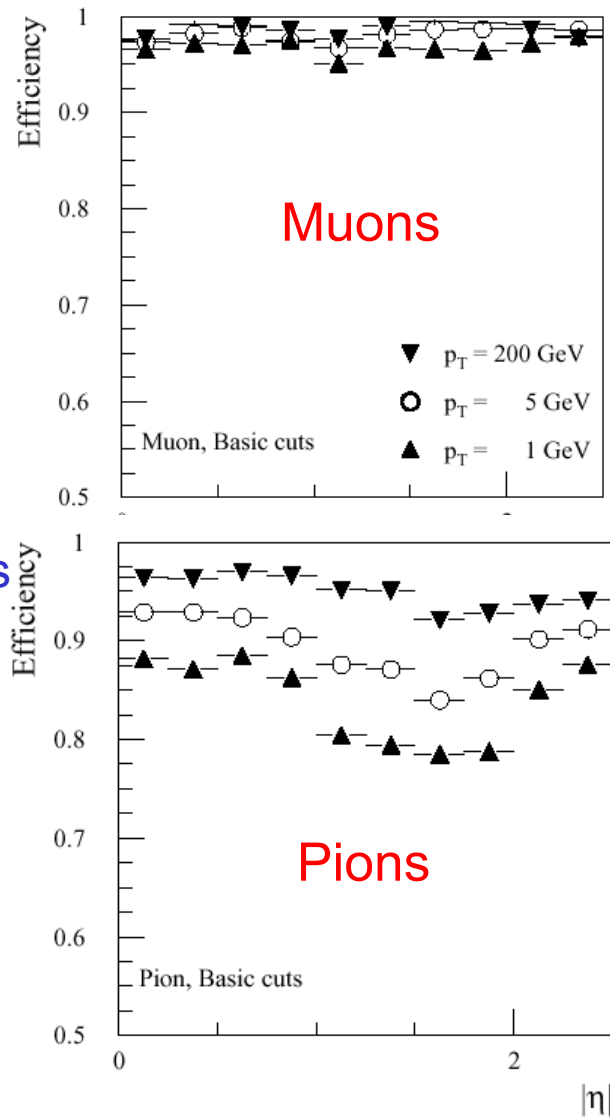


Fig.20

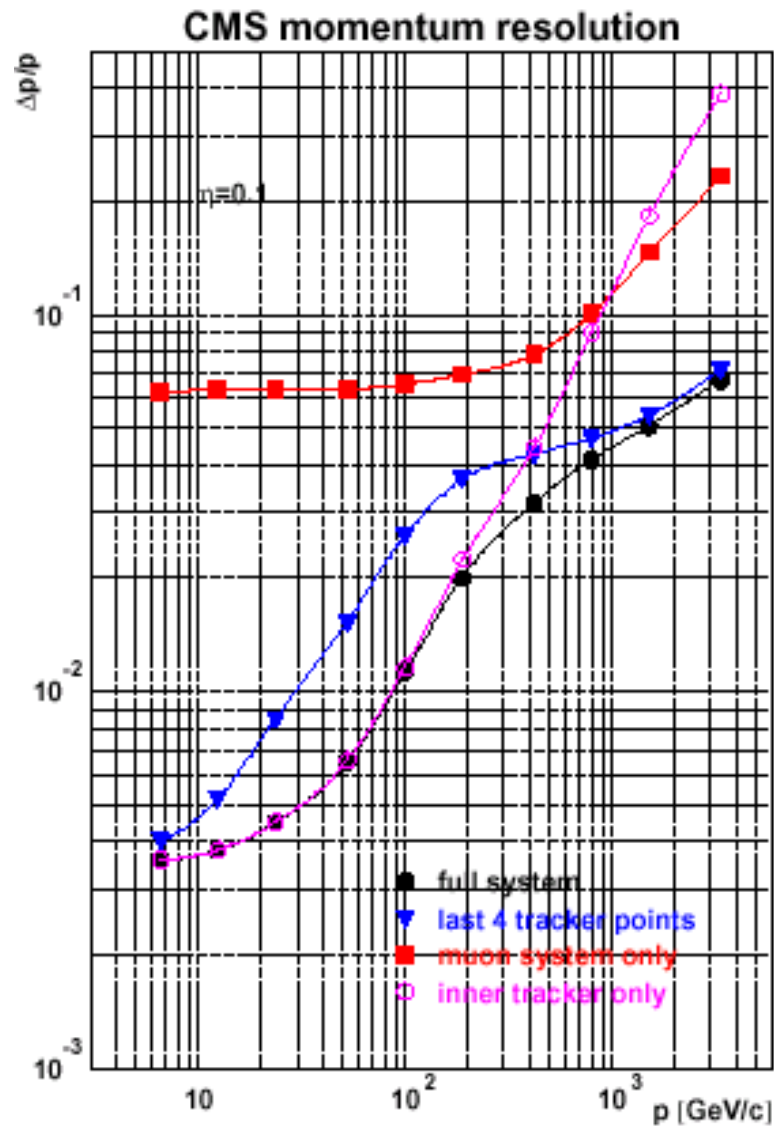


Fig.21

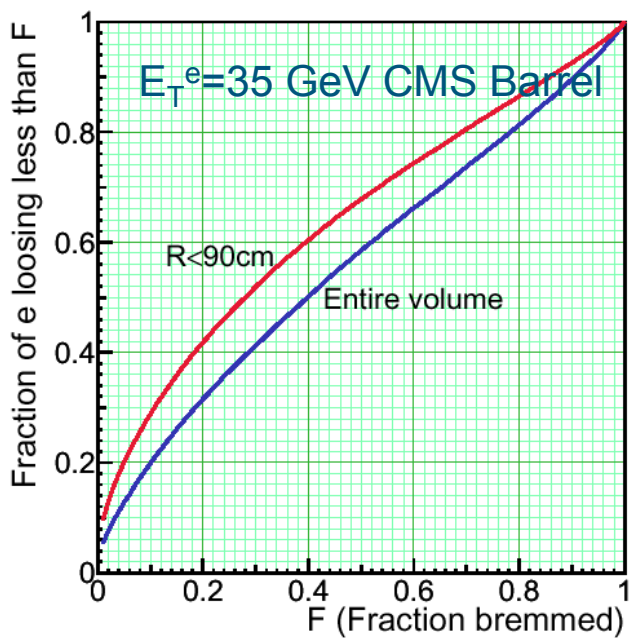


Fig.22a

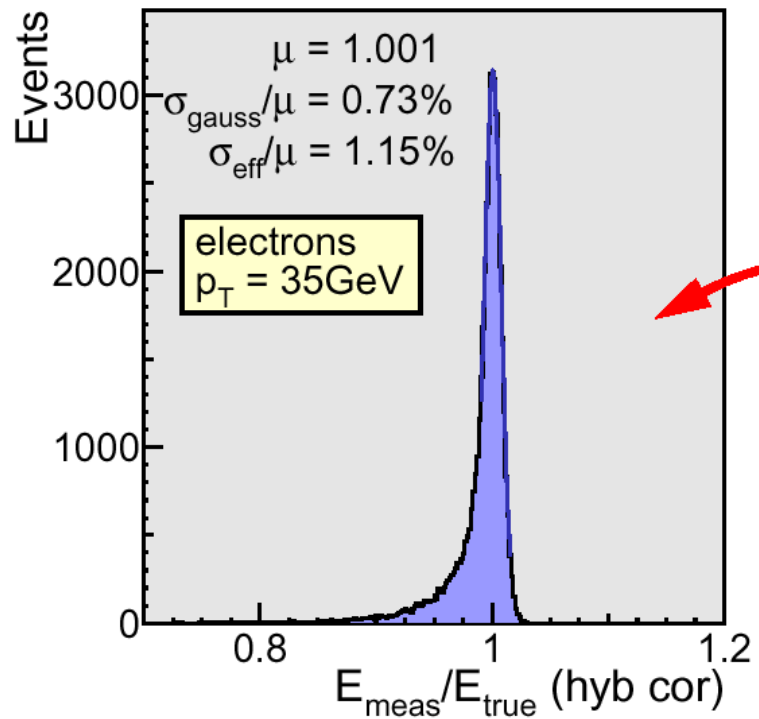
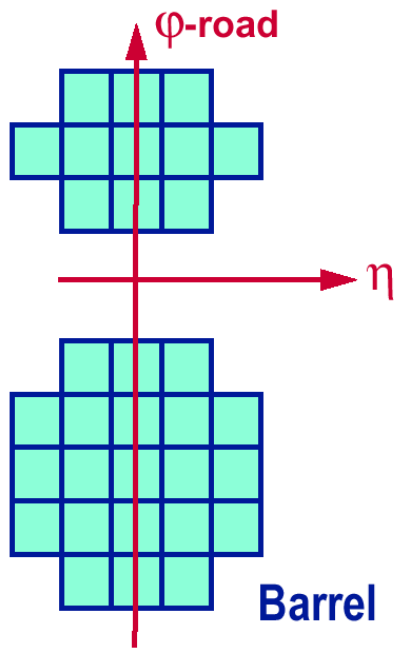
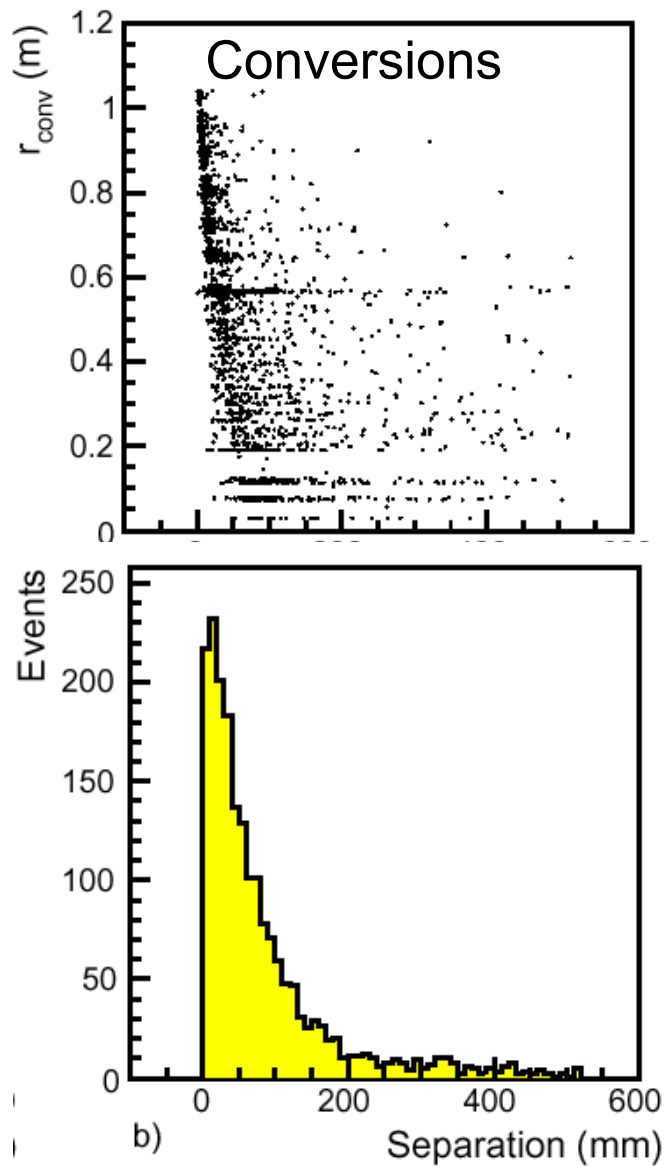


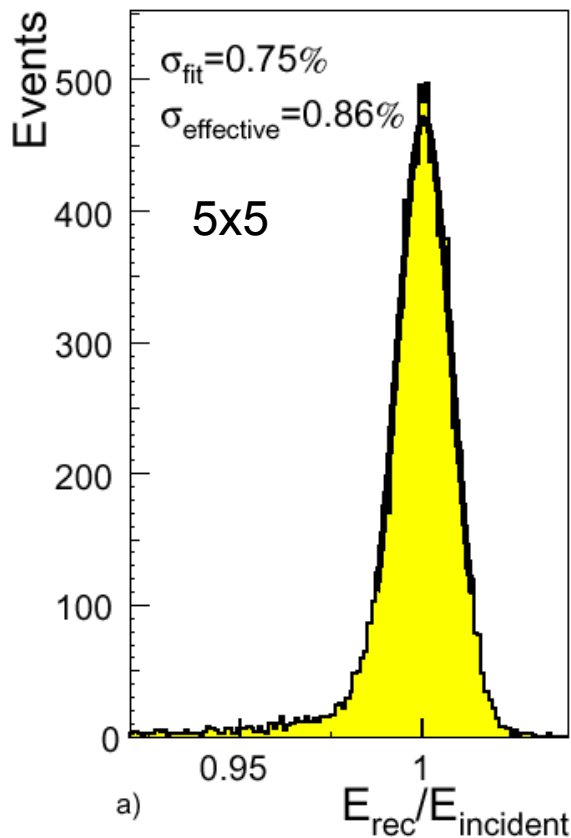
Fig.22b



CMS Barrel
 Higgs $\rightarrow \gamma\gamma$
 $\epsilon_\gamma \sim 90\%$

$\frac{1}{4}$ of conversions
 cannot be
 reconstructed

Unconverted γ s



Converted γ s

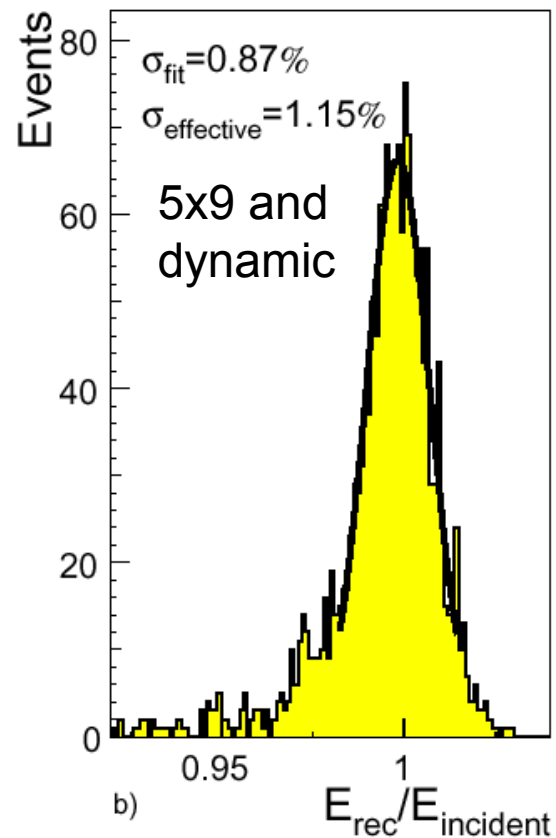


Fig.23

Classical 'cone' algorithm - jet built around a seed

- parameters: E_T^{seed} cut, cone opening radius ΔR

ATLAS: $W \rightarrow$ jet-jet mass resolution

p_T^W (GeV)	ΔR	σ_{LoL}	σ_{HiL} (GeV)
$p_T < 50$	0.4	9.5	13.8
$100 < p_T < 200$	0.4	7.7	12.9
$200 < p_T < 700$	0.3	5.0	6.9

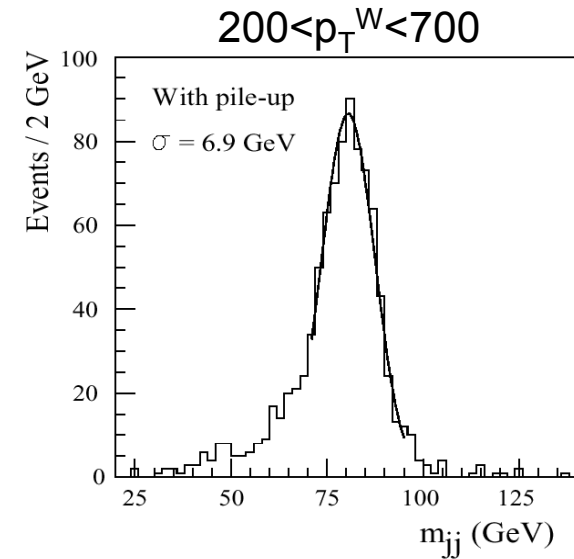
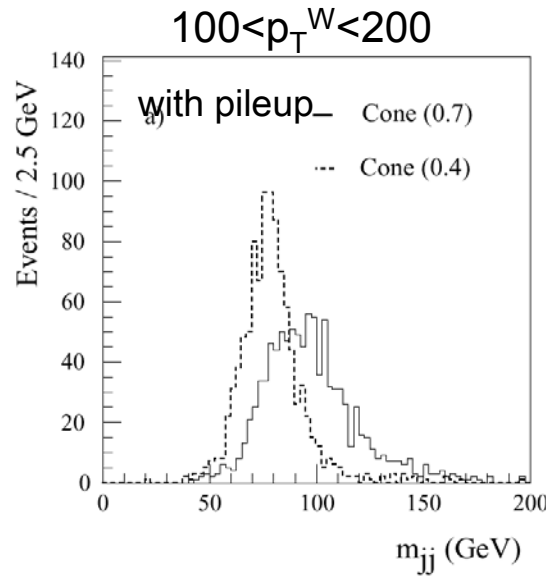
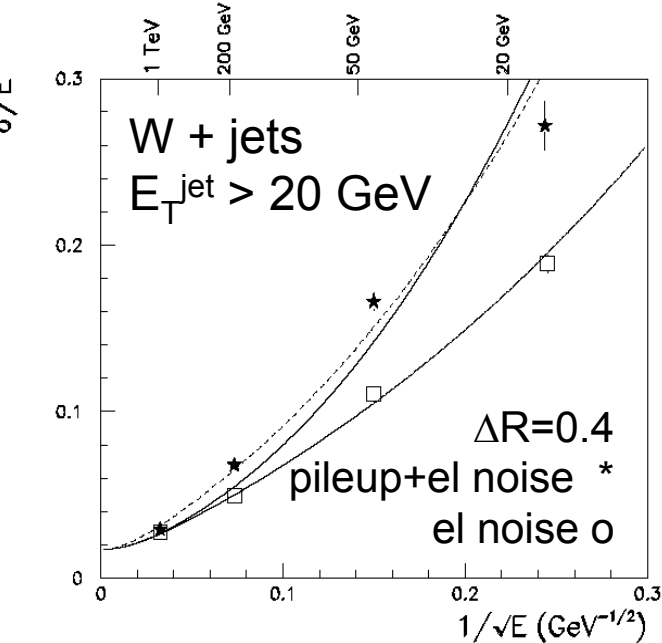
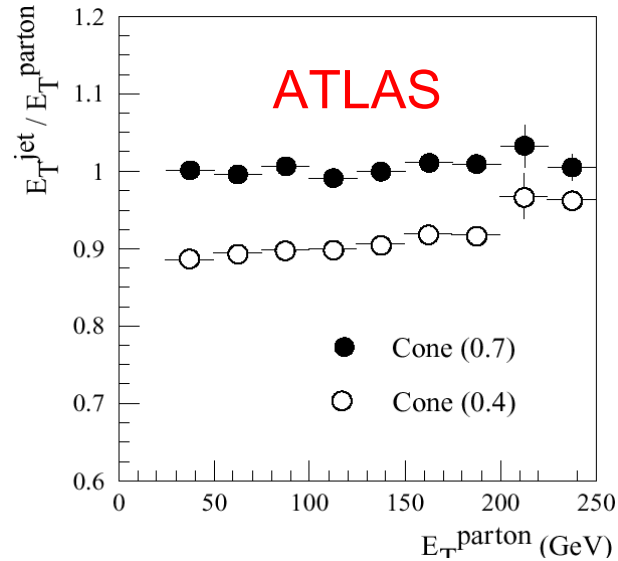


Fig.24

$A \rightarrow \tau\tau$ $m_A=150$ geV

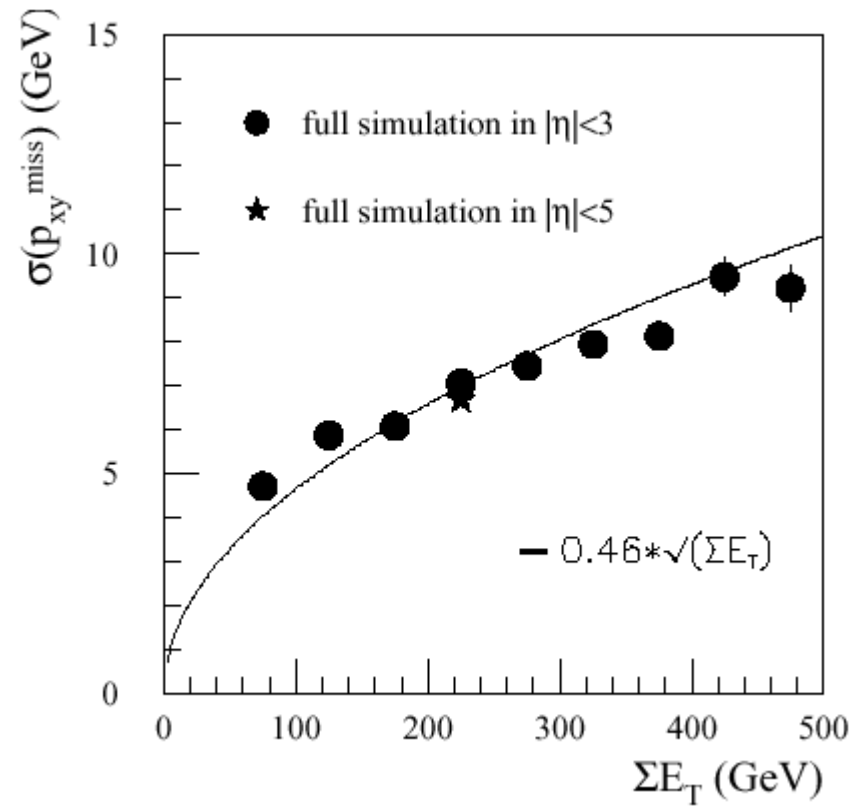


Fig.25

Cuts (ATLAS)

$E_{T\gamma1}, E_{T\gamma2} > 40, 25$ GeV with $|\eta| < 2.5$

E_{H1}/E_{em}

$E_{em2}^{3\times3}/E_{em2}^{7\times7}$

Shower width in η

Track Veto

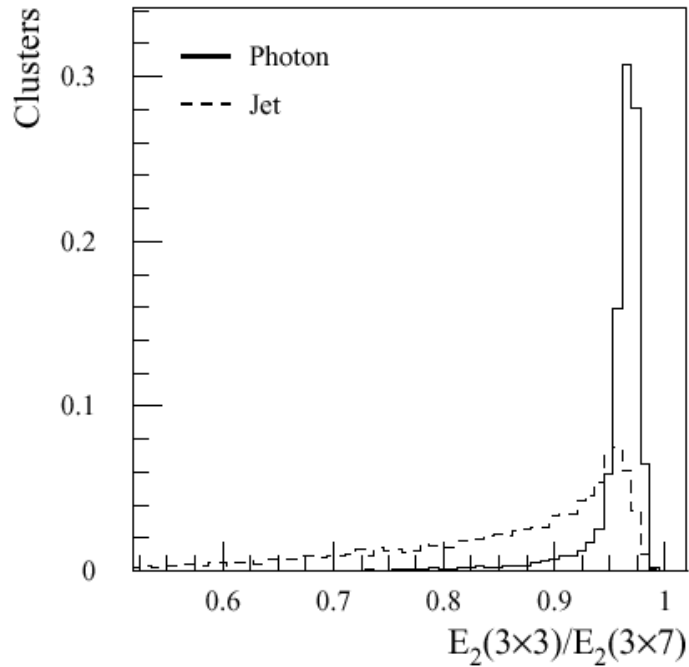
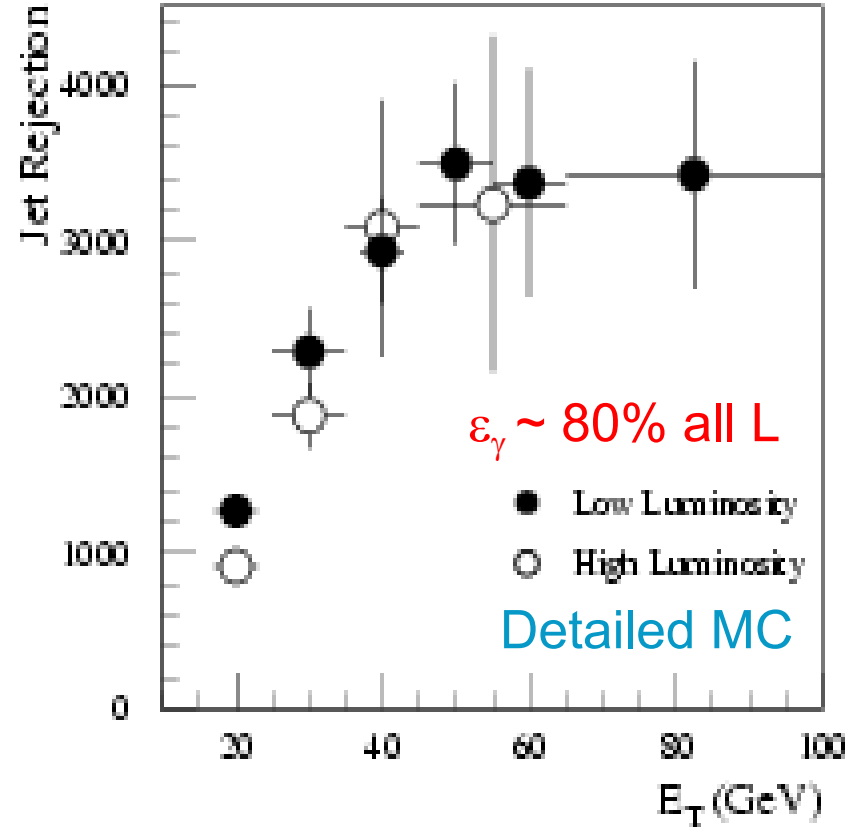


Fig.26a

ATLAS EM calorimeter

4 mm η -strips in first compartment

3 longitudinal segments



$\Rightarrow (\gamma\text{-jet} + \text{jet-jet}) < 40\% \gamma\gamma$

Fig.26b

Likelihood method

Form significance S_i for i -th trk in jet

Form $r_i = f_b(S_i)/f_u(S_i)$

Form Jet weight $W = \text{Slog } r_i$

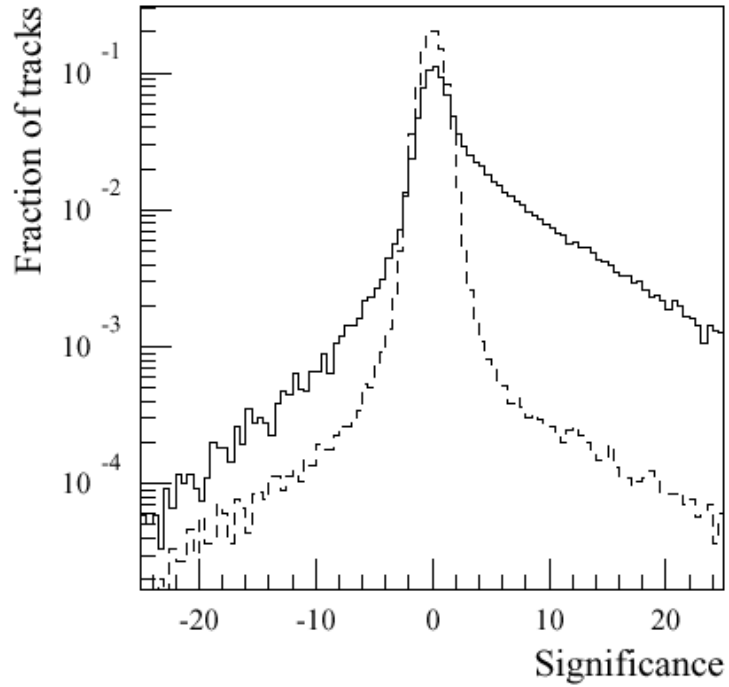


Fig.27a

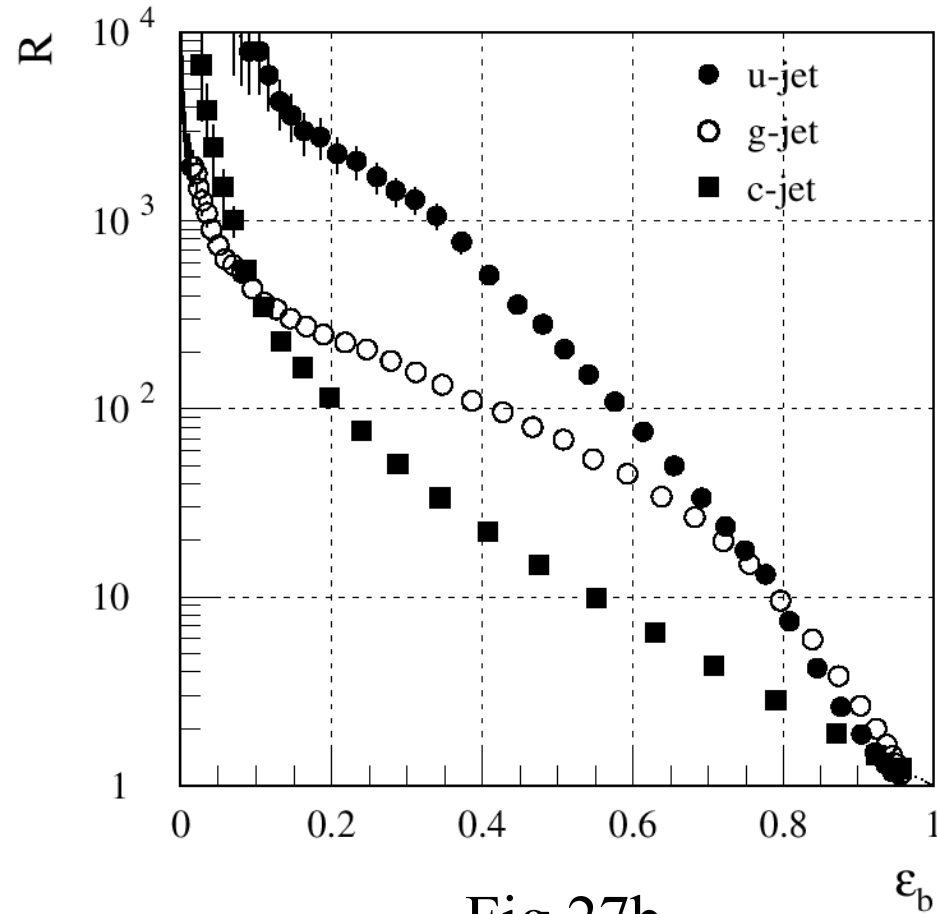


Fig.27b

ATLAS

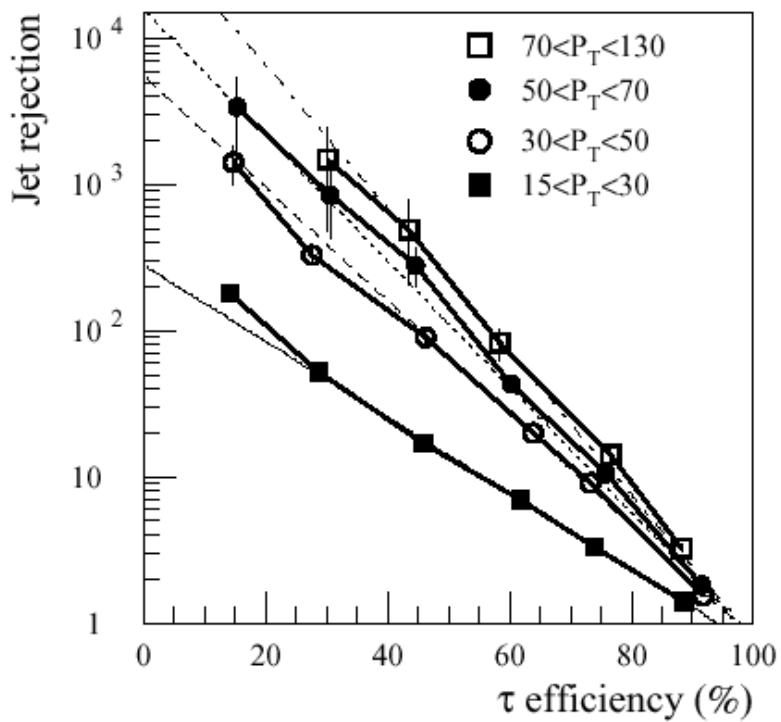


Fig.28a

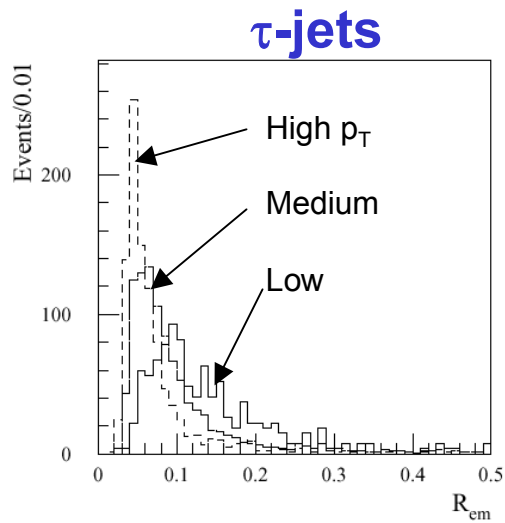


Fig.28b

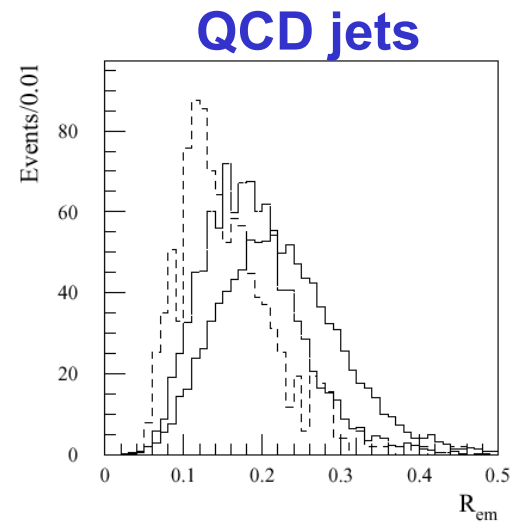


Fig.28c

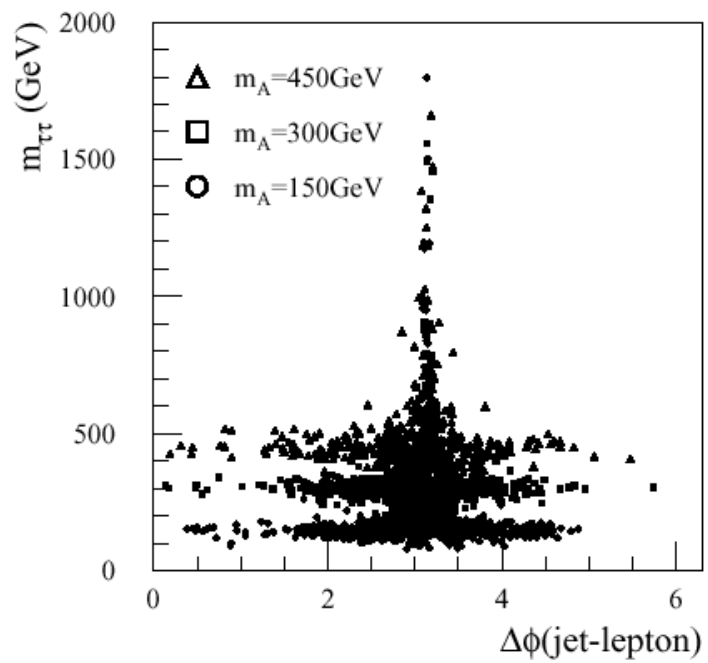
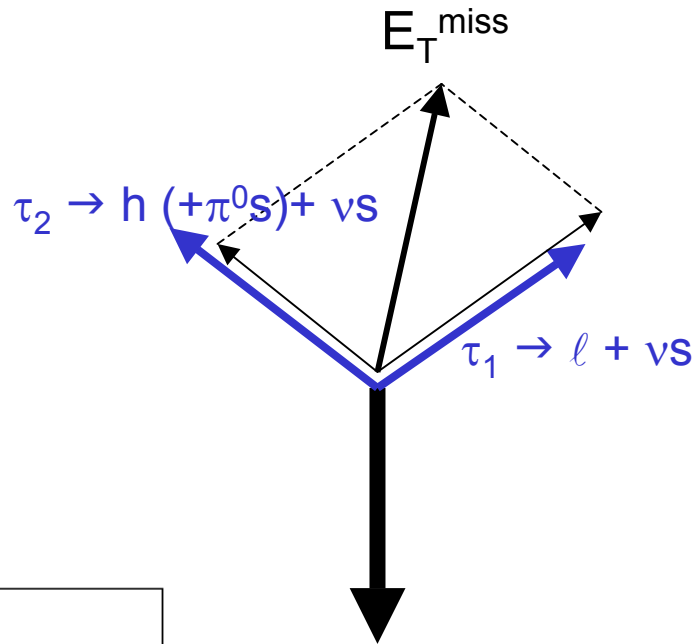


Fig.29a

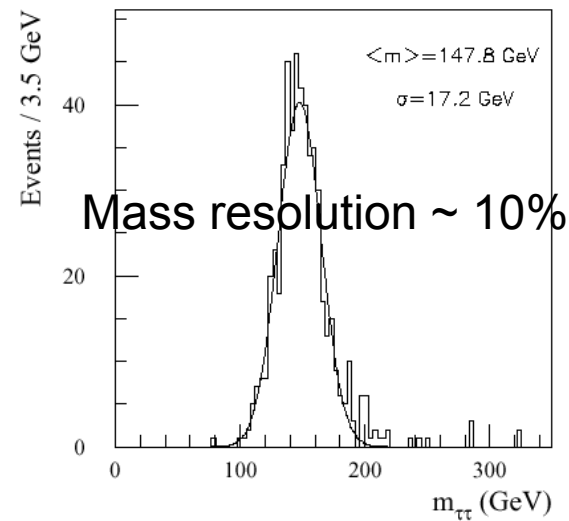


Fig.29b

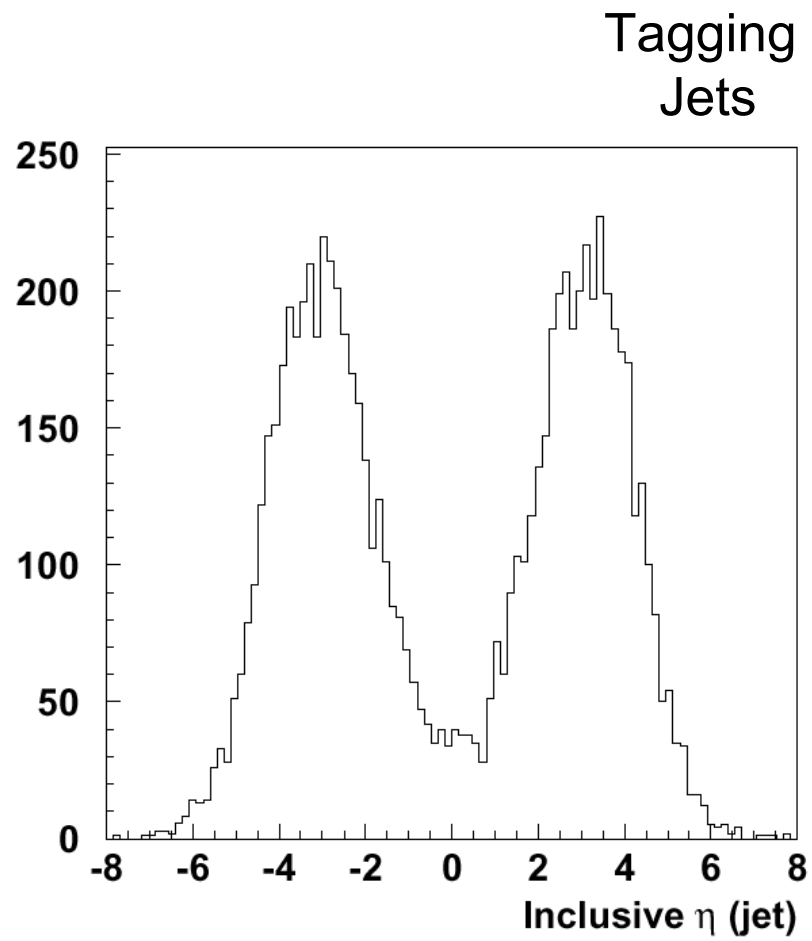
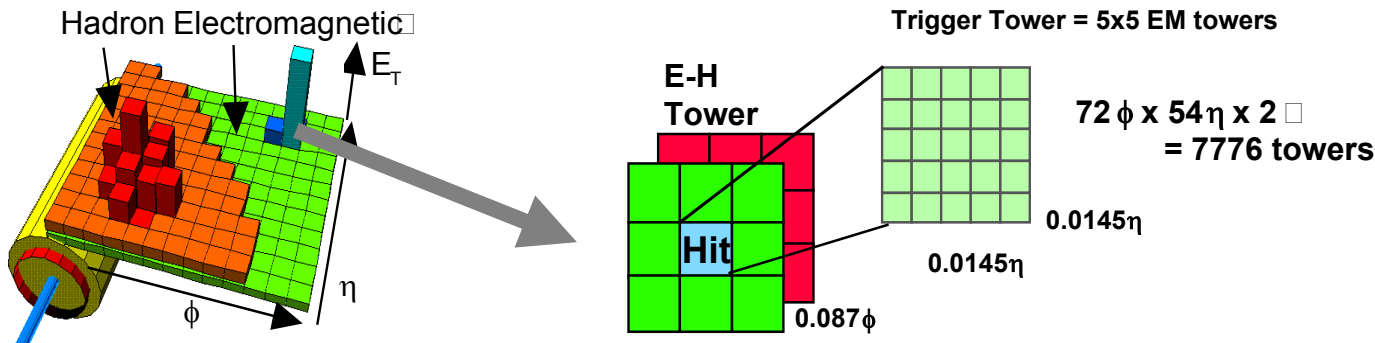


Fig.30



$$E_T(\text{Hit Tower}) + \max E_T(\text{Surrounding Towers}) > E_T^{\min}$$

$$E_T(\text{Surrounding Towers}) / E_T(\text{Hit Tower}) < HoE^{\max}$$

$$\text{At least 1 } E_T(\text{Surrounding Towers}) < E_{\text{iso}}^{\max}$$

$$\text{Fine-grain: } \geq 1(\text{Fine-grain Grids}) > R E_T^{\min}$$

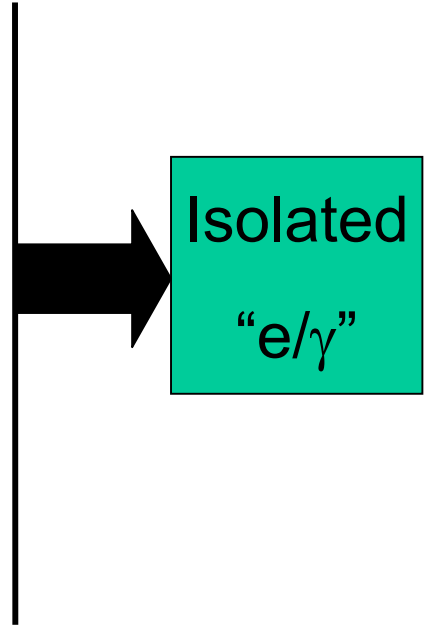


Fig.31

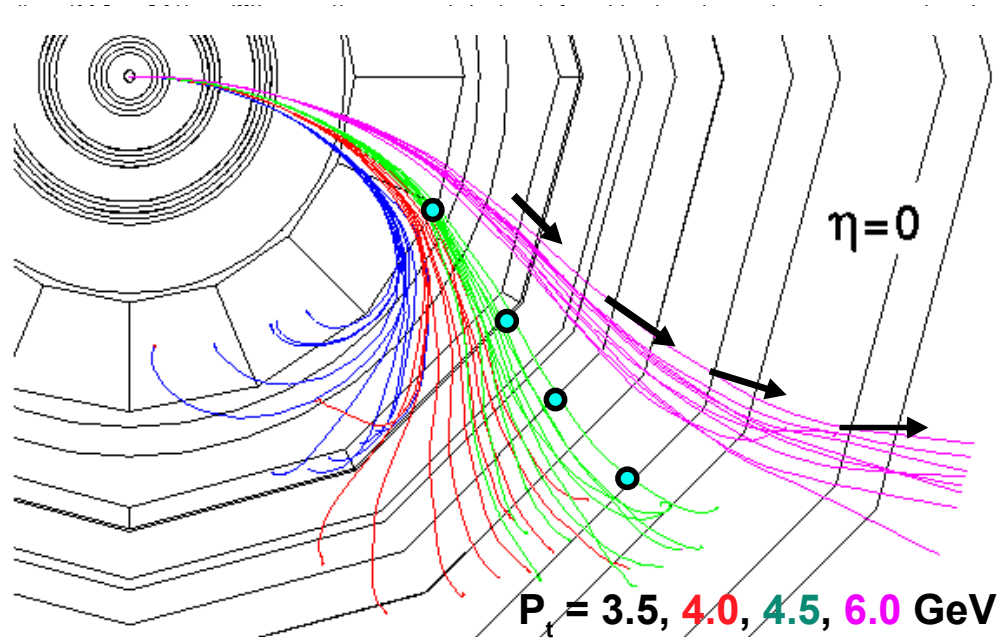


Fig.32

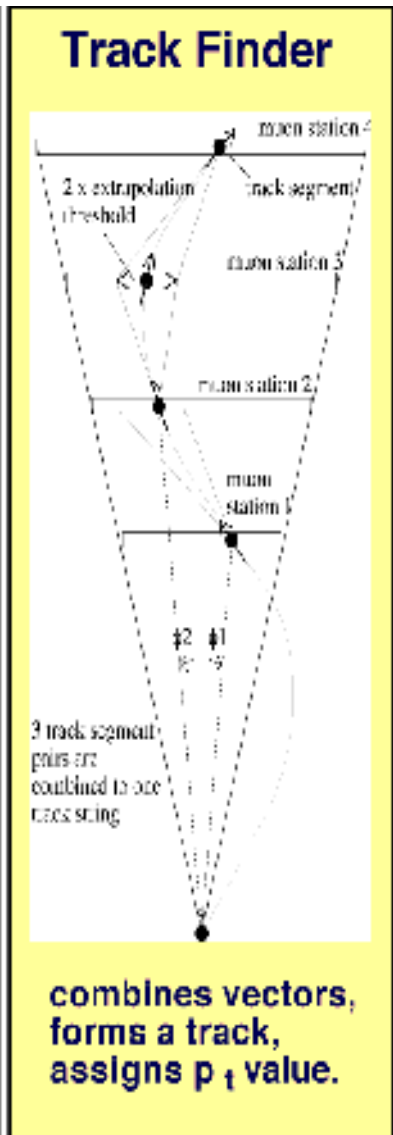
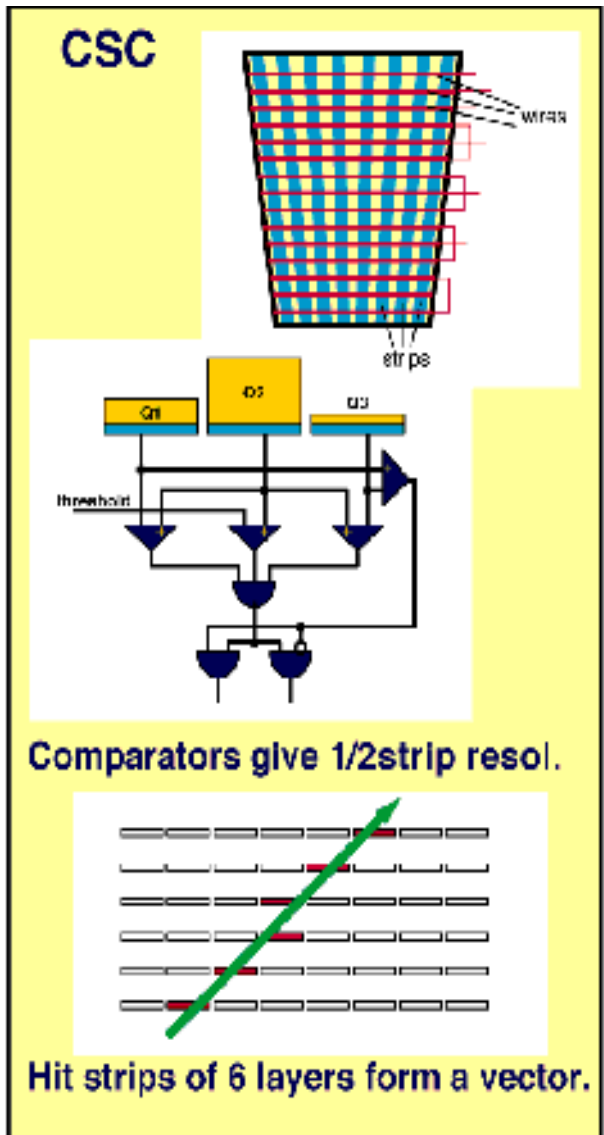
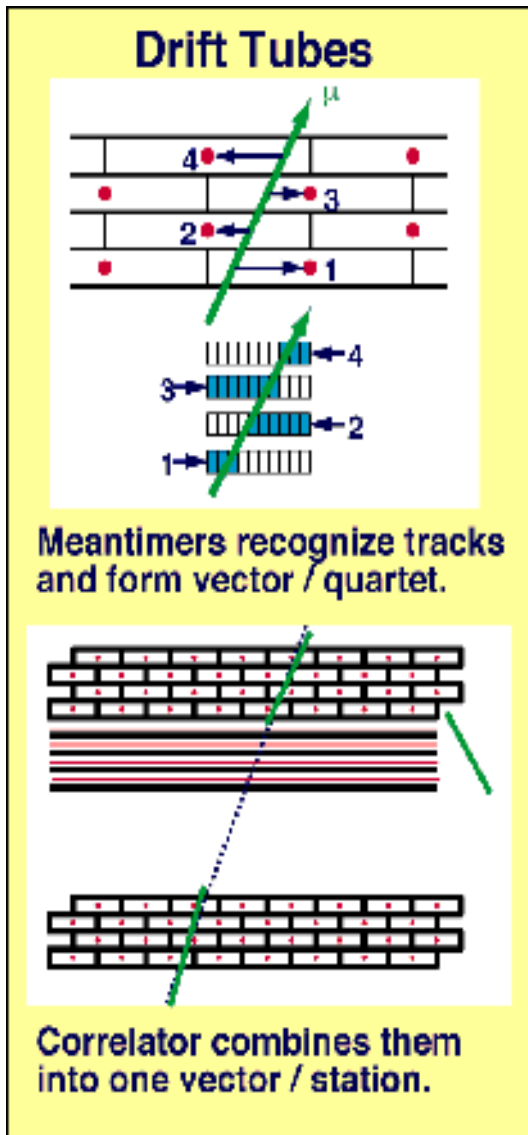


Fig.33

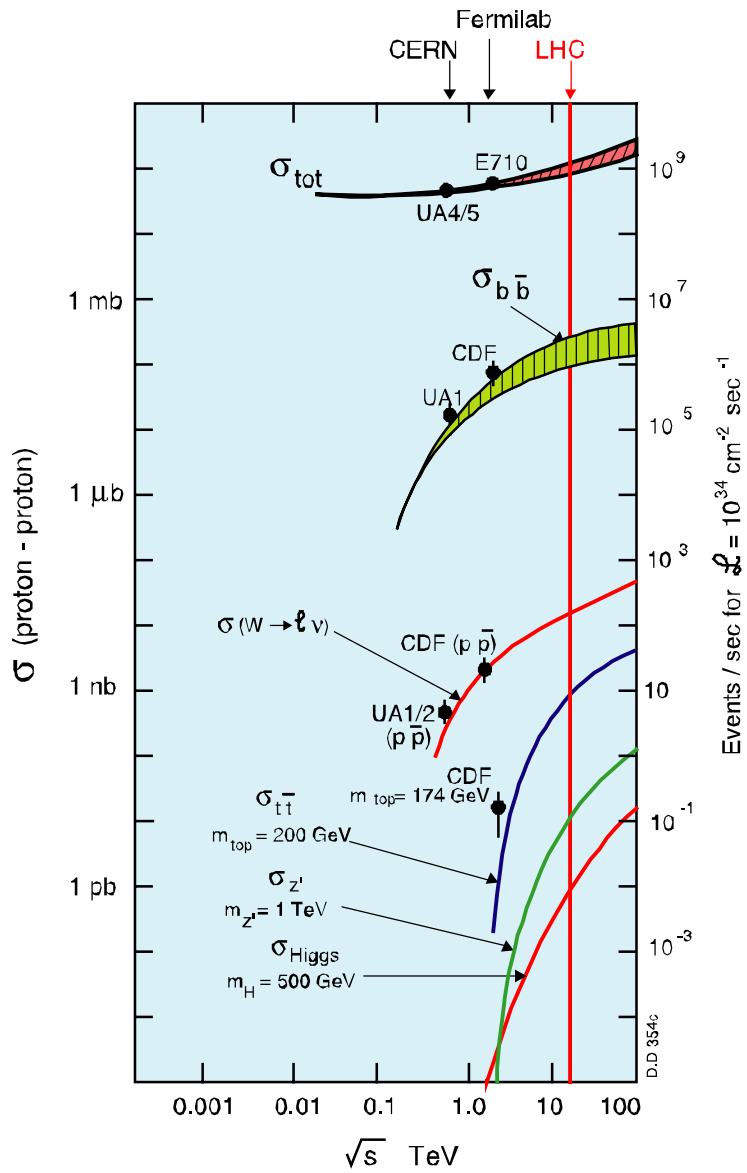


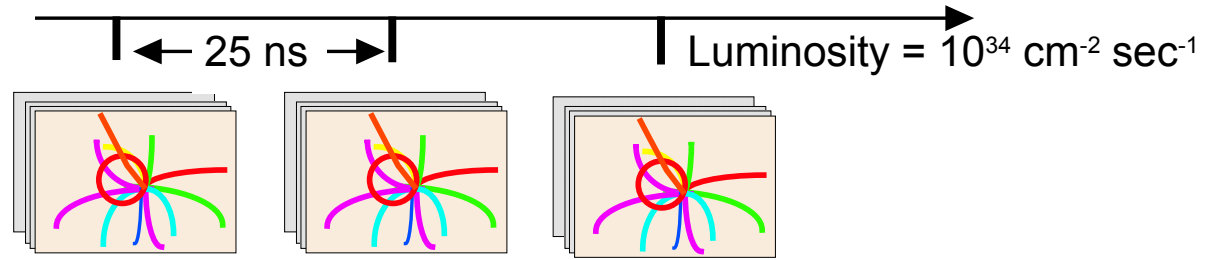
Fig.34

- 30 Collisions/25ns

(10^9 event/sec)

10^7 channels

(10^{16} bit/sec)



Multilevel trigger and readout systems

Trigger Rate

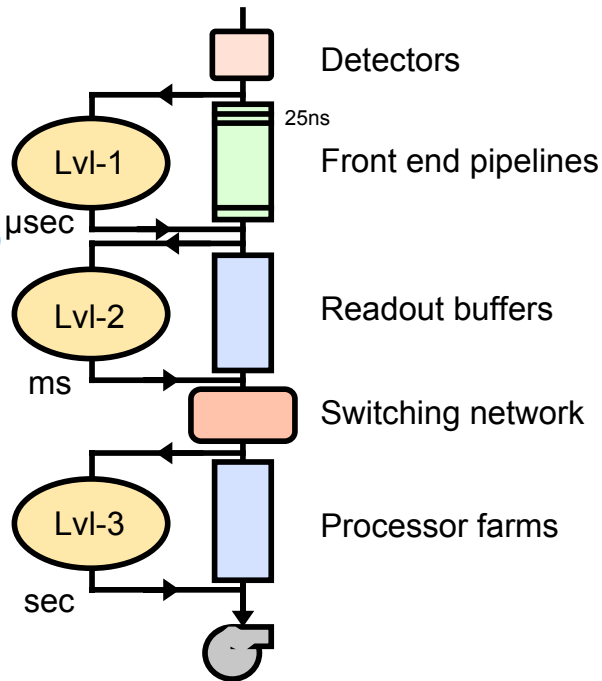
40 MHz

10^5 Hz

10^3 Hz

10^2 Hz

ATLAS



Trigger Rate

40 MHz

10^5 Hz

10^2 Hz

CMS

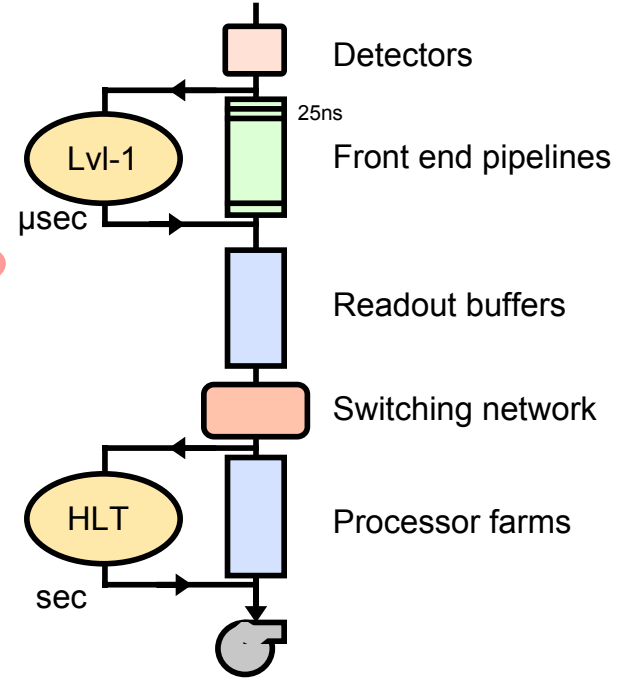


Fig.35

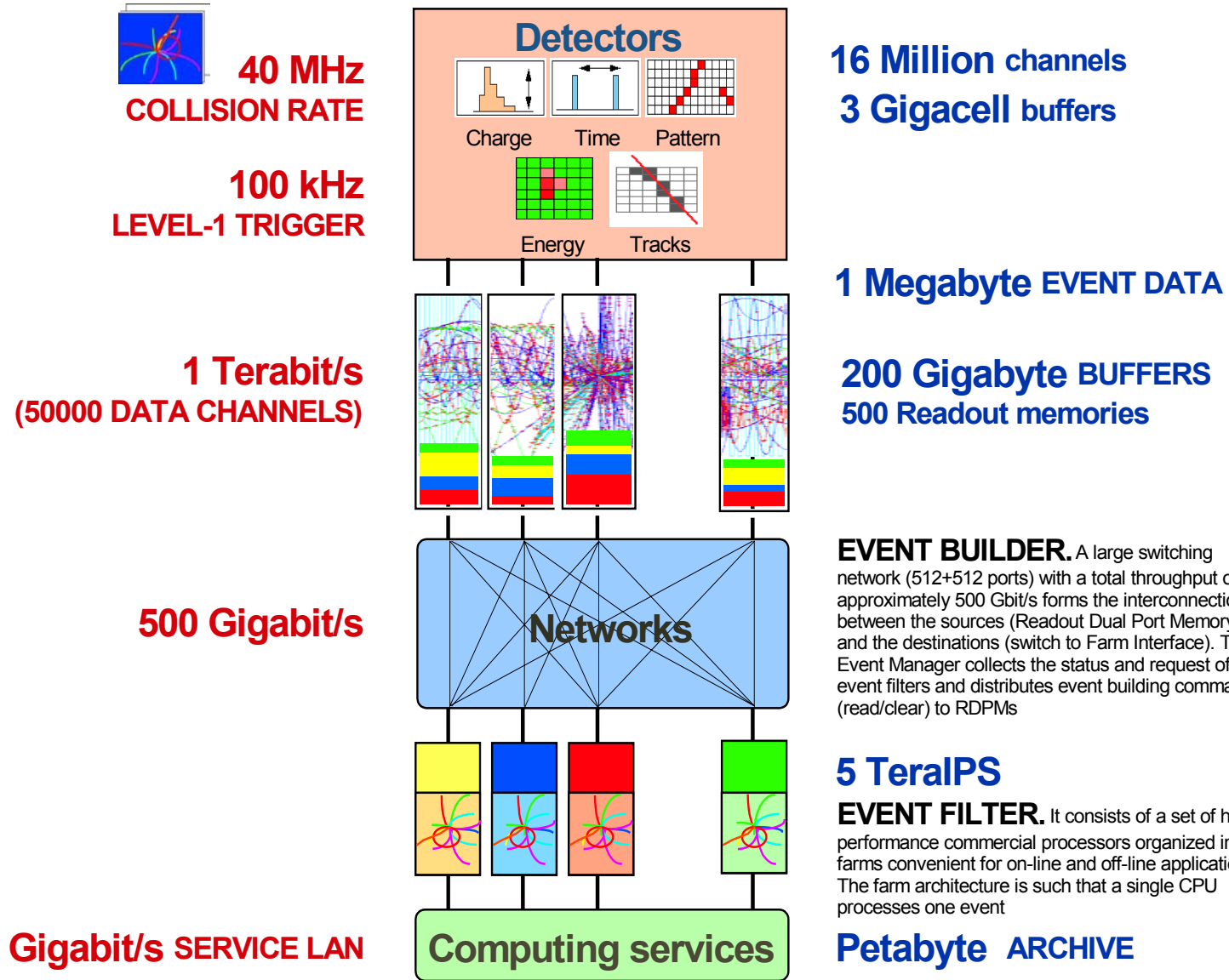


Fig.36

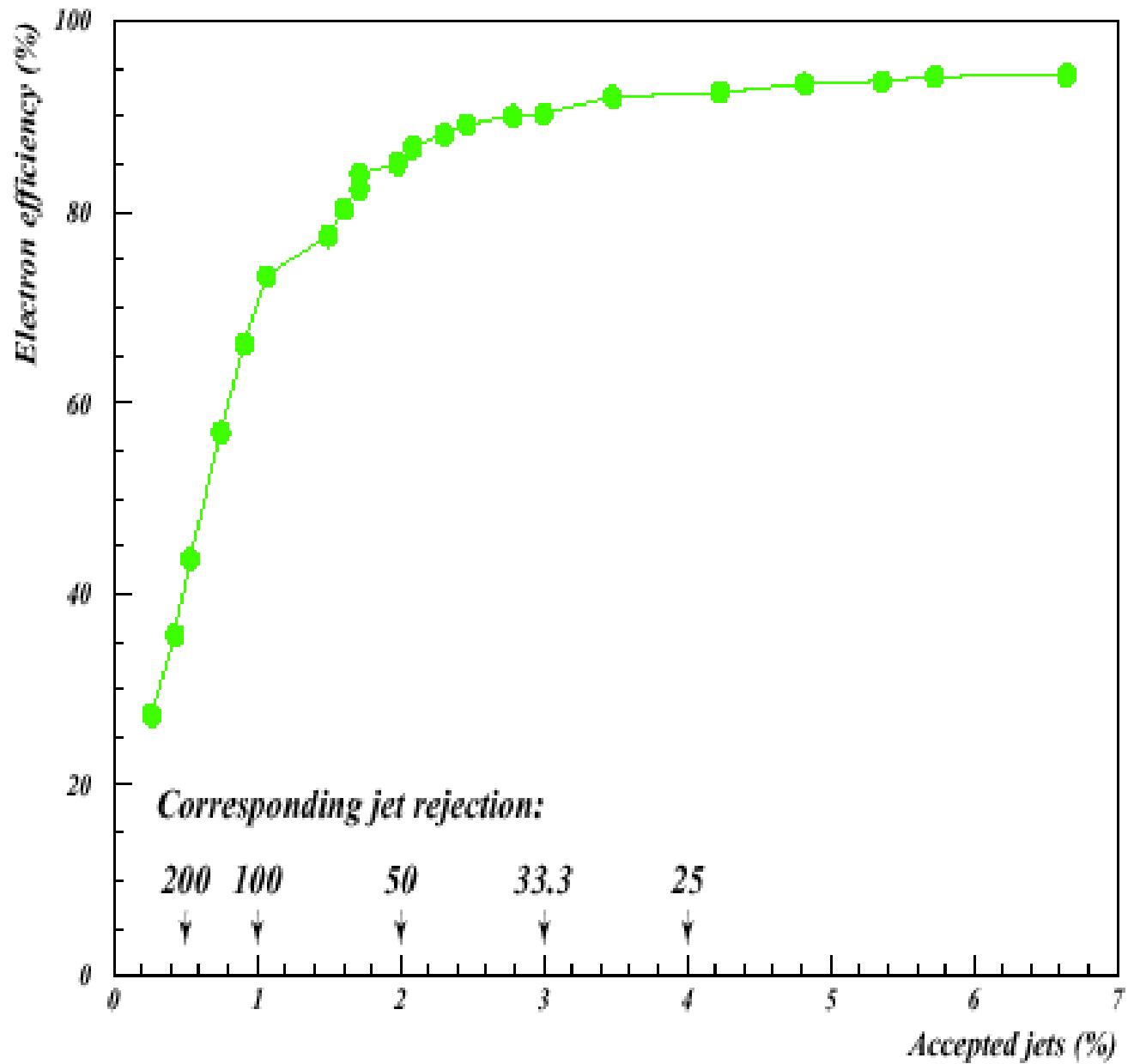


Fig.37

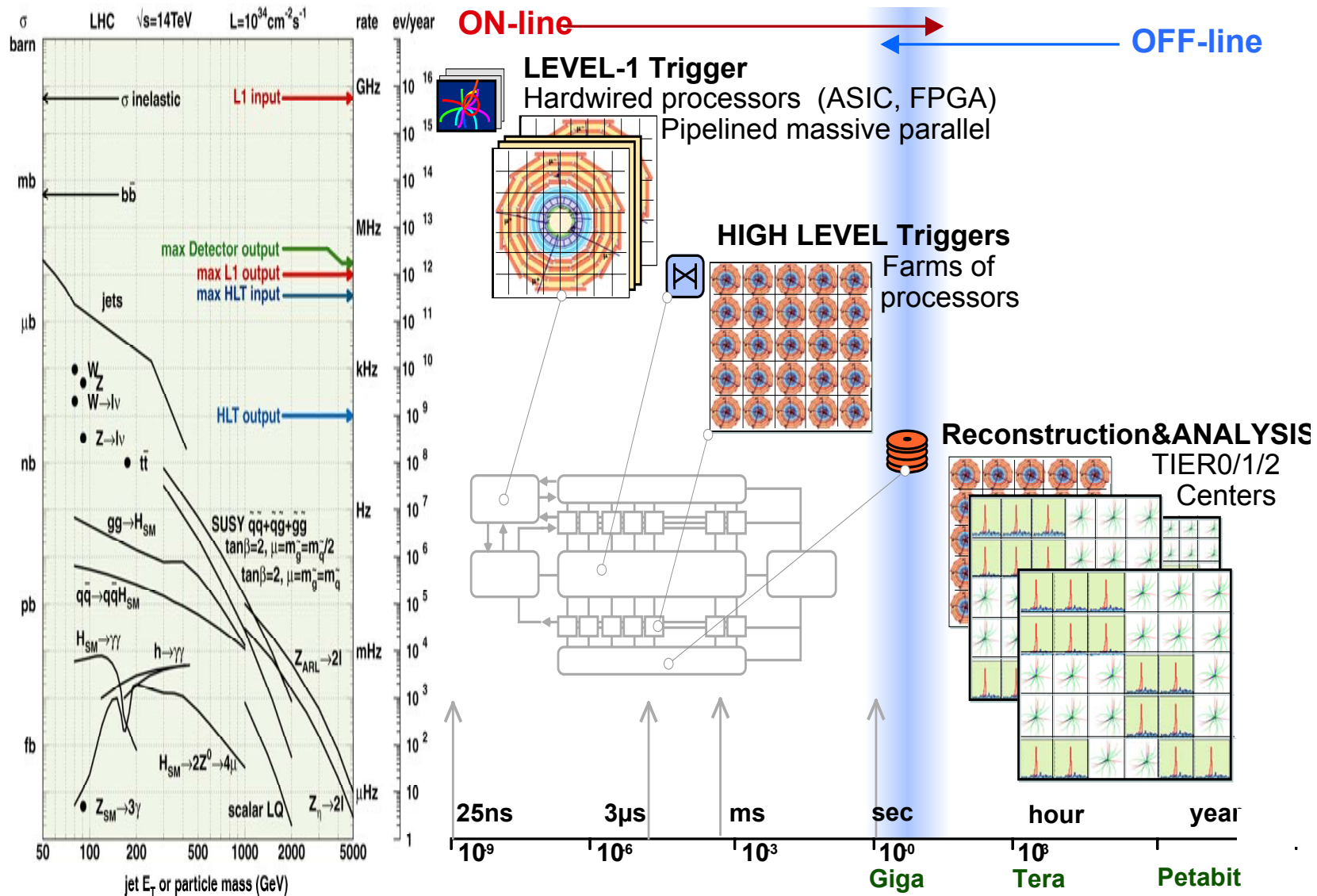


Fig.38

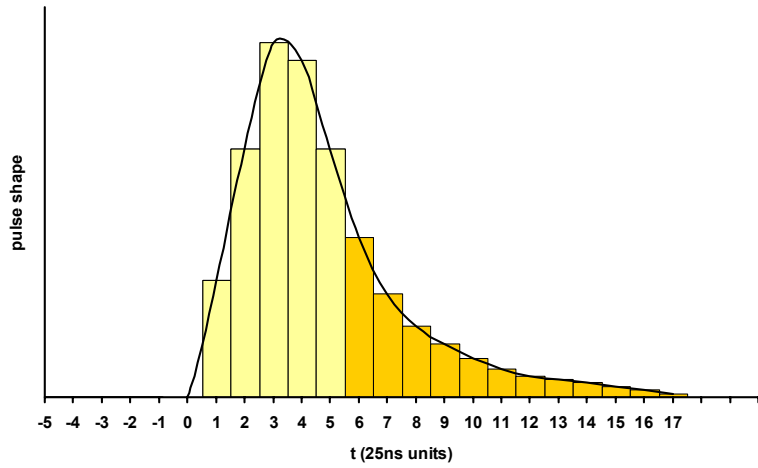


Fig.39a

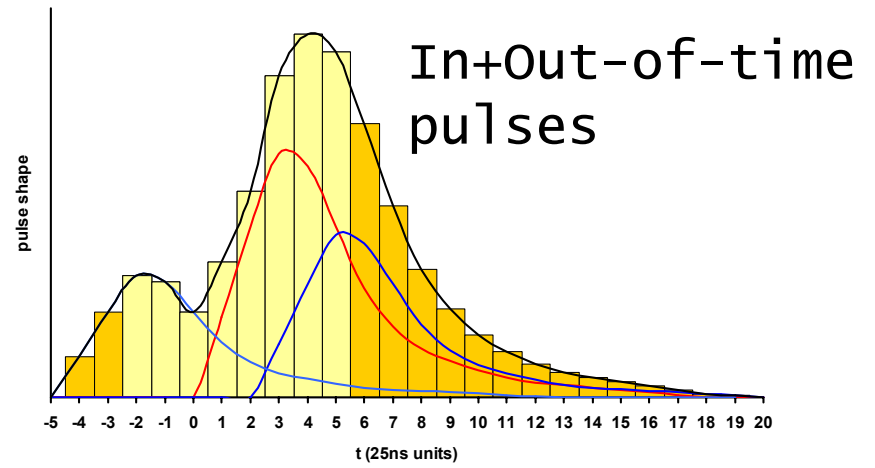
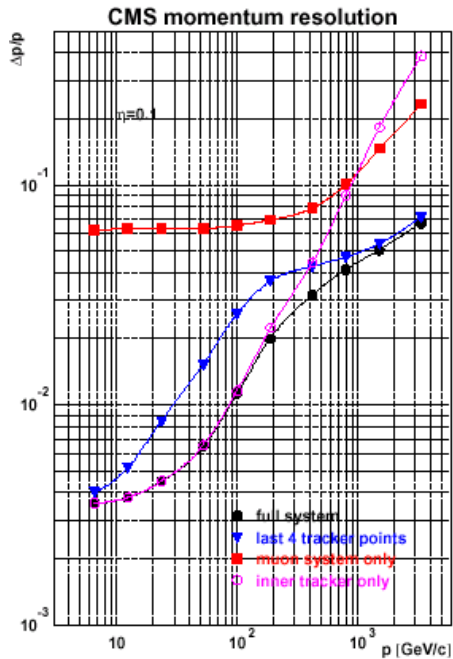


Fig.39b

Muon Momentum Resolution

Spatial resolution
 $\approx 100 \mu\text{m}/\text{station}$

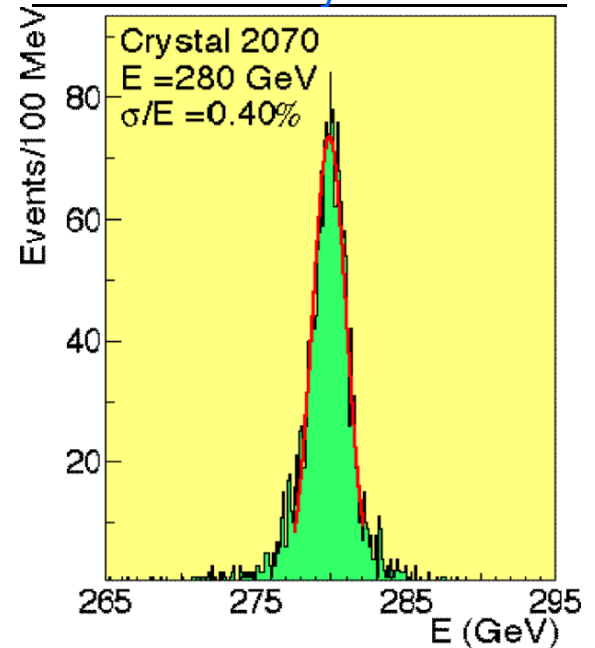


$\delta p_t/p_t - 10\%$
 at $p_t=500 \text{ GeV}$ at $\eta=2$

Fig.40a

PbWO₄ CRYSTAL ELECTROMAGNETIC CALORIMETER

Energy reconstructed
 in 3 x 3 crystals



$\sigma/E - 2.7\% / \sqrt{E} \oplus 0.5\% \oplus 20\%/E$
 (E in GeV)

Fig.40b

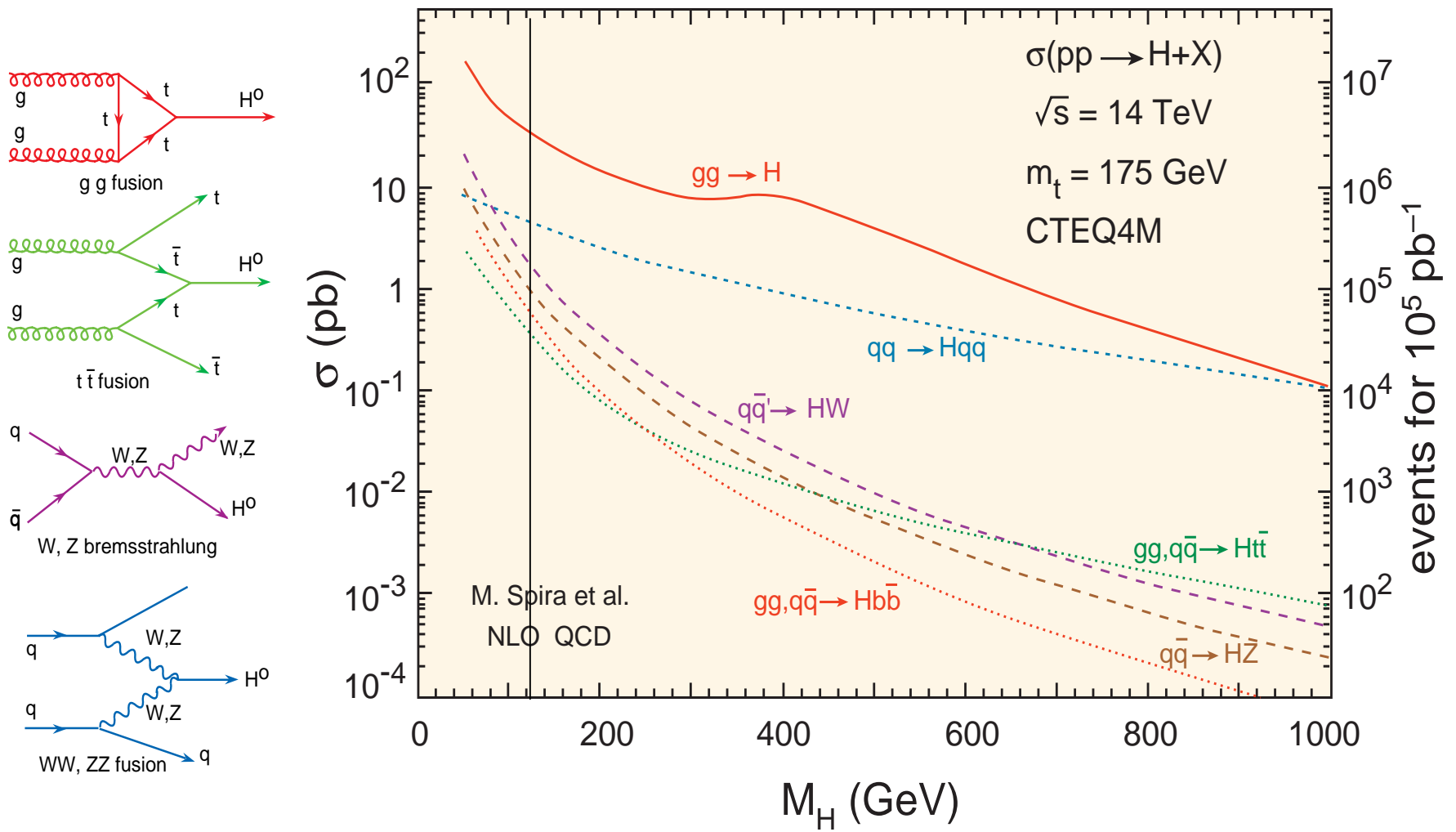


Fig.41

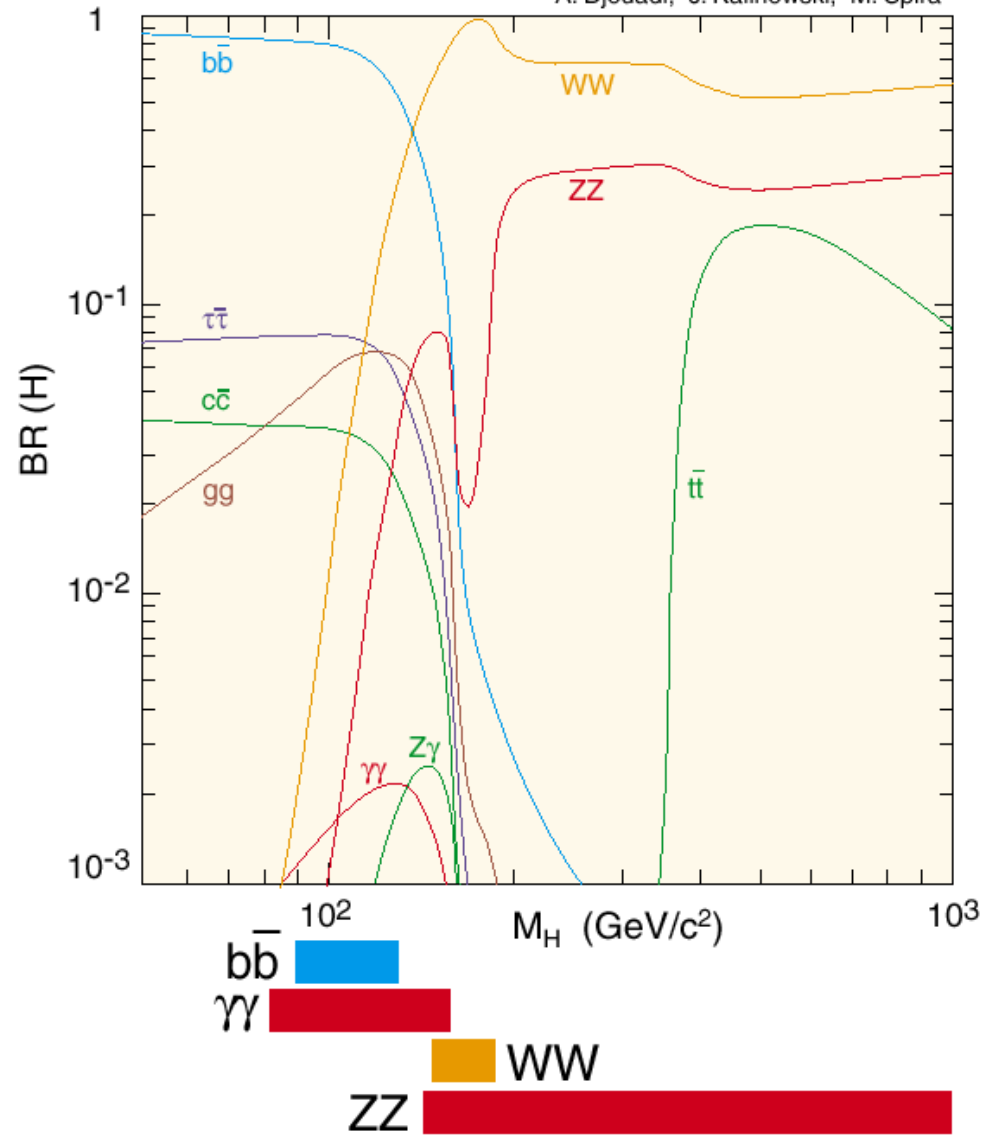


Fig.42

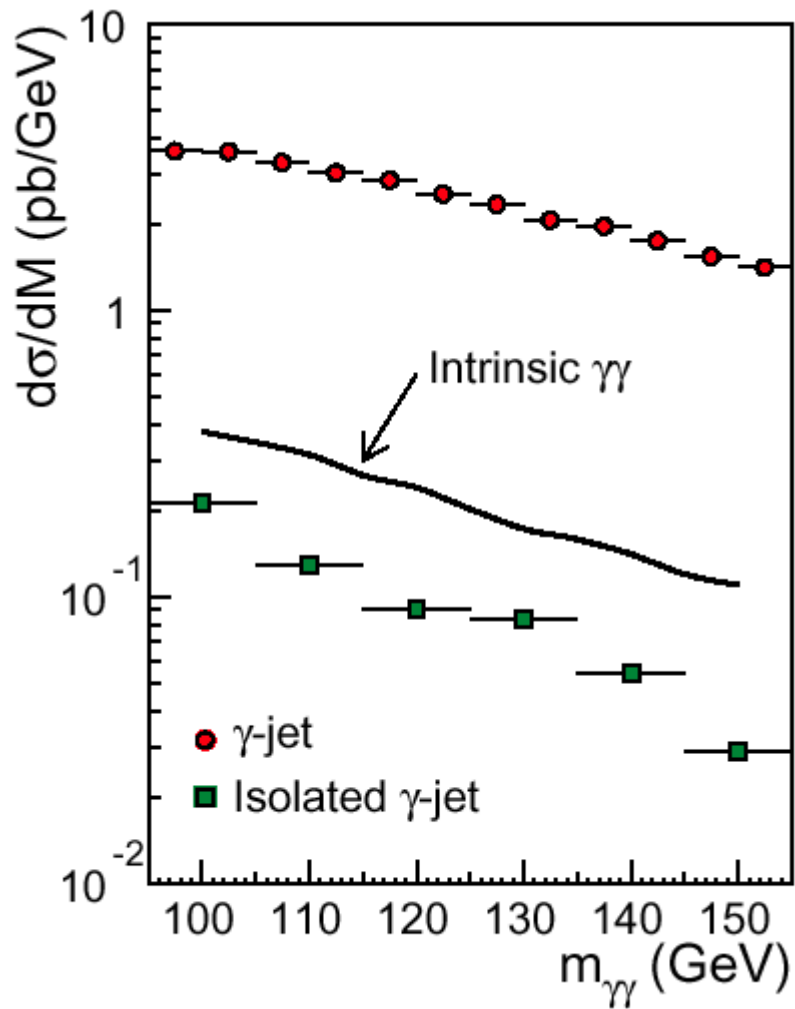


Fig.43a

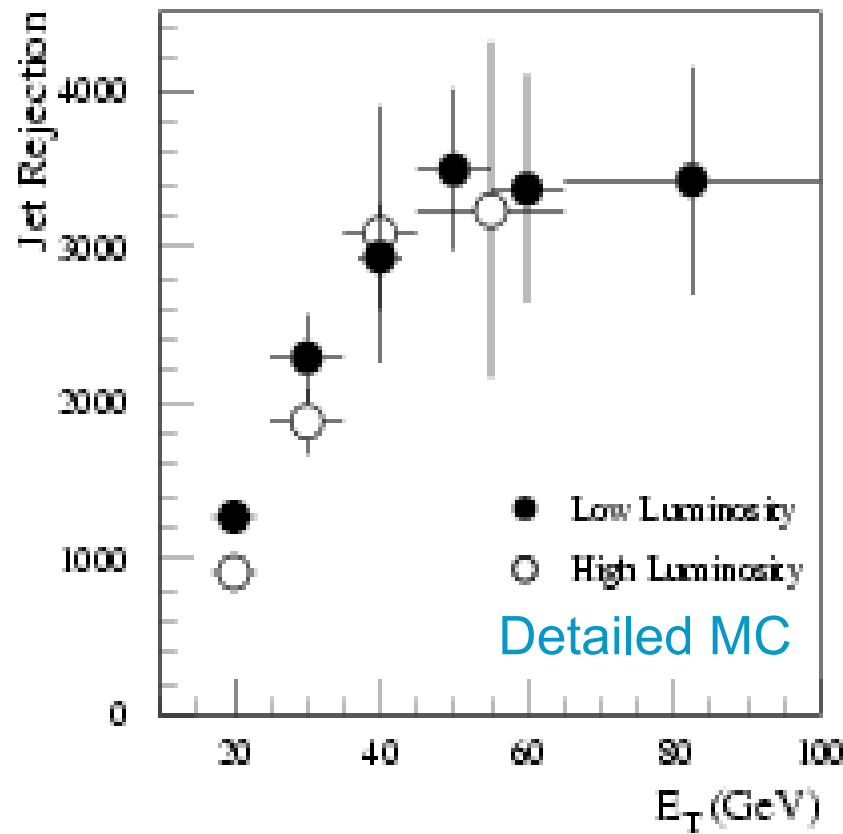


Fig.43b

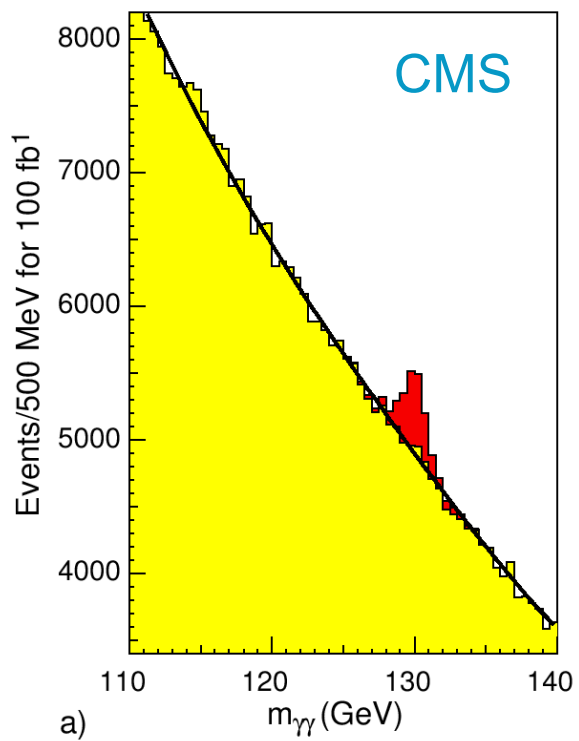


Fig.44a

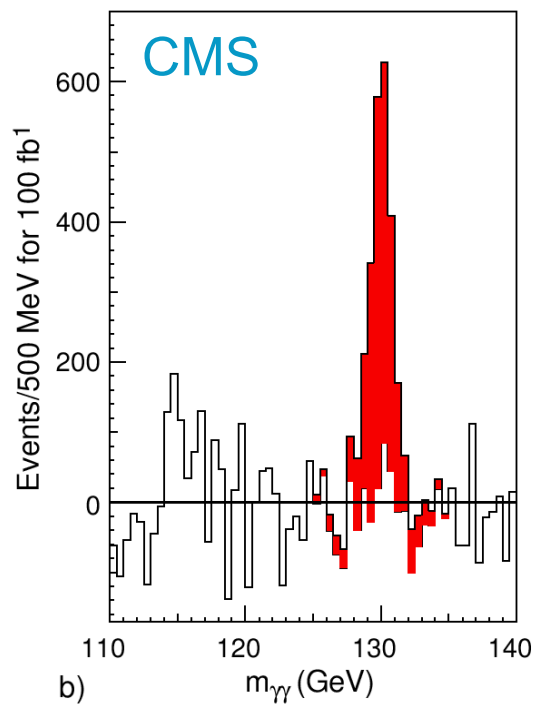


Fig.44b

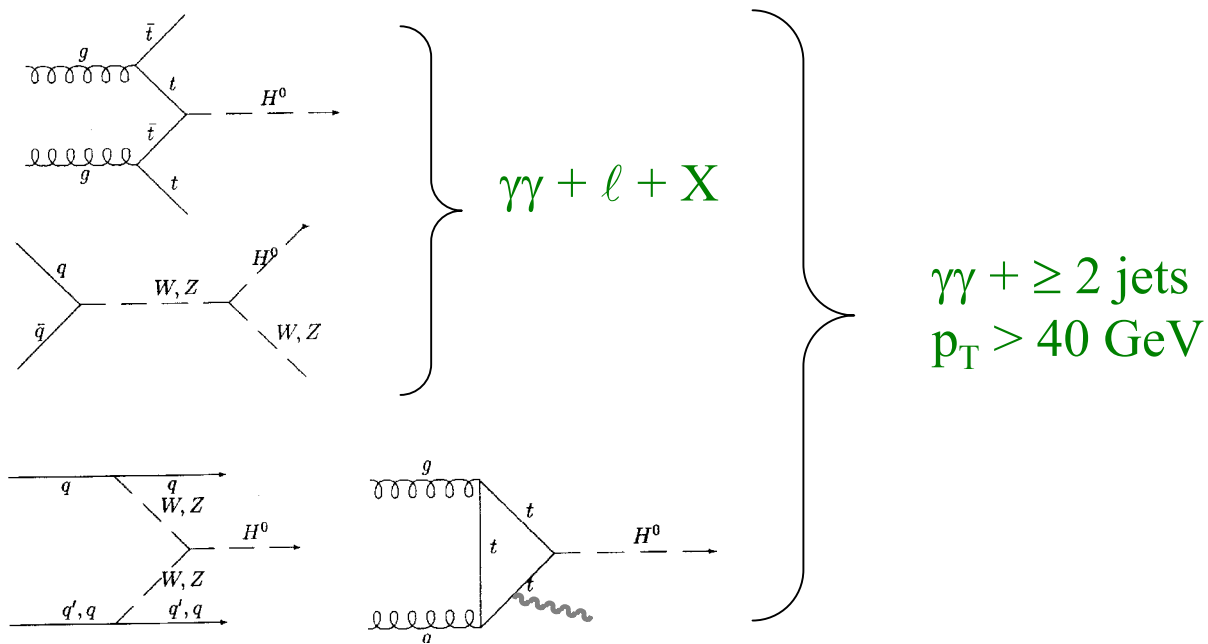


Fig.45

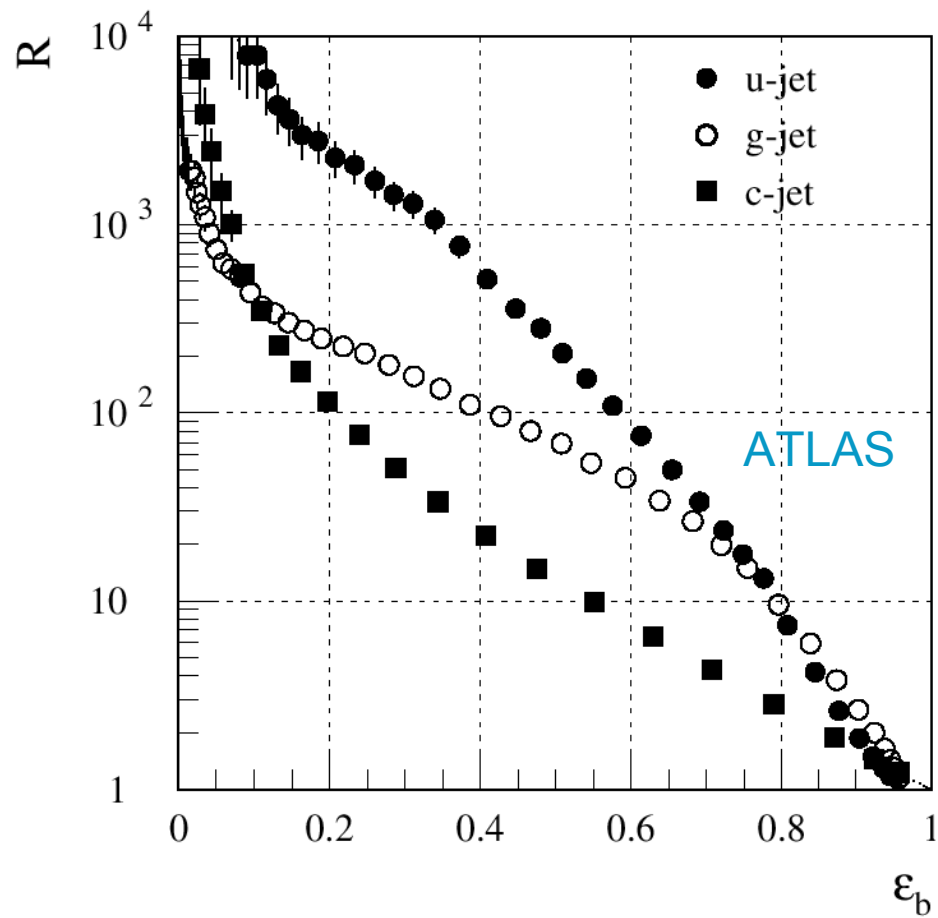


Fig.46

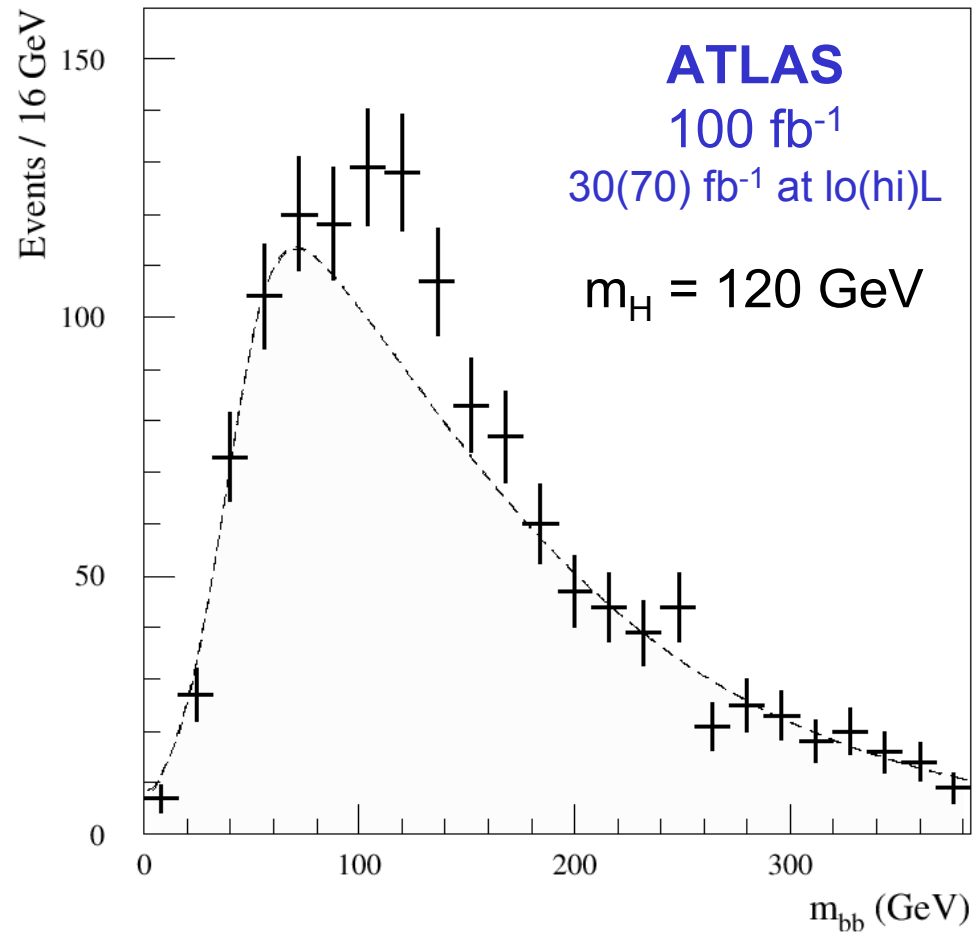


Fig.47

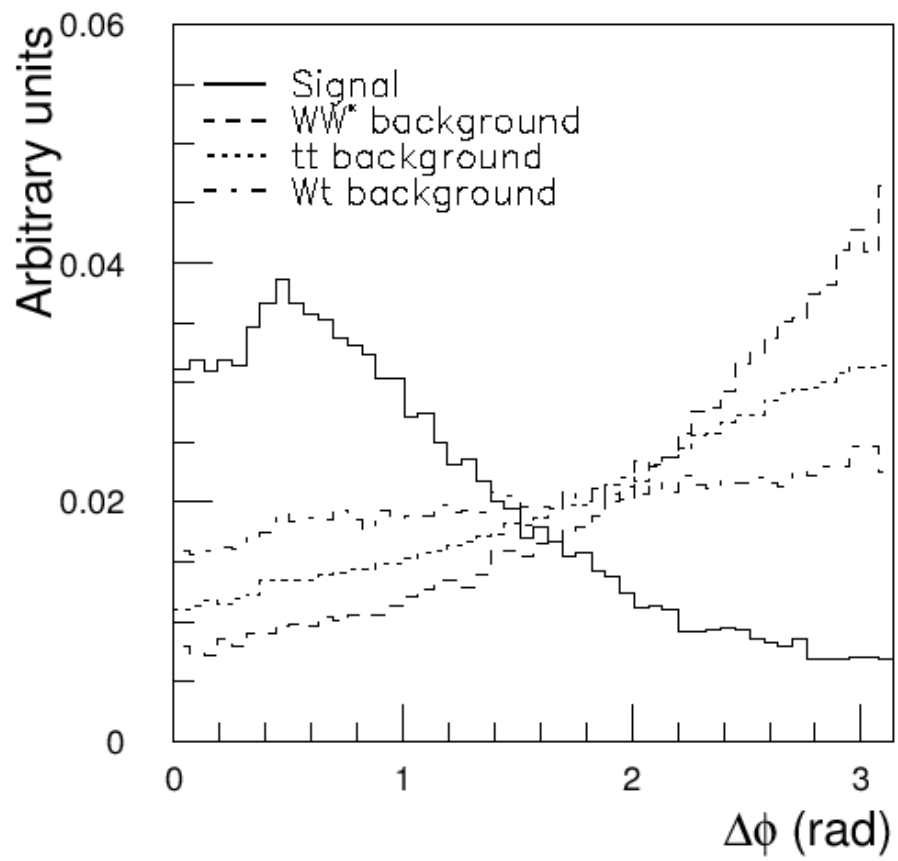


Fig.48

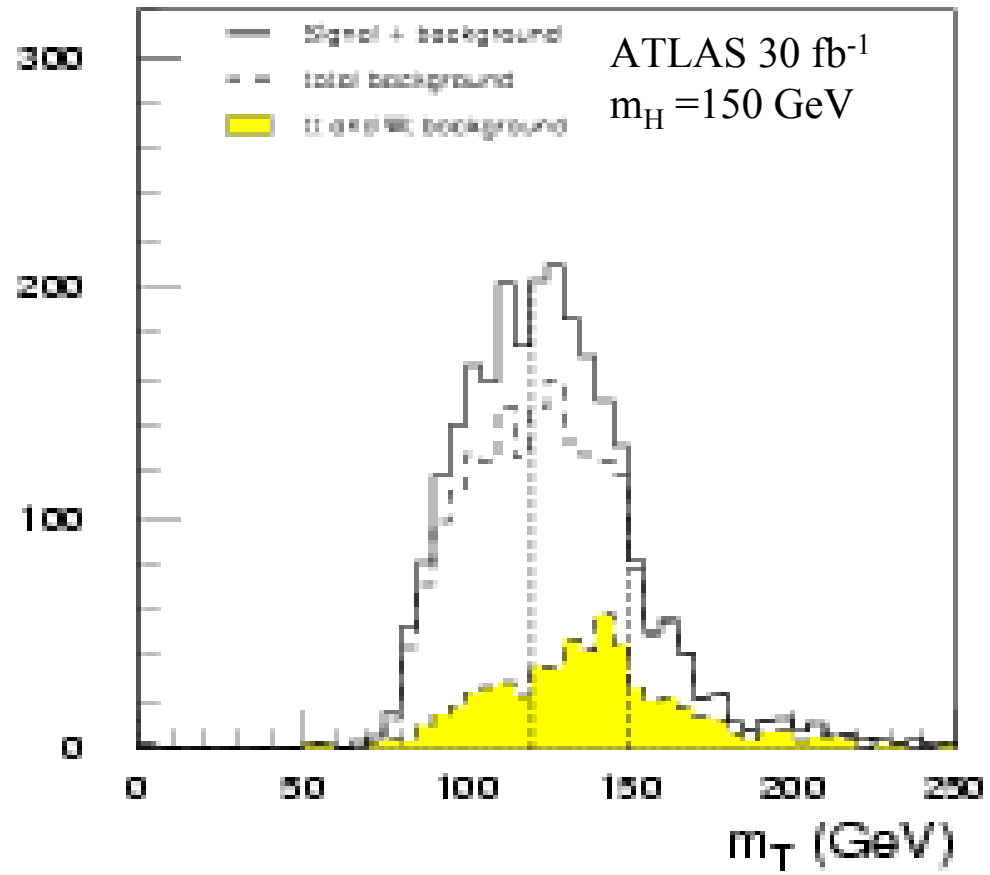


Fig.49

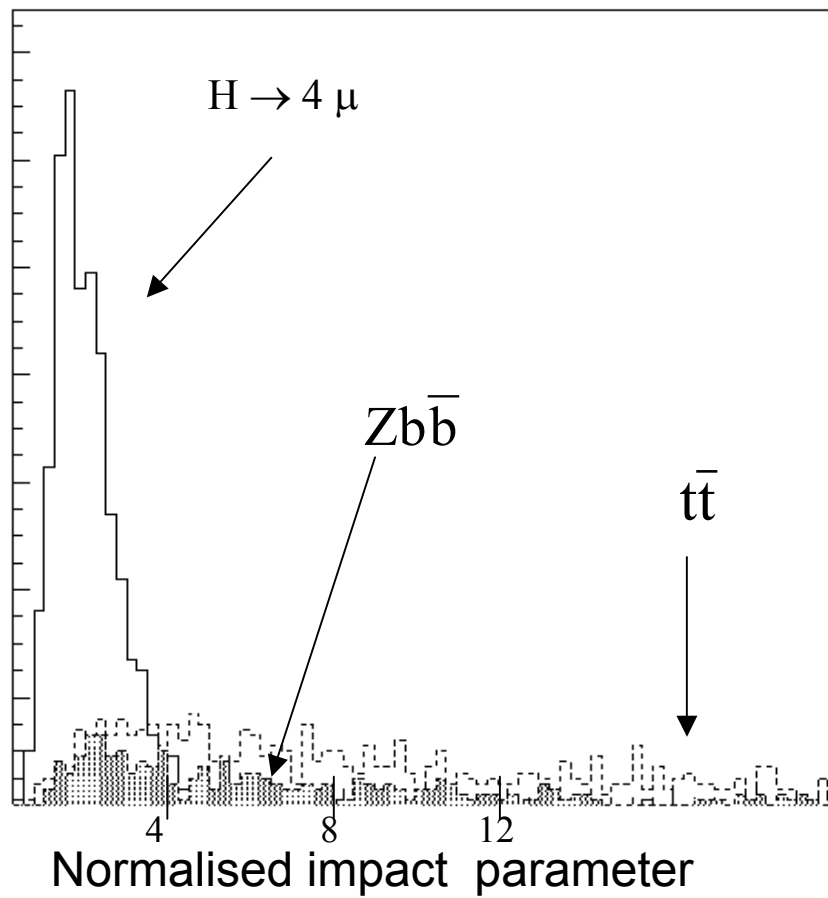


Fig.50

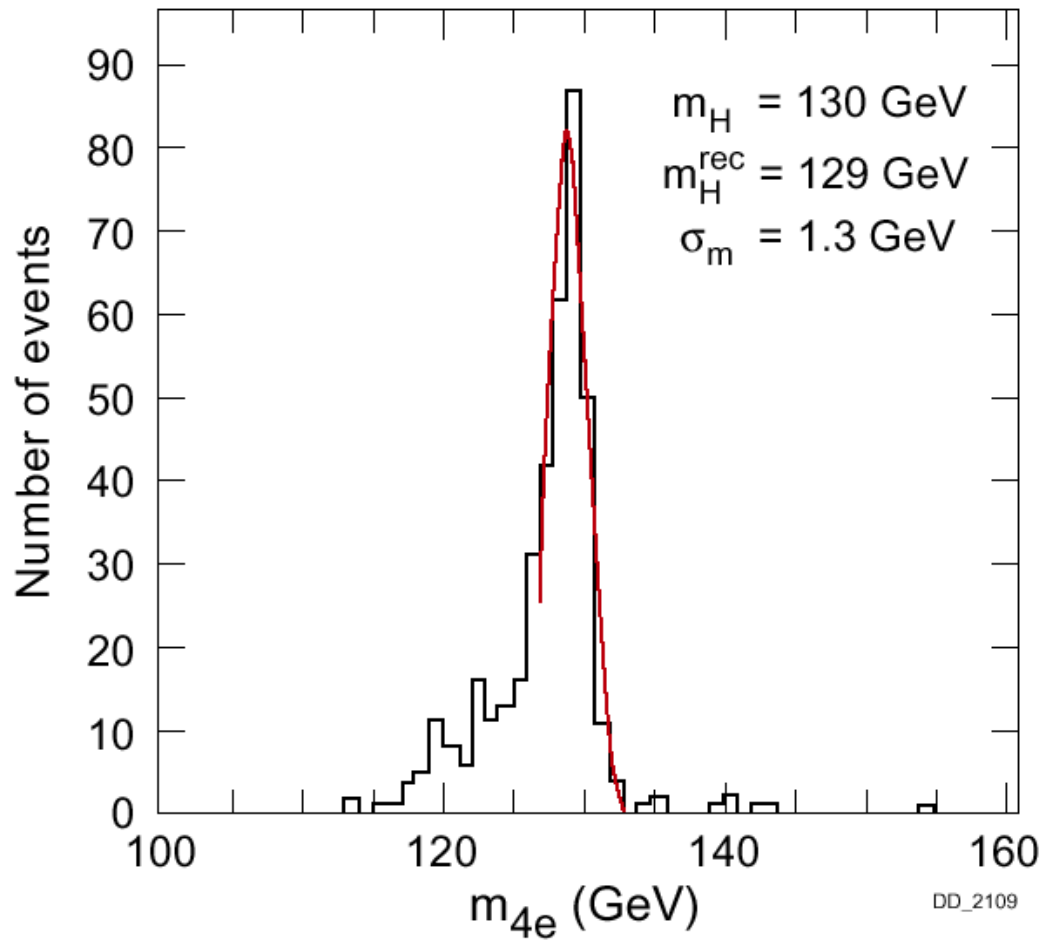


Fig.51

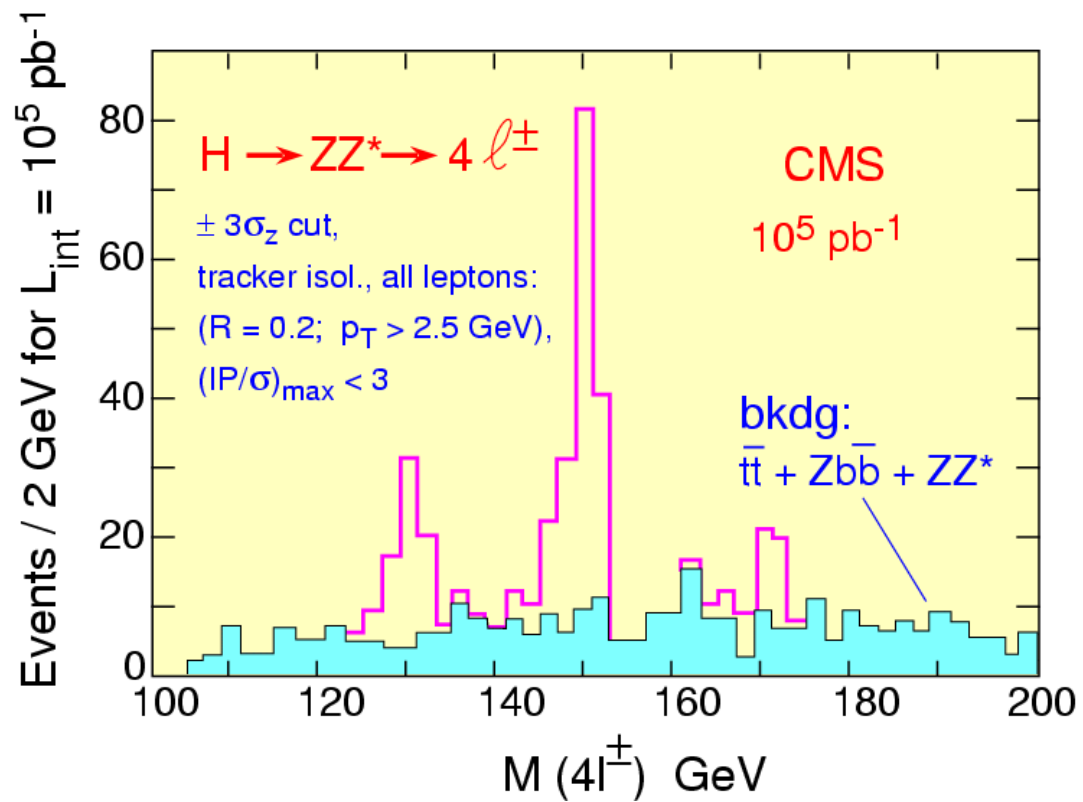
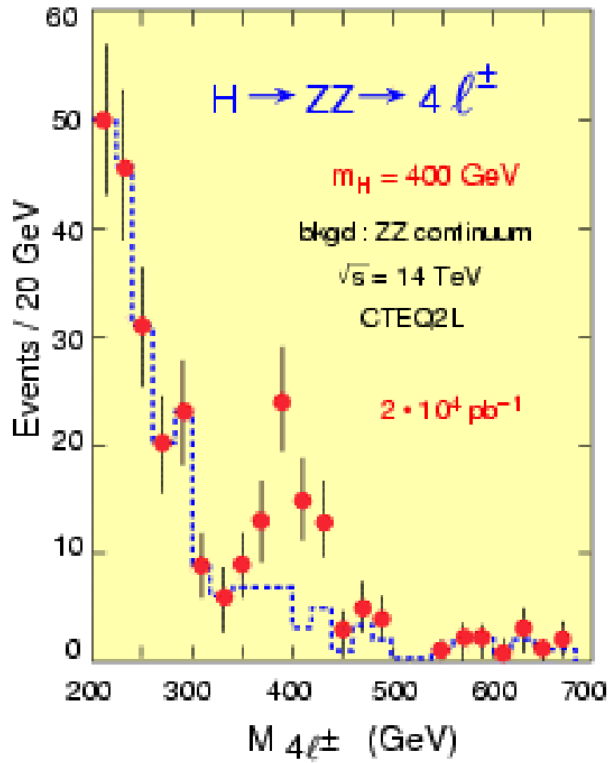


Fig.52

20 fb⁻¹



100 fb⁻¹

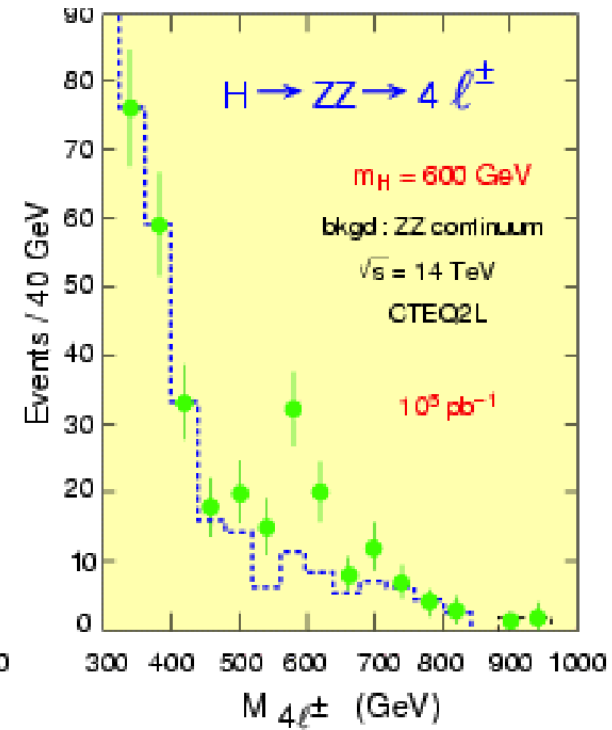
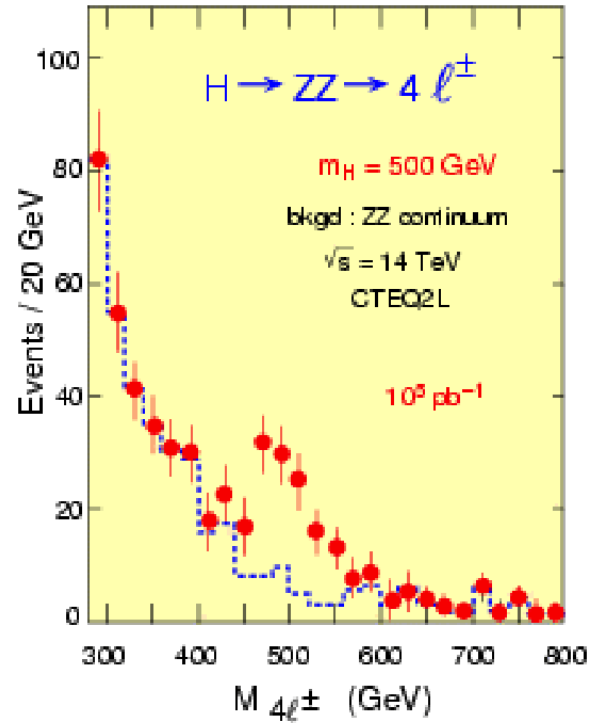


Fig.53

ATLAS : 100 fb⁻¹

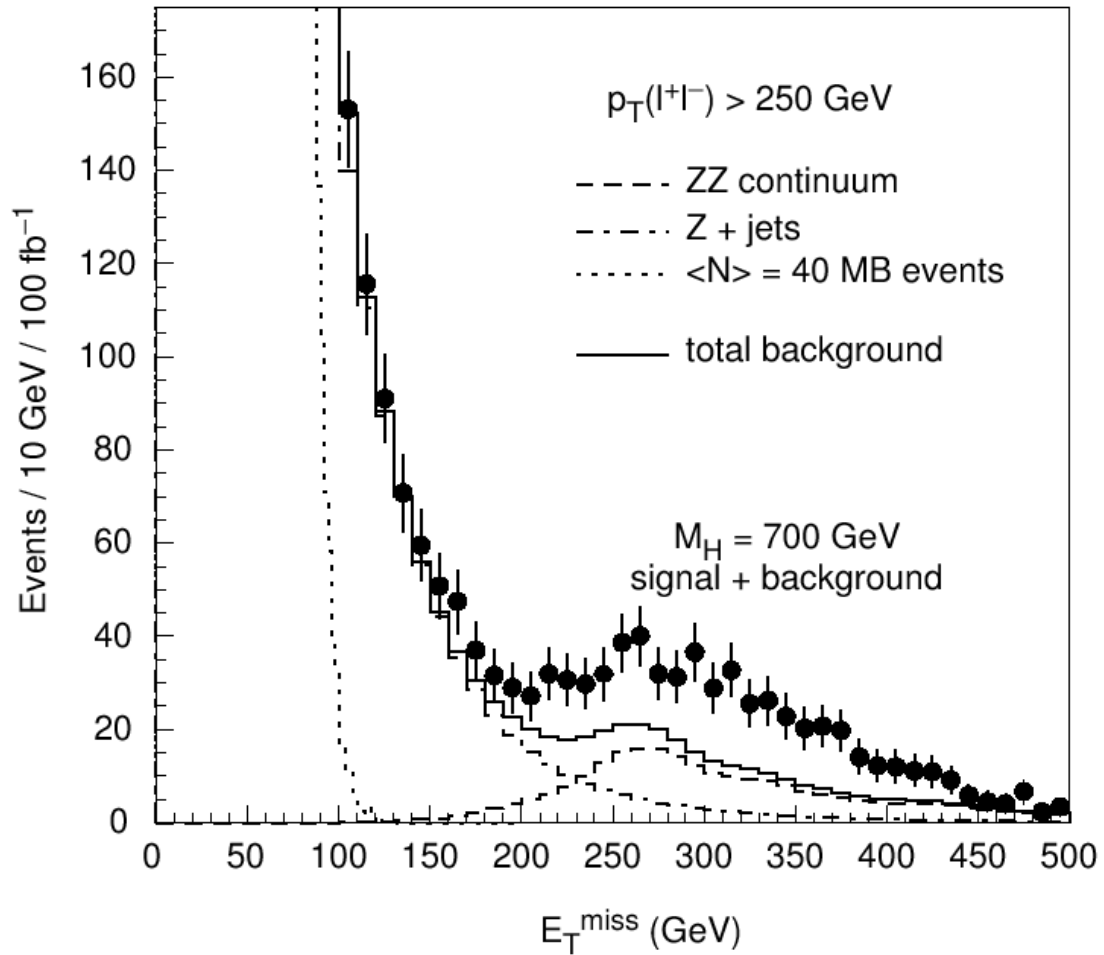
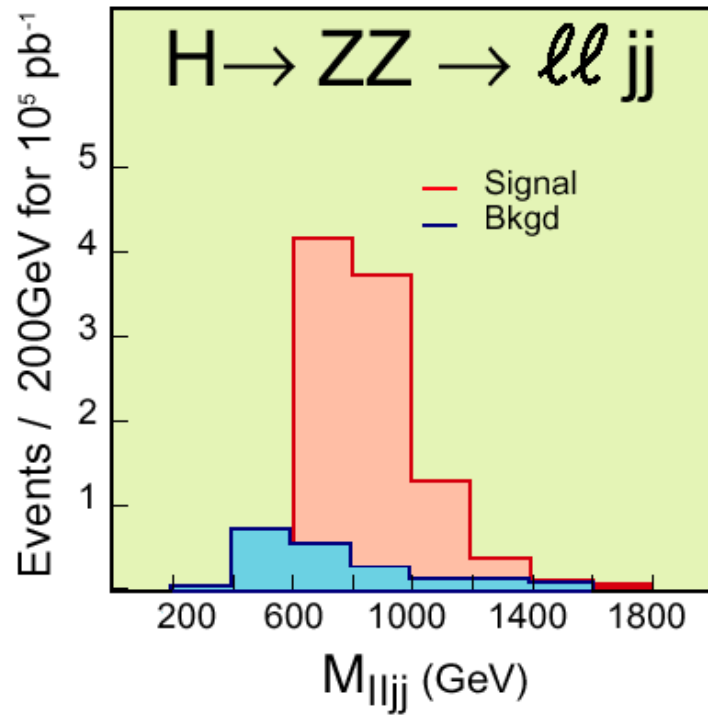


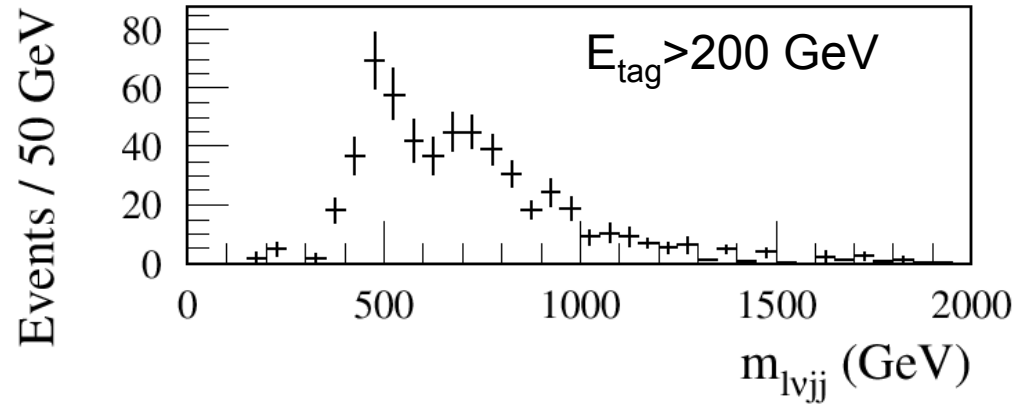
Fig.54



CMS

Fig.55

ATLAS
 $m_H = 1\text{TeV}, 30\text{fb}^{-1}$



$m_H = 800$ GeV, 30fb^{-1}

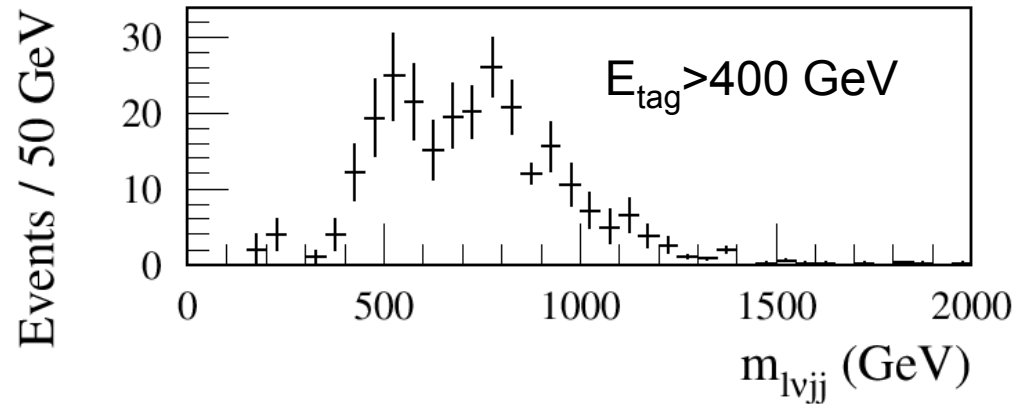


Fig.56

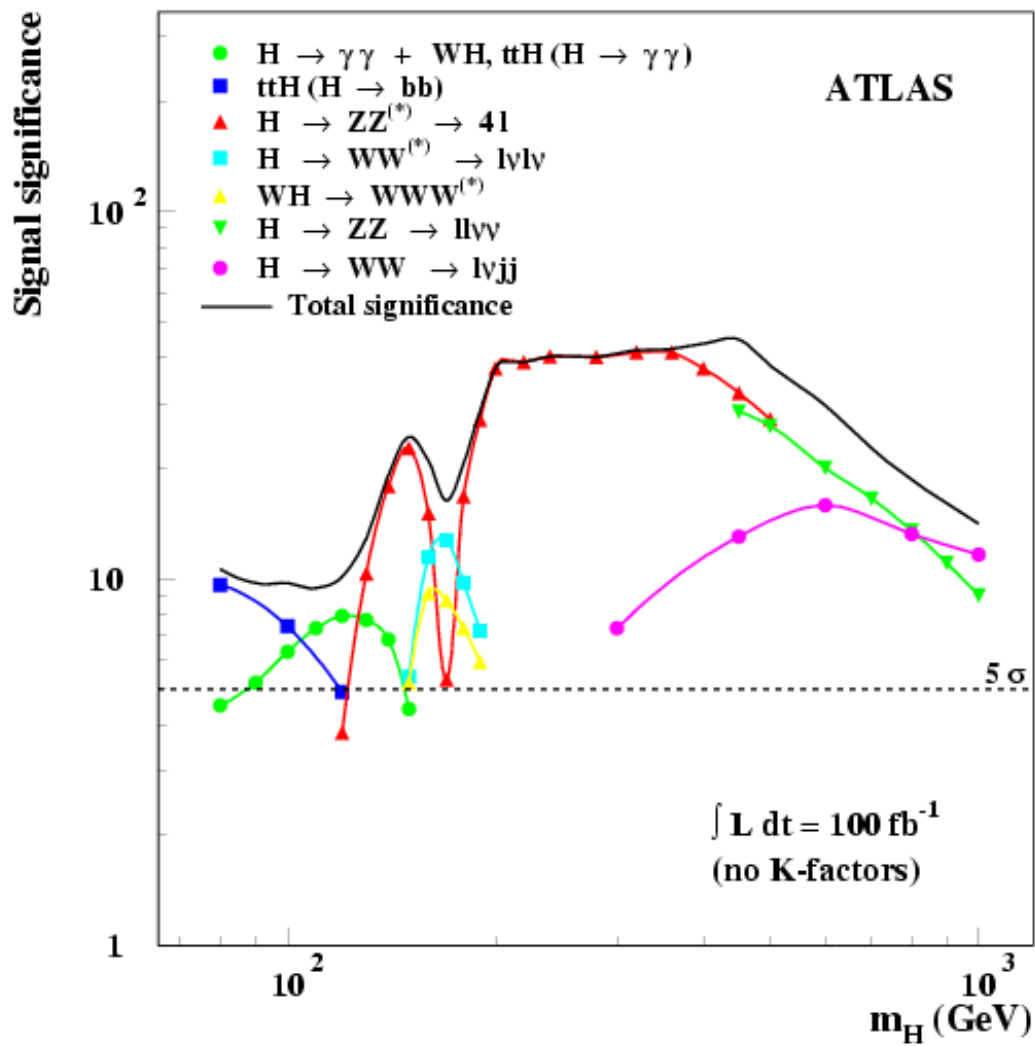


Fig.57

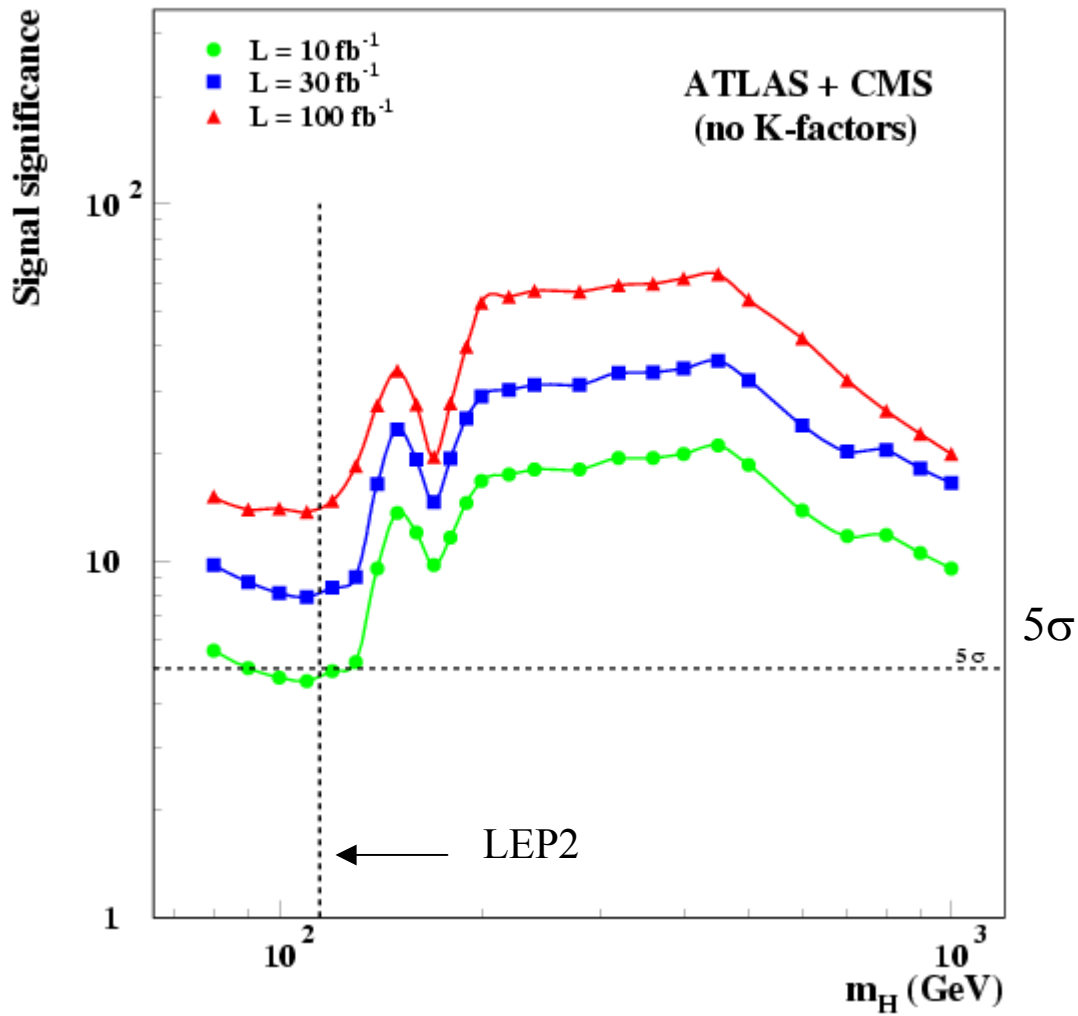


Fig.58

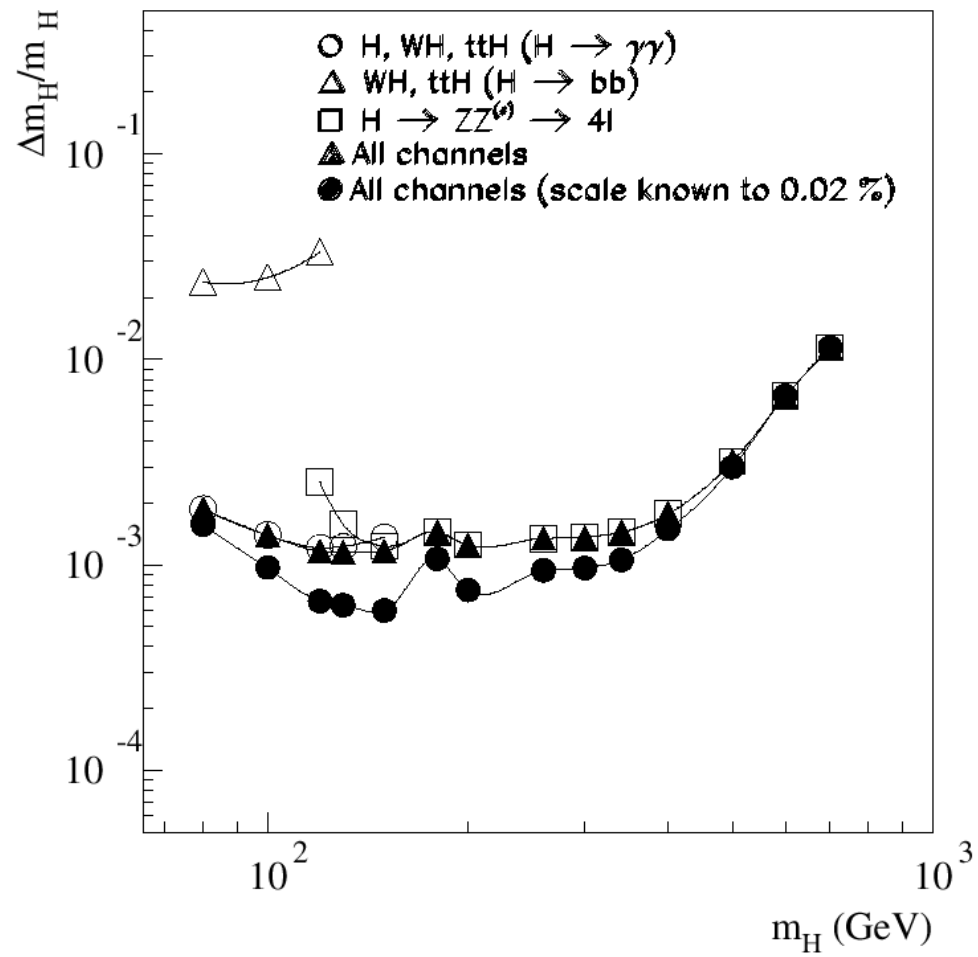


Fig.59

Higgs production via WW fusion

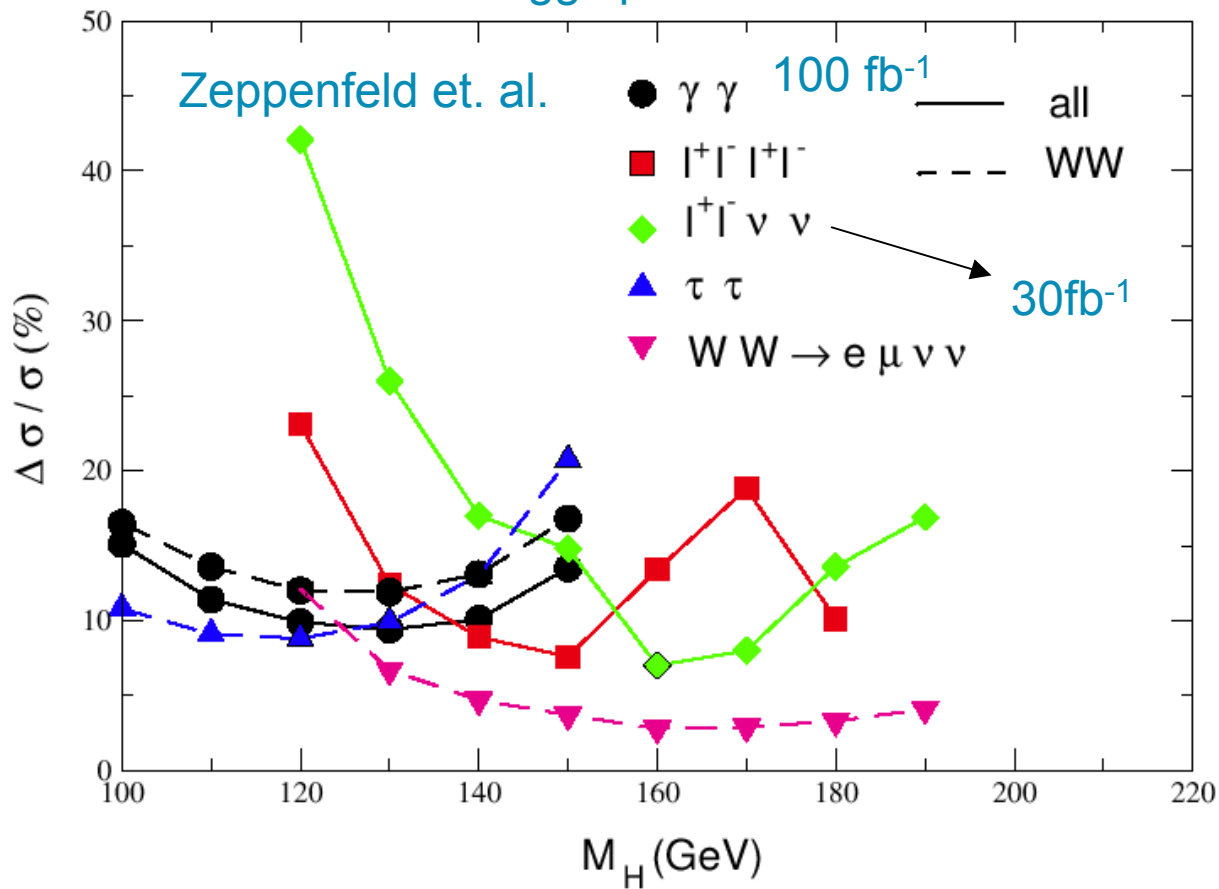


Fig.60

Mass spectra for $M_{\text{SUSY}} > 1 \text{ TeV}$

Two-loop / RGE-improved radiative corrections included

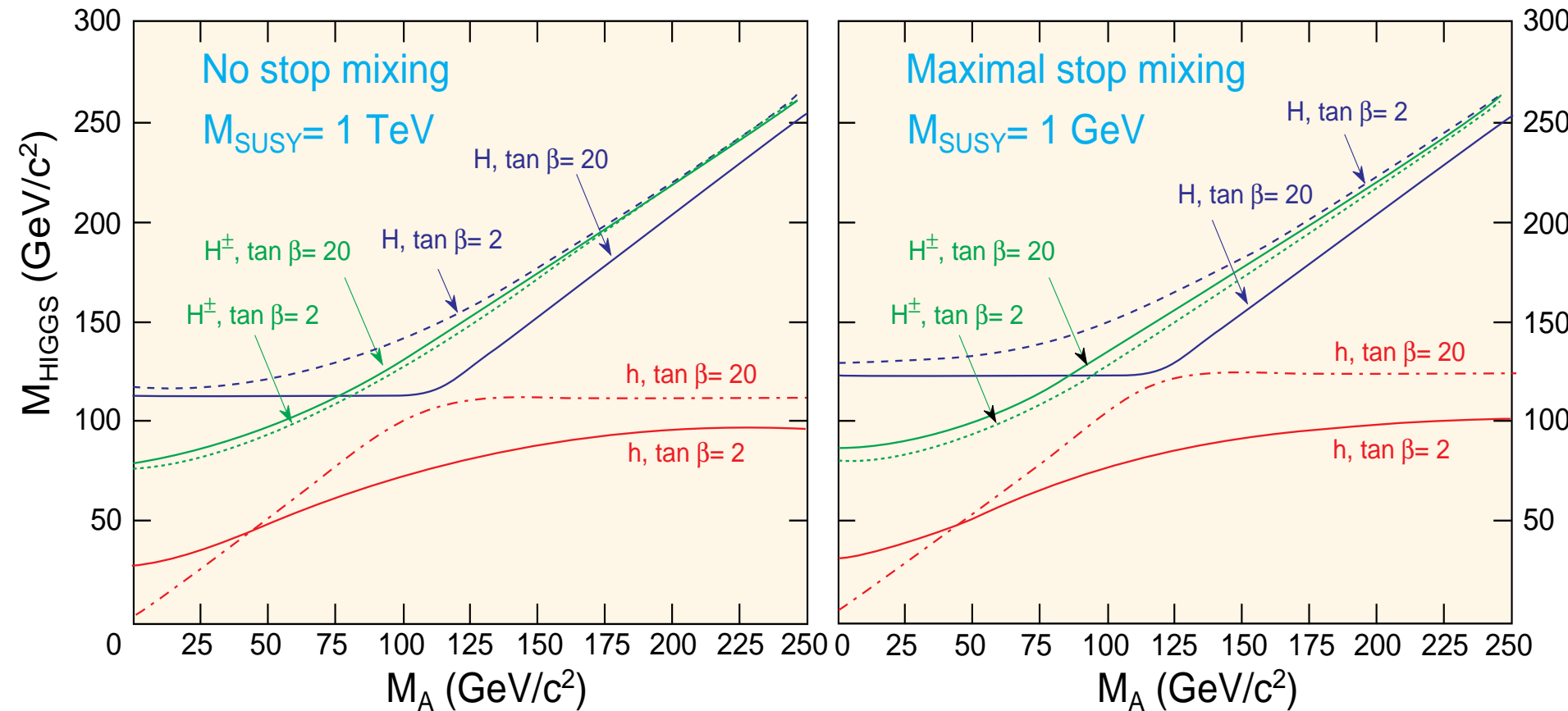


Fig.62

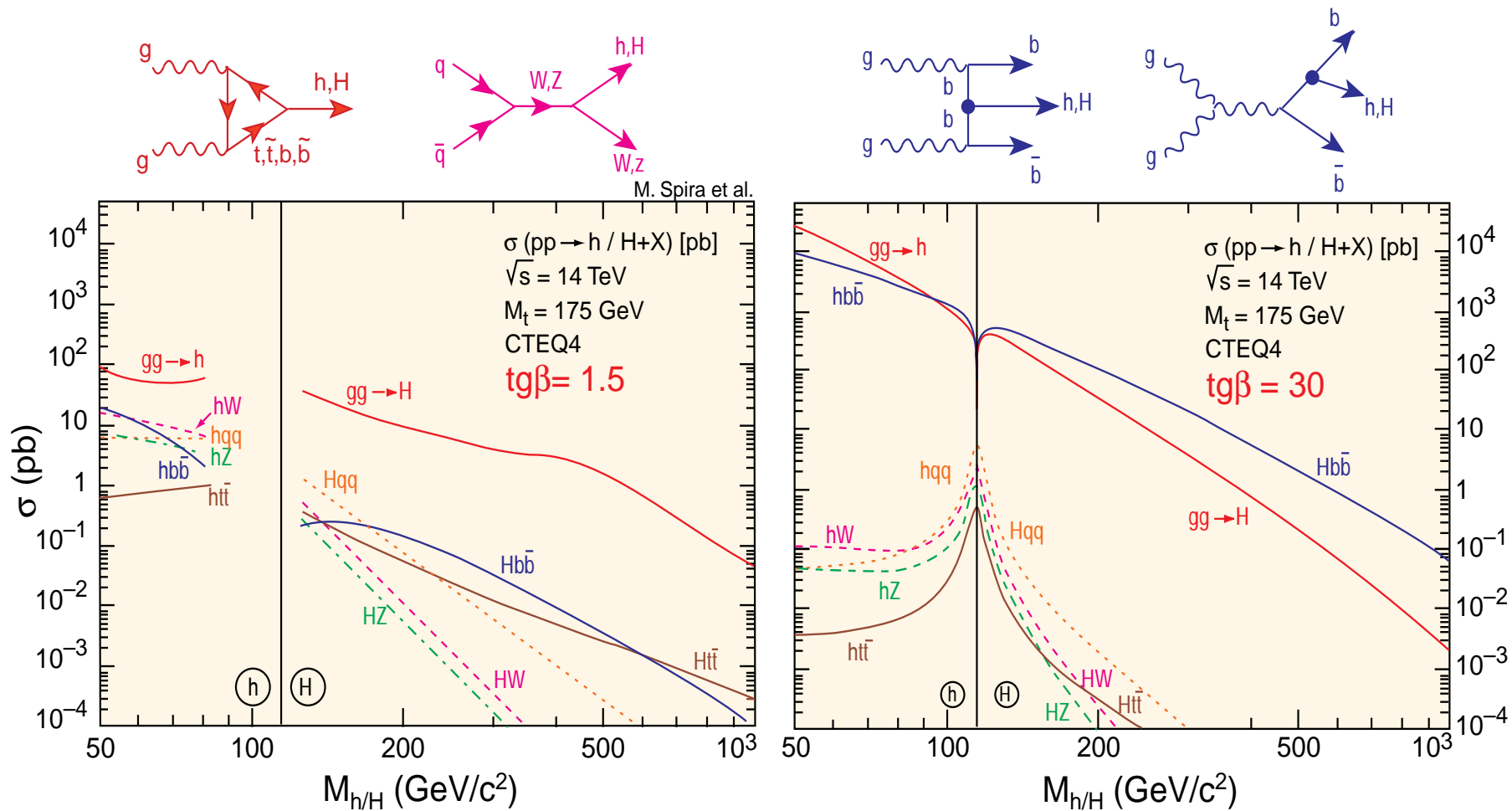


Fig.63

No mixing, $M_S=1\text{TeV}$

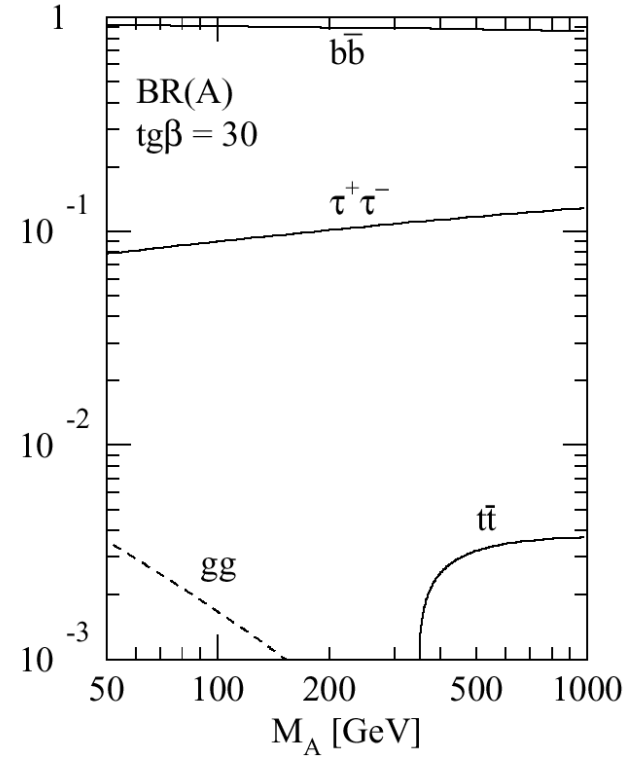
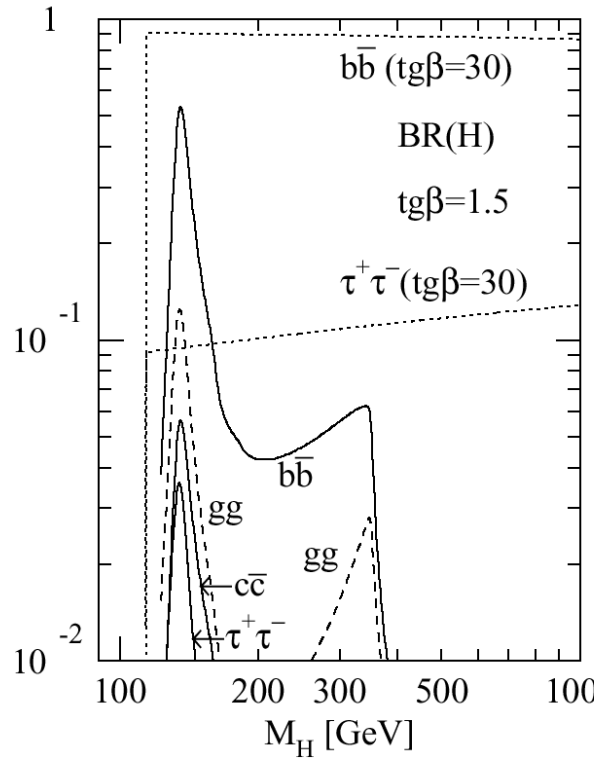
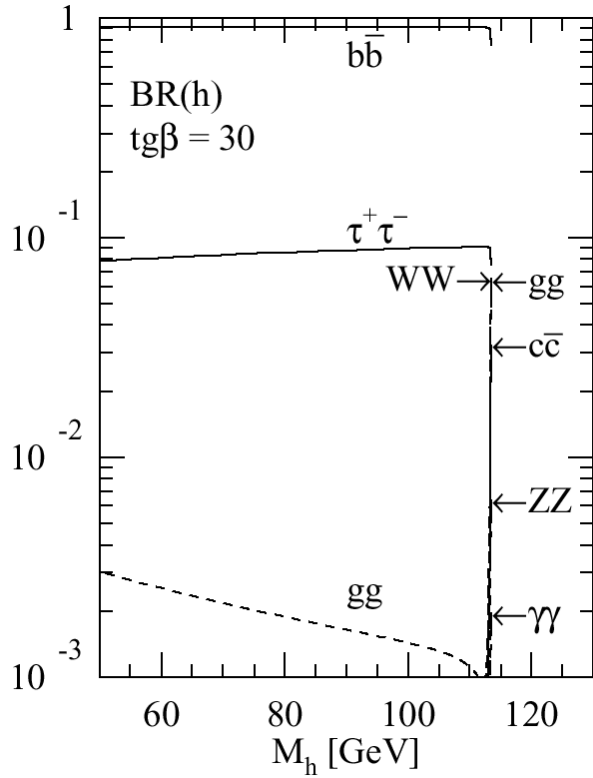


Fig.64

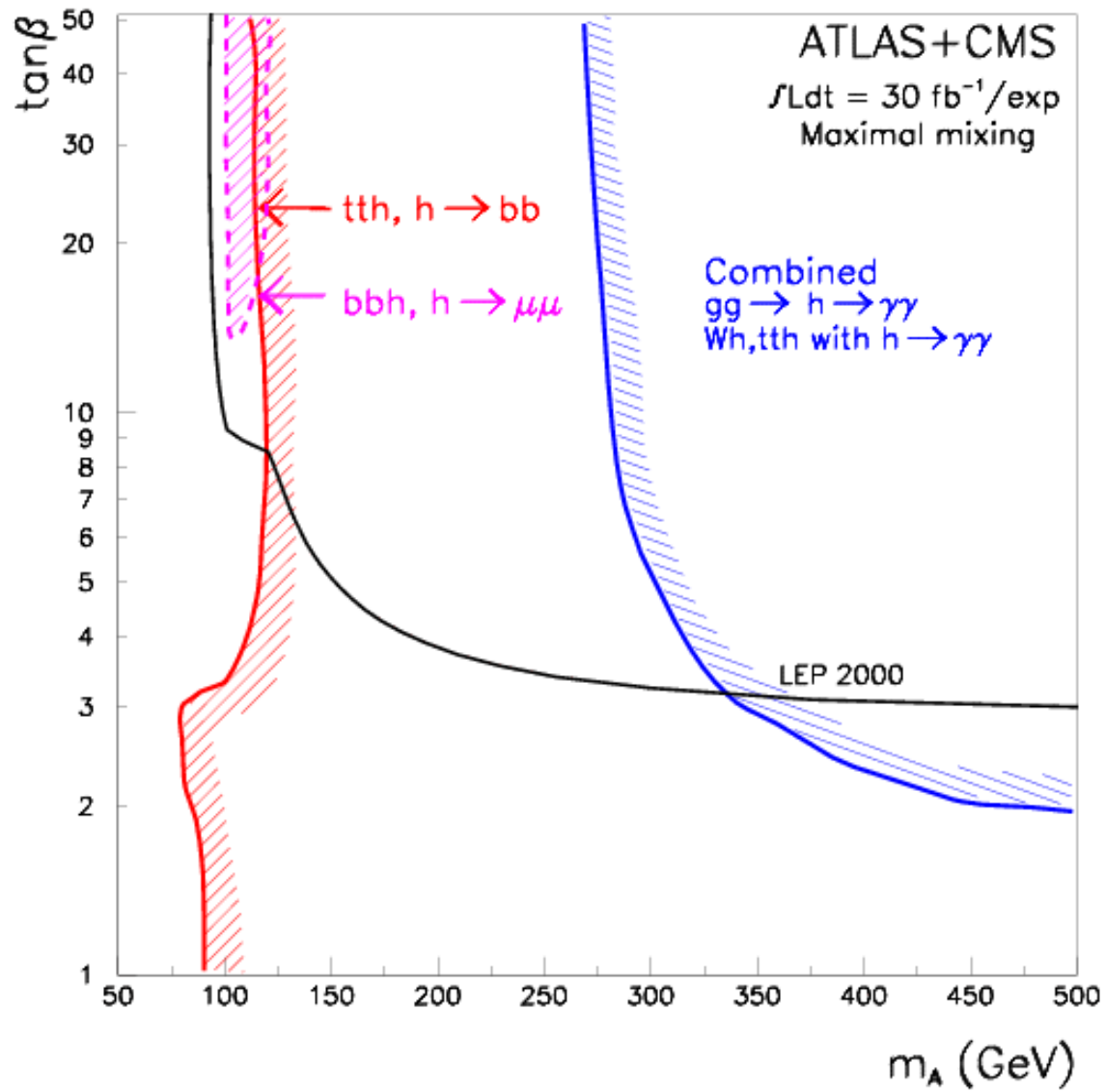


Fig.65

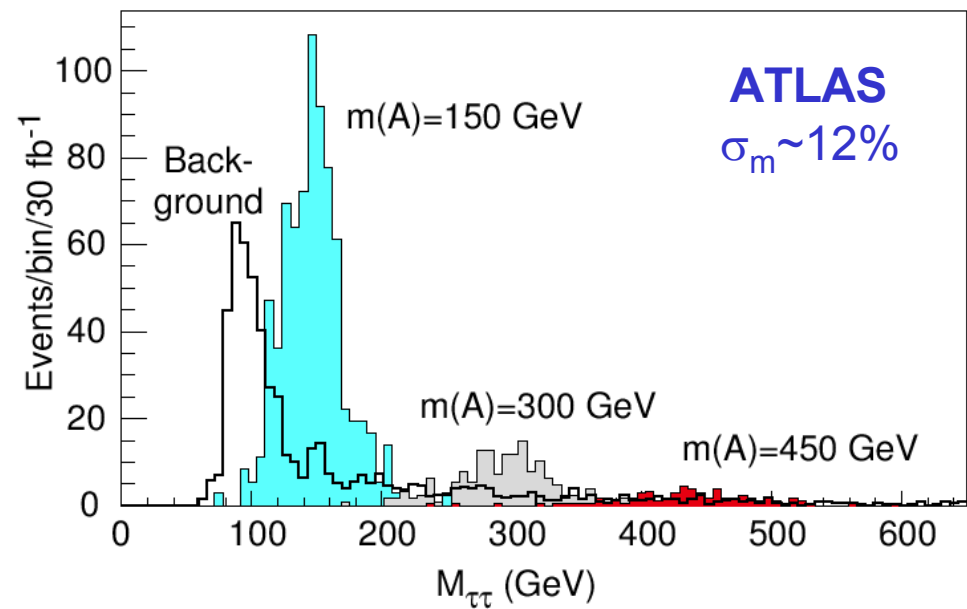


Fig.66a

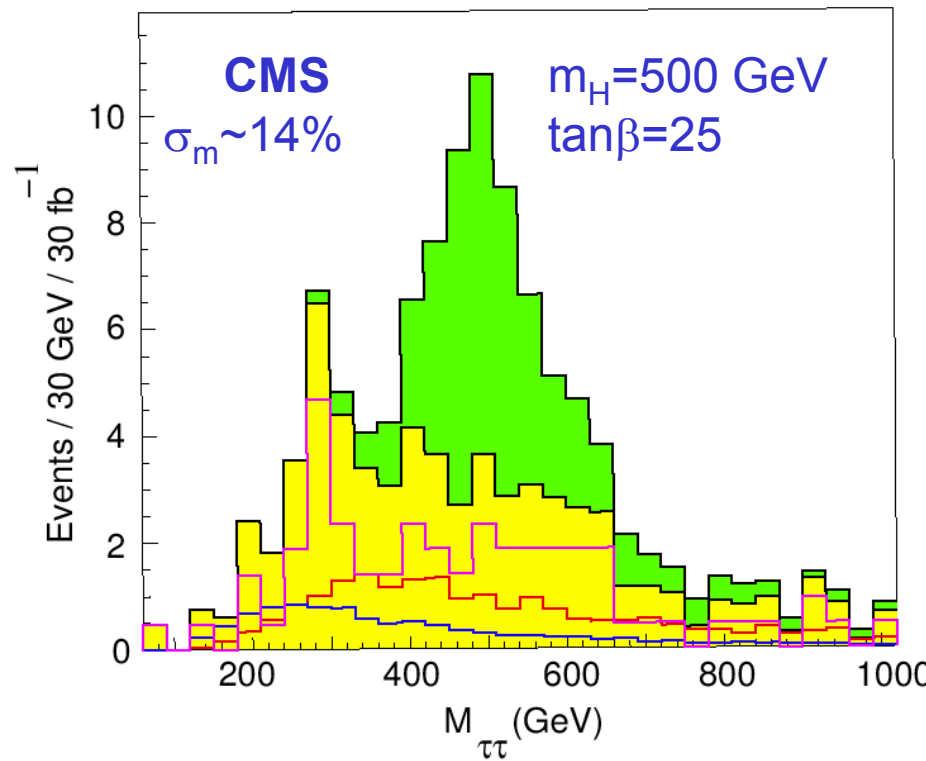


Fig.66b

CMS 30 fb⁻¹

Fig.67a

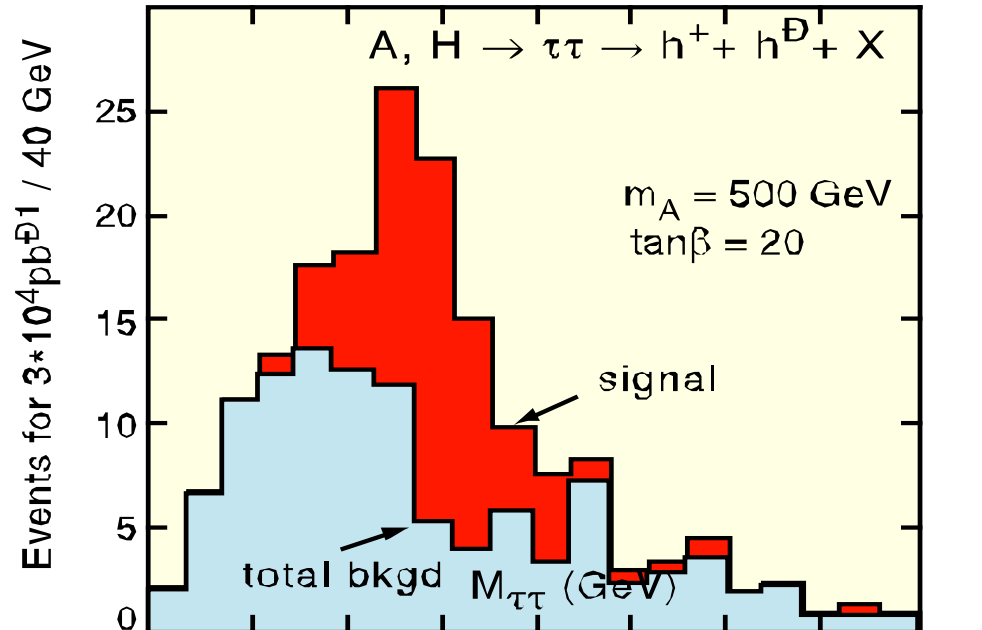
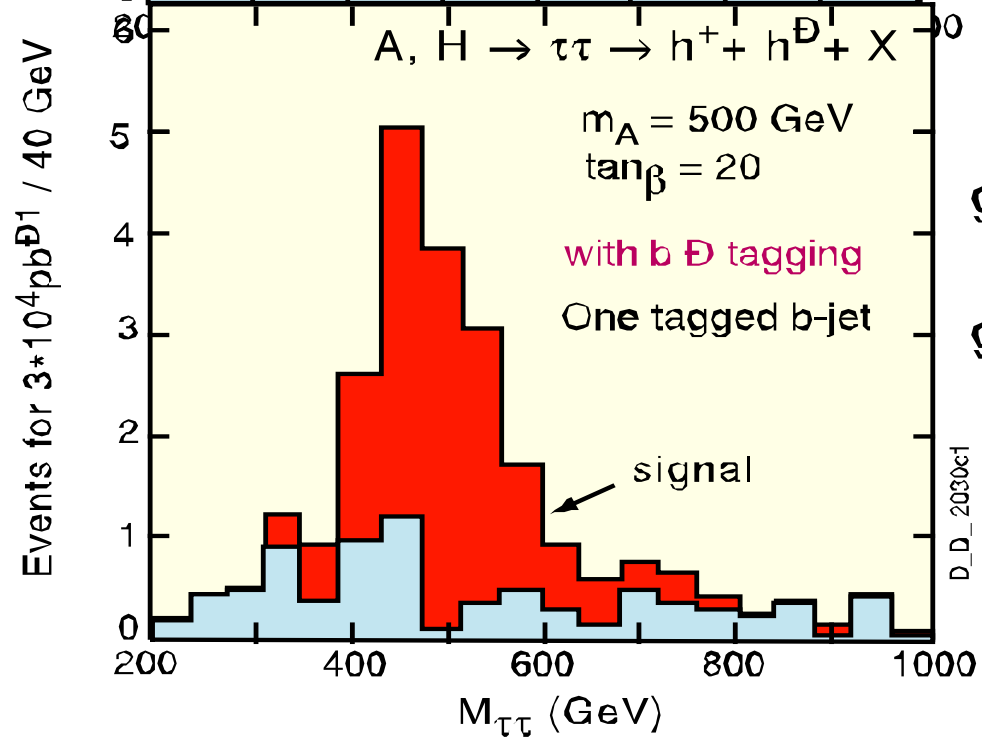


Fig.67b



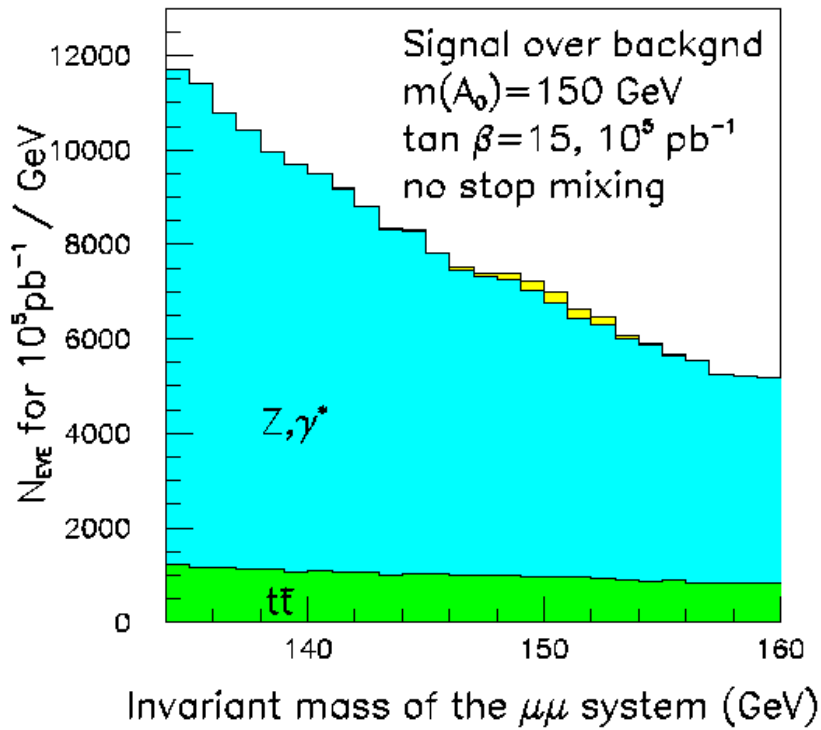


Fig.68a

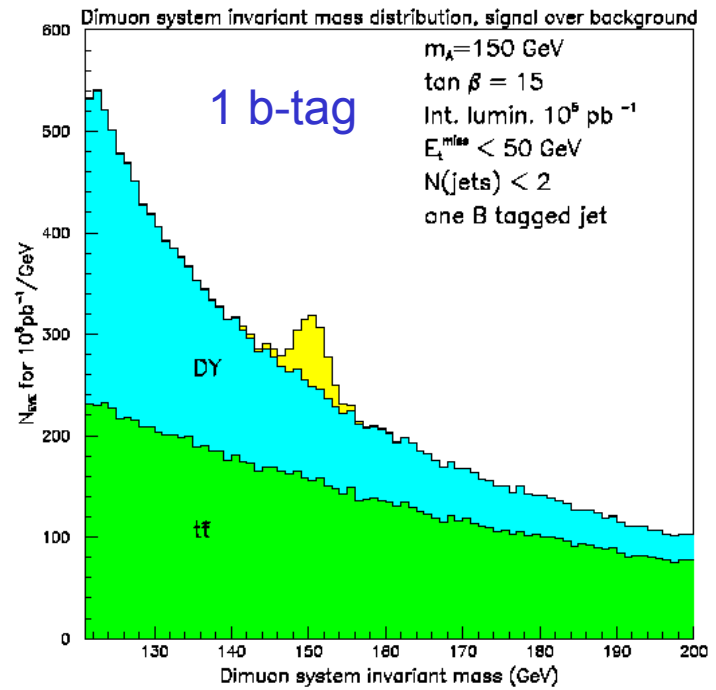


Fig.68b

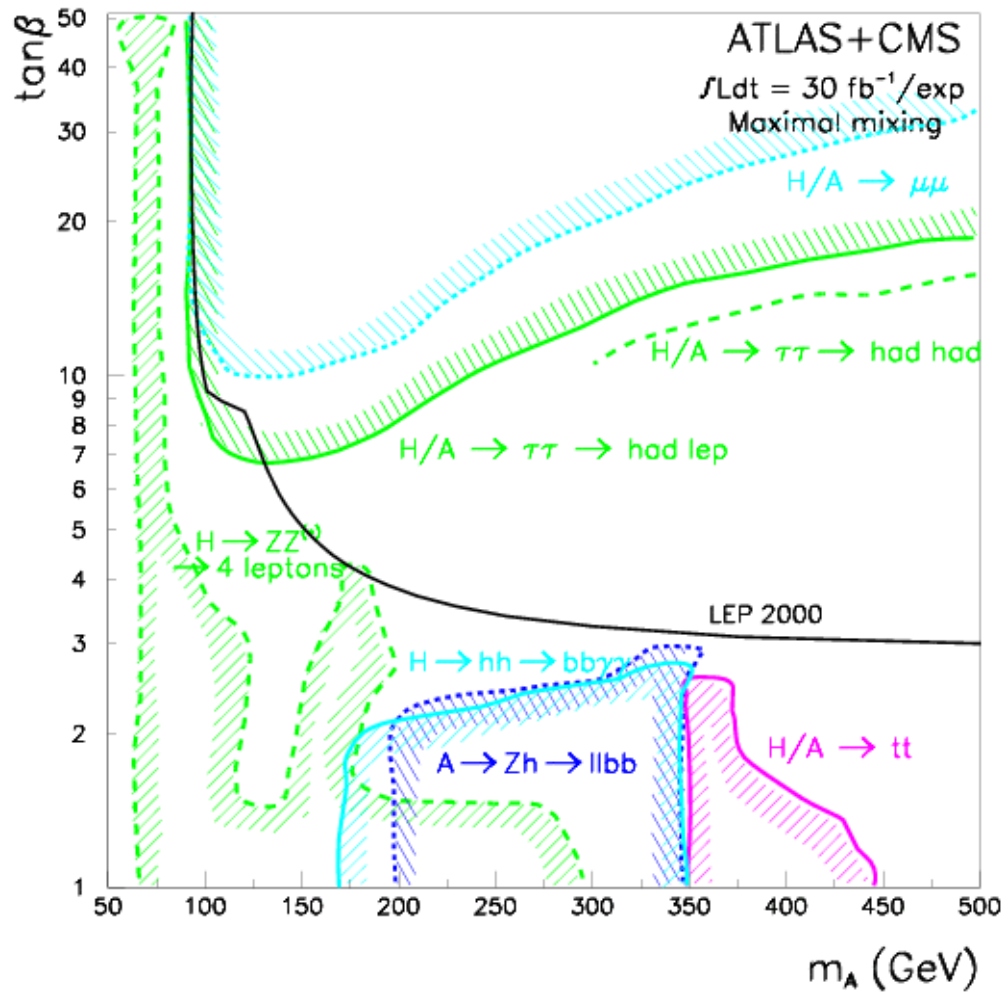


Fig.69

H^\pm Branching ratios, no stop mixing

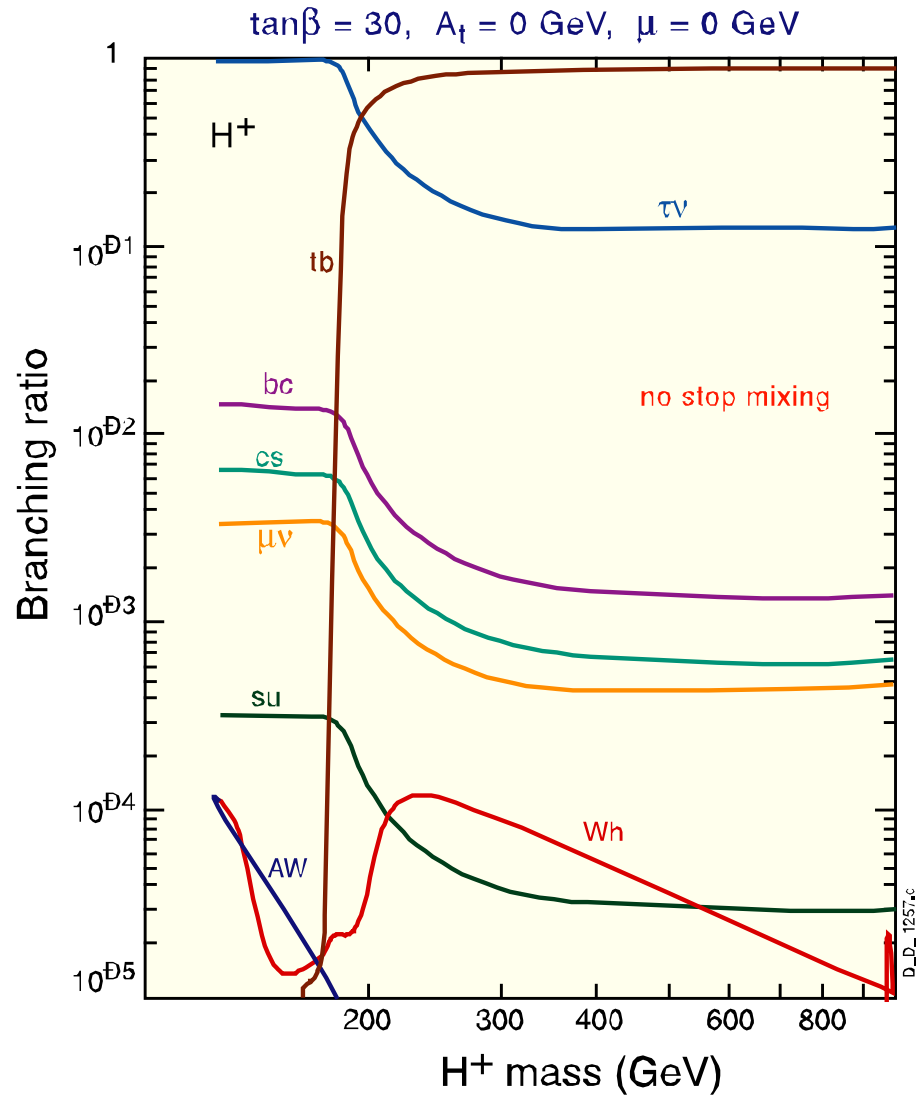


Fig.70

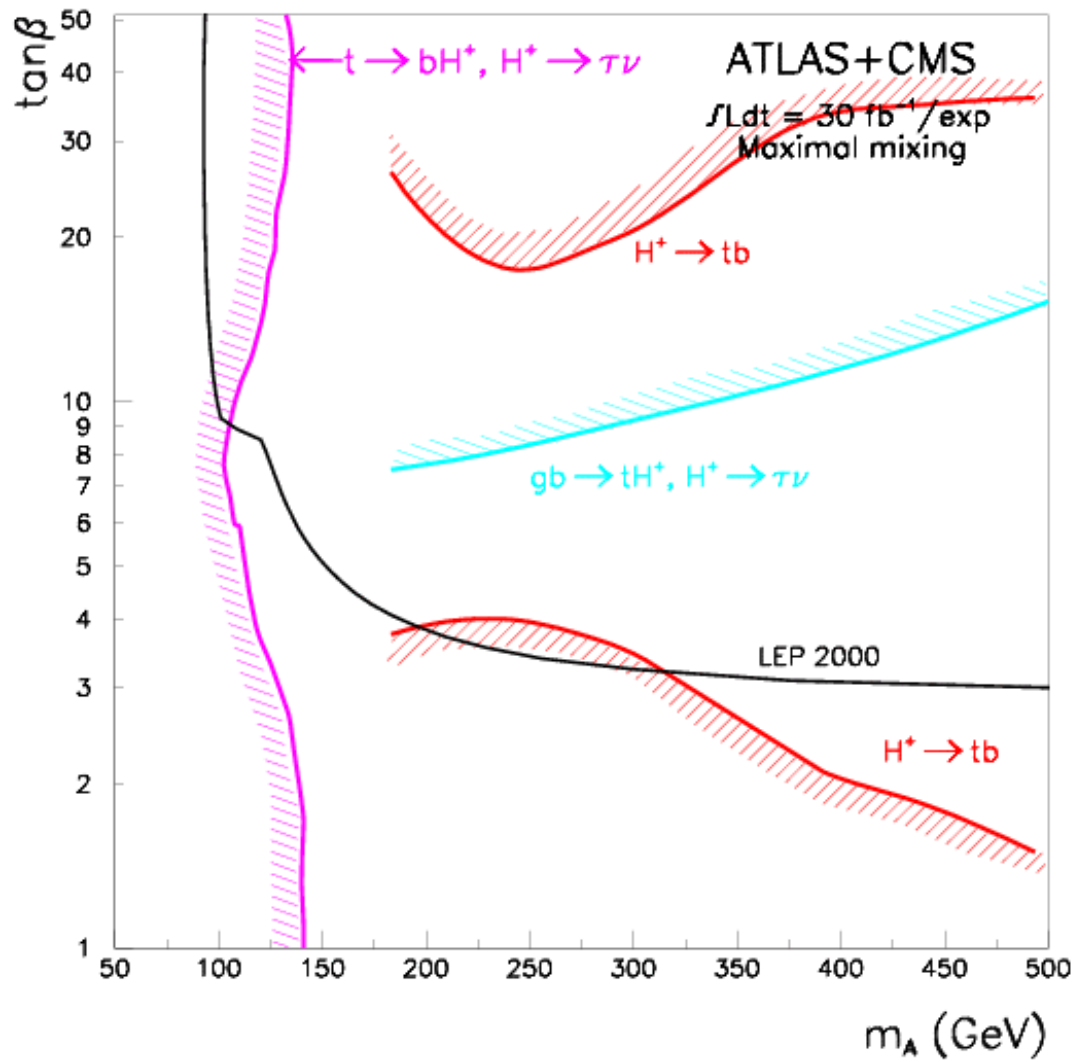
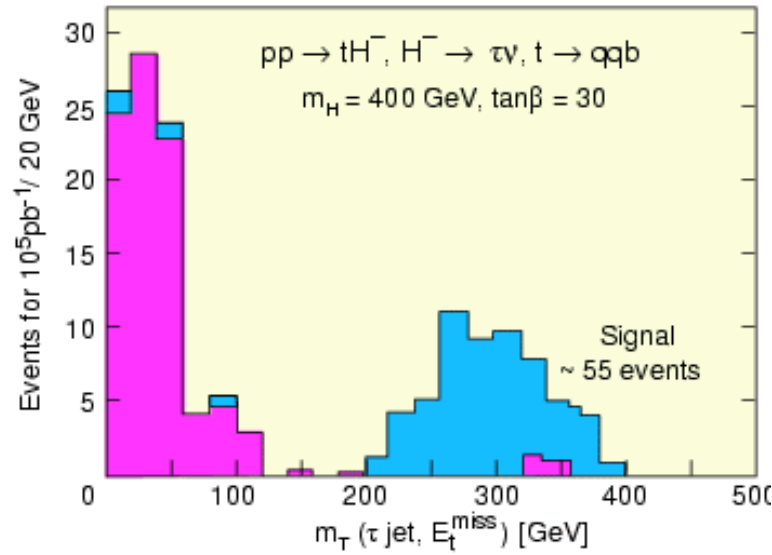


Fig.71

a



b

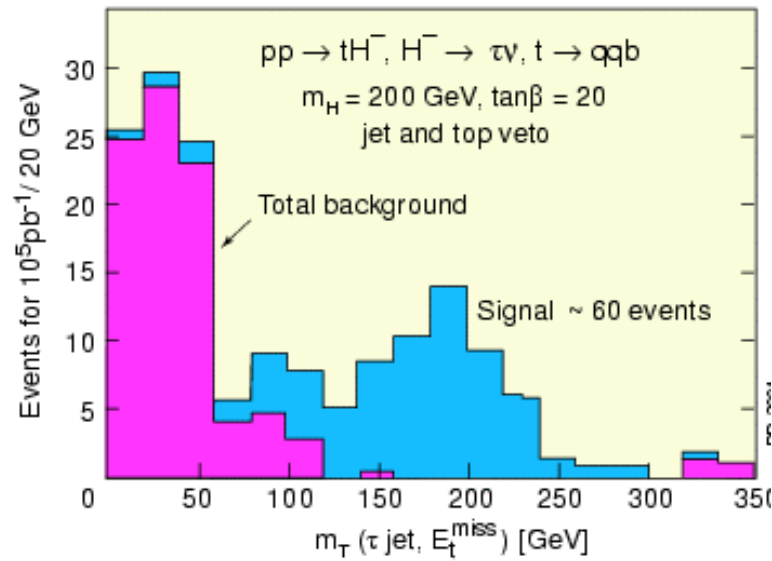
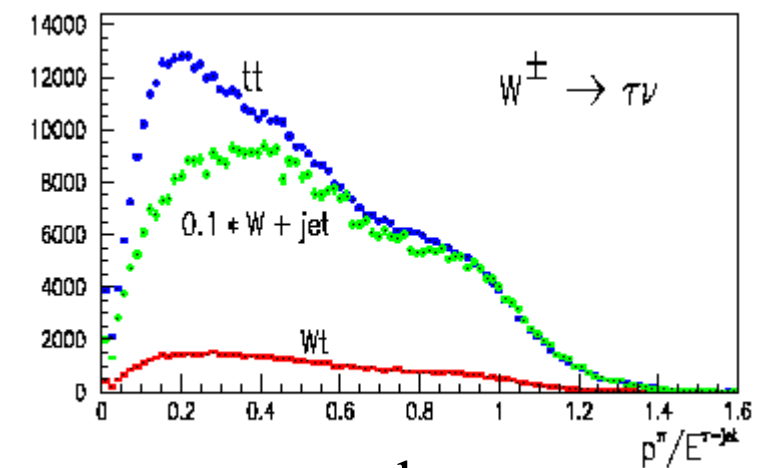
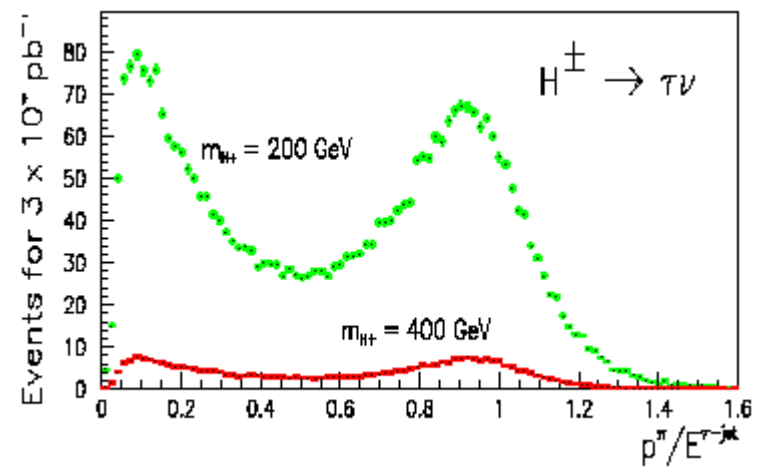
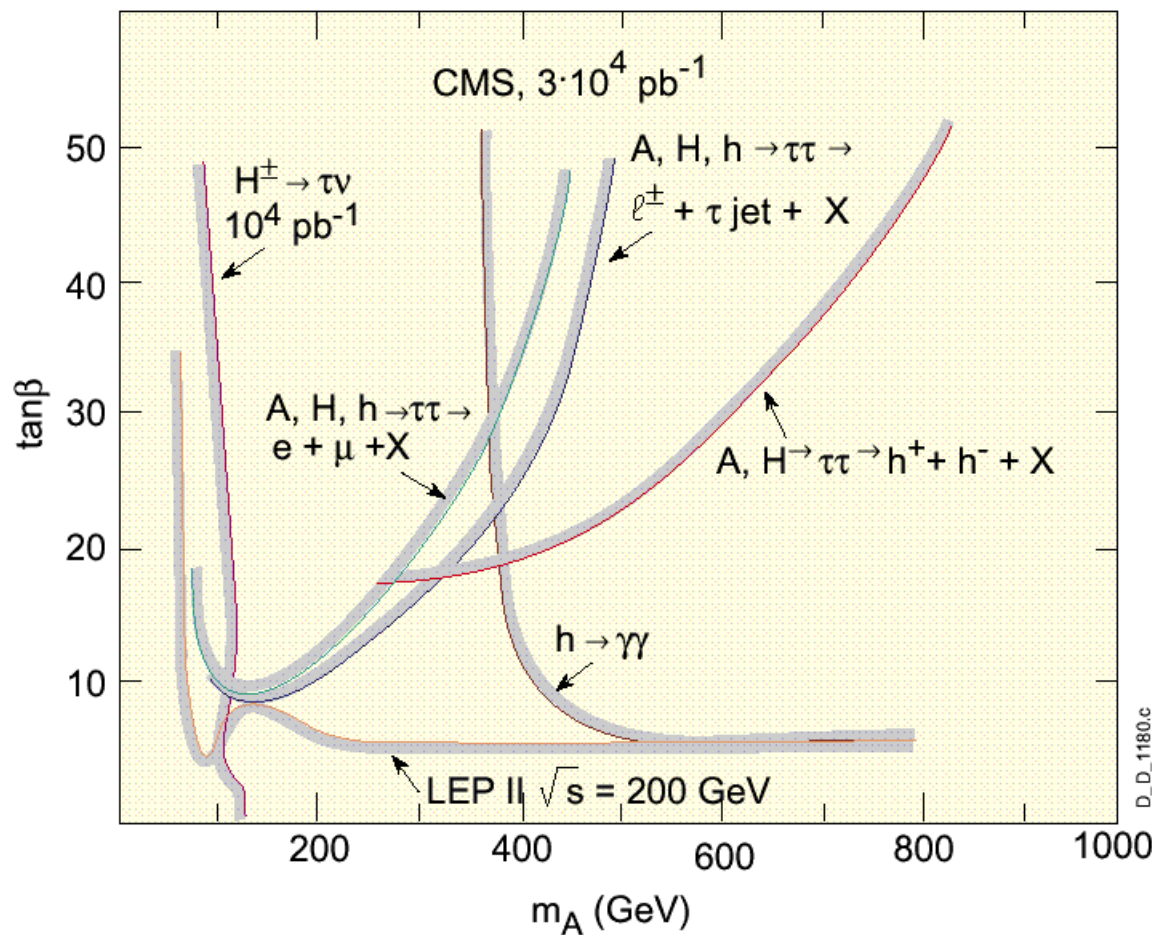


Fig.72

a



b



c

Fig.73

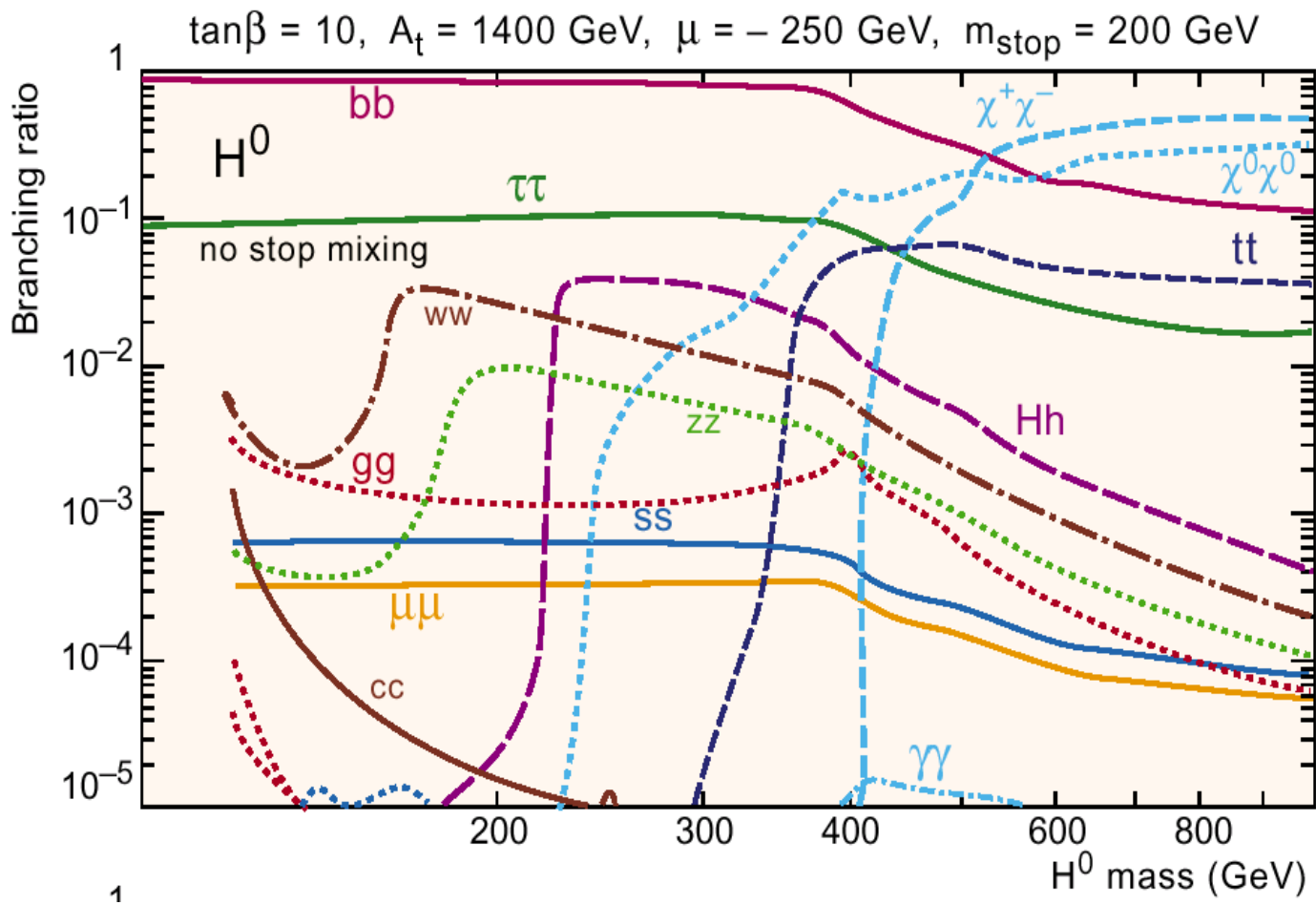


Fig.74

Adding $b\bar{b}$ on the τ modes can “close” the plane

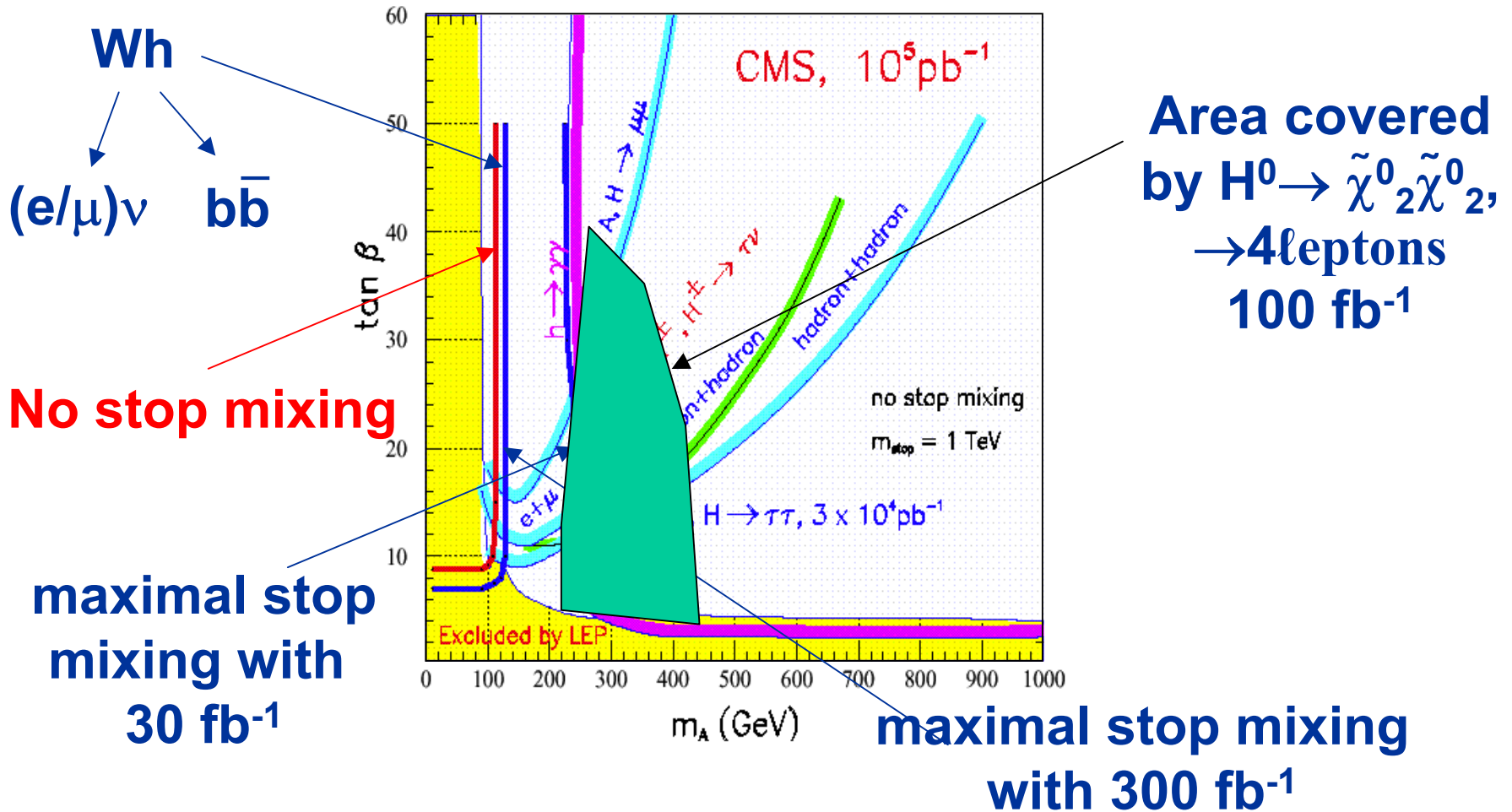


Fig.75

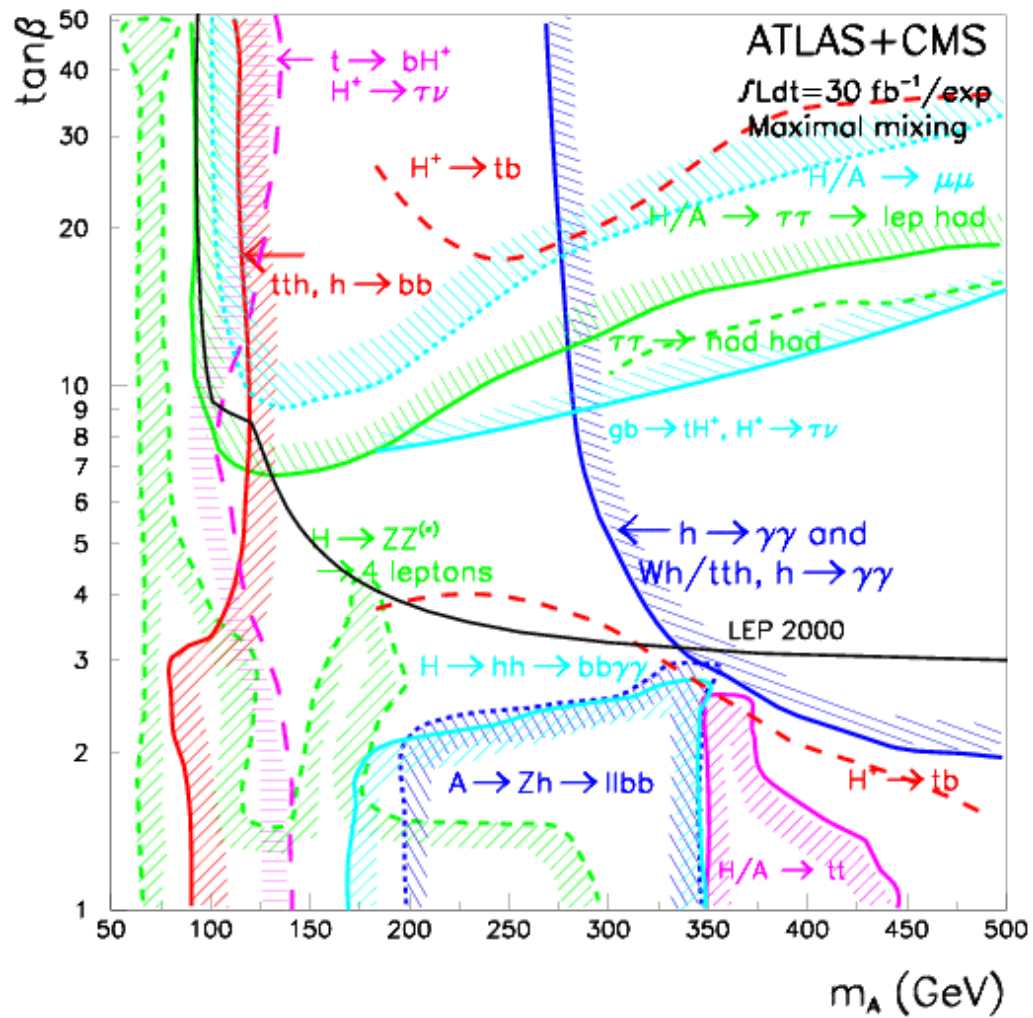
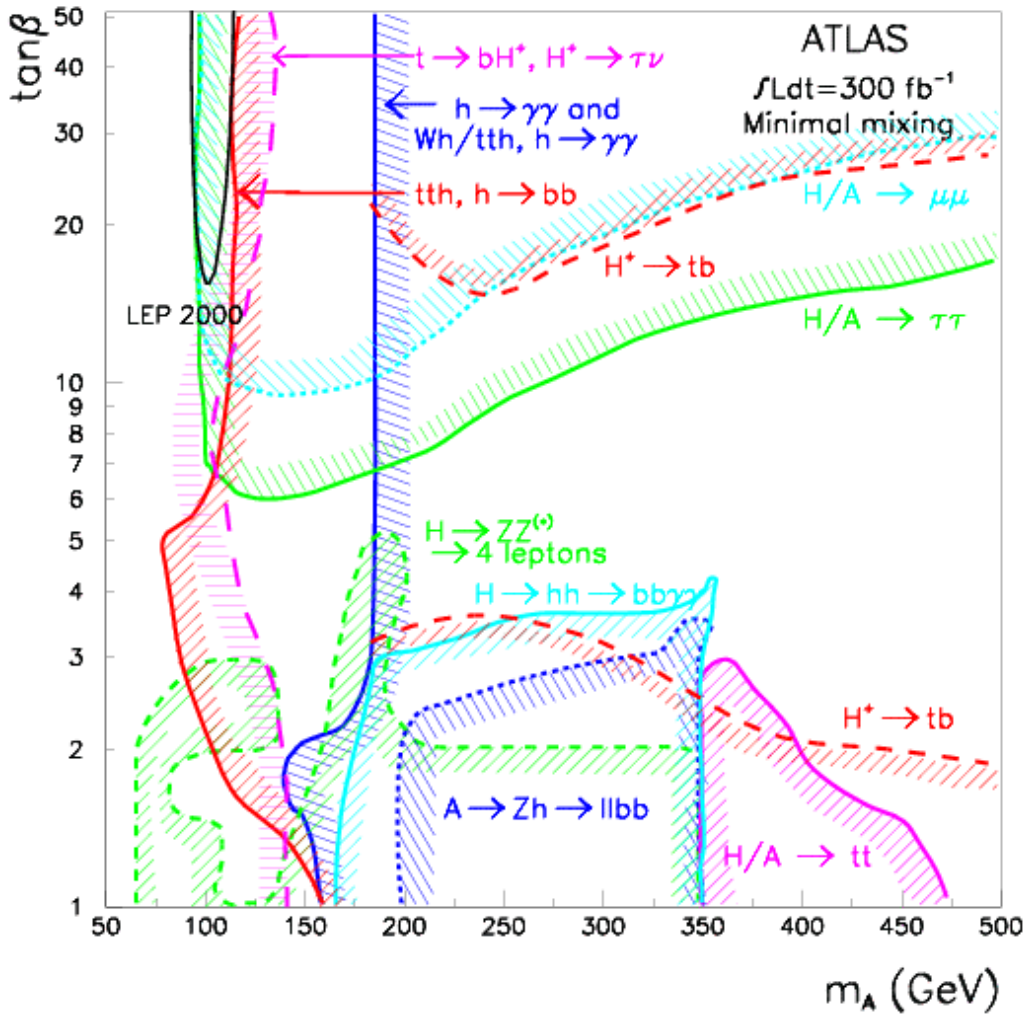


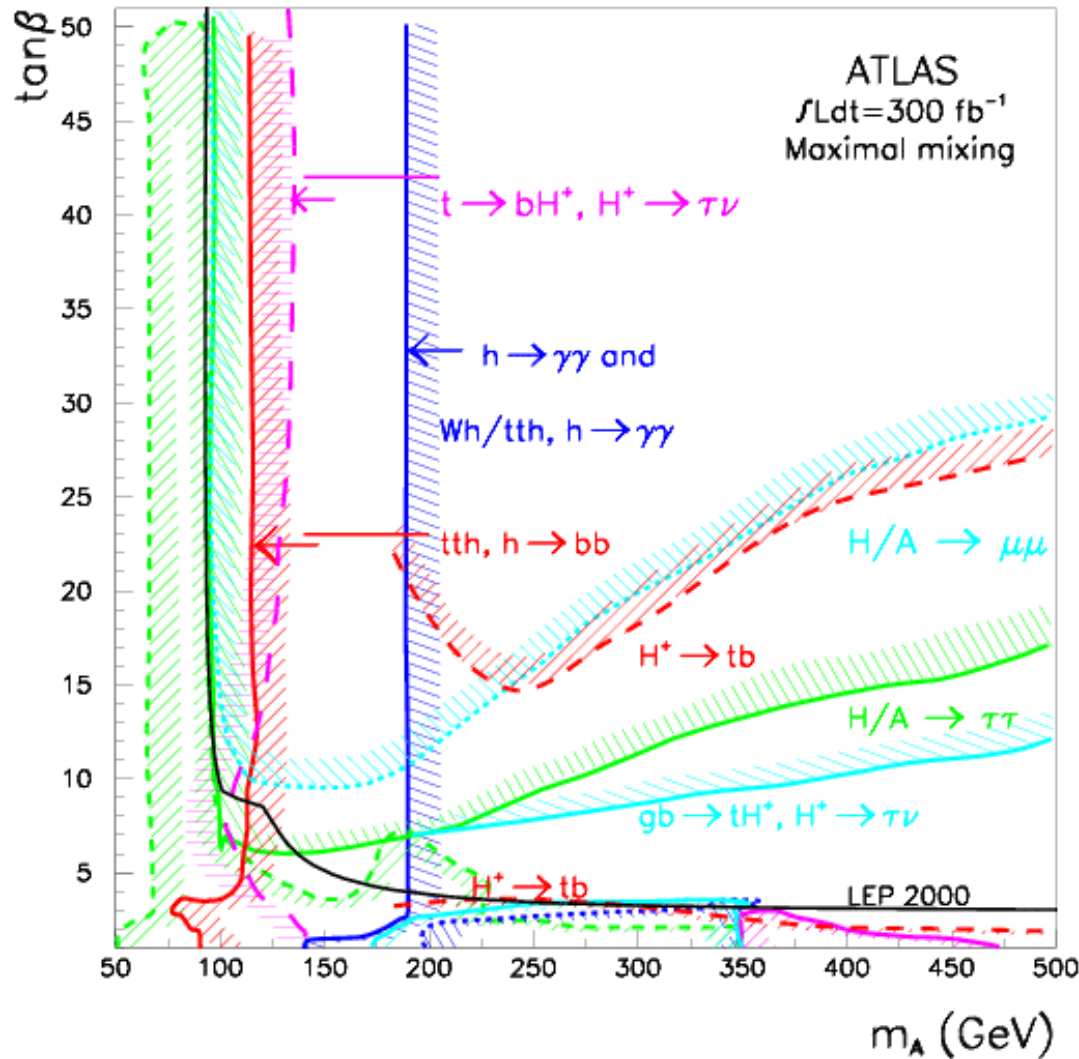
Fig.76



Minimal mixing
 $(m_h < 115.5 \text{ GeV})$
 NB: log scale

Caveat: coverage
 depends strongly on
 exact upper bound on m_h

Fig.77

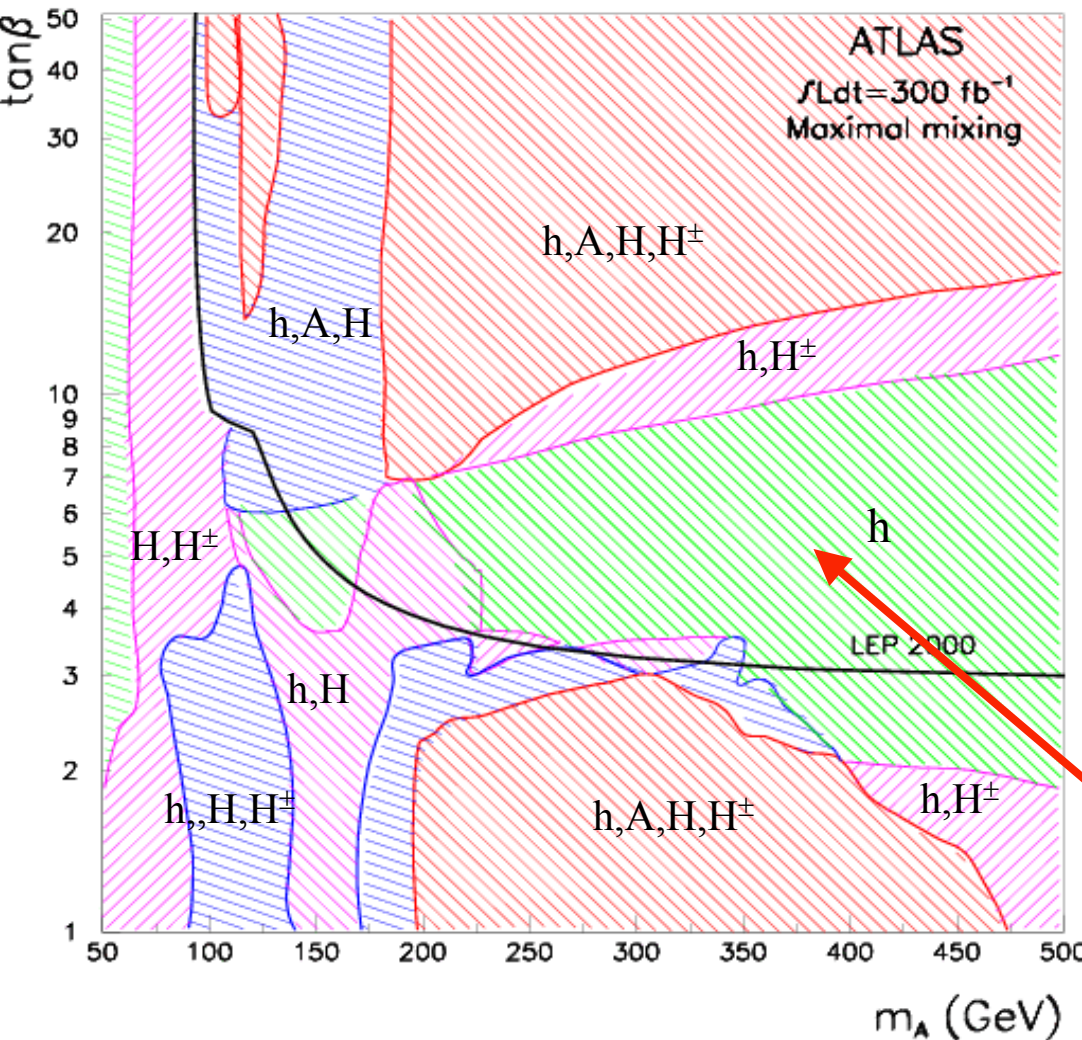


Maximal mixing
 ($m_h < 130 \text{ GeV}$)
 NB: linear scale

Caveat: possible
 suppression of e.g. bbH
 coupling could affect
 significantly
 H observation at LHC

Fig.78

MSSM Higgs bosons



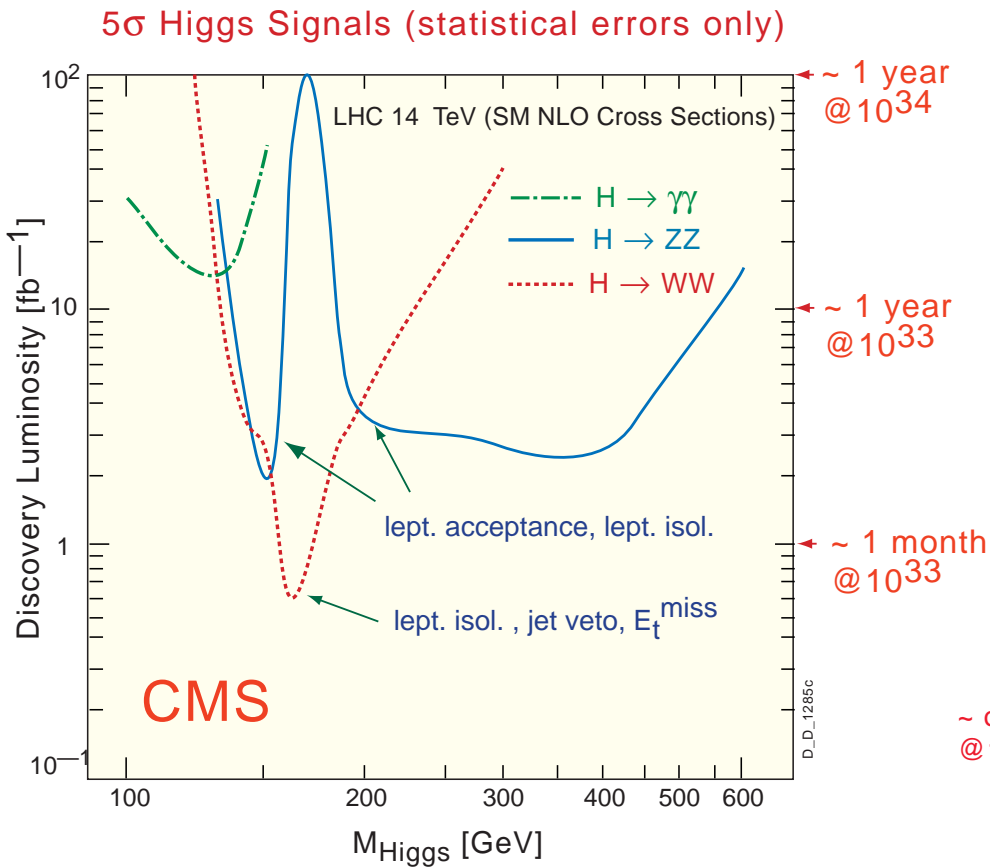
- 4 Higgs observable
- 3 Higgs observable
- 2 Higgs observable
- 1 Higgs observable

5 σ contours

Assuming decays to SM particles only

In this region only h observable (h \approx SM Higgs)
 → disentangle SM /MSSM ?

Fig.79



CMS \tilde{q}, \tilde{g} mass reach in E_T^{miss} + jets inclusive channel for various integrated luminosities

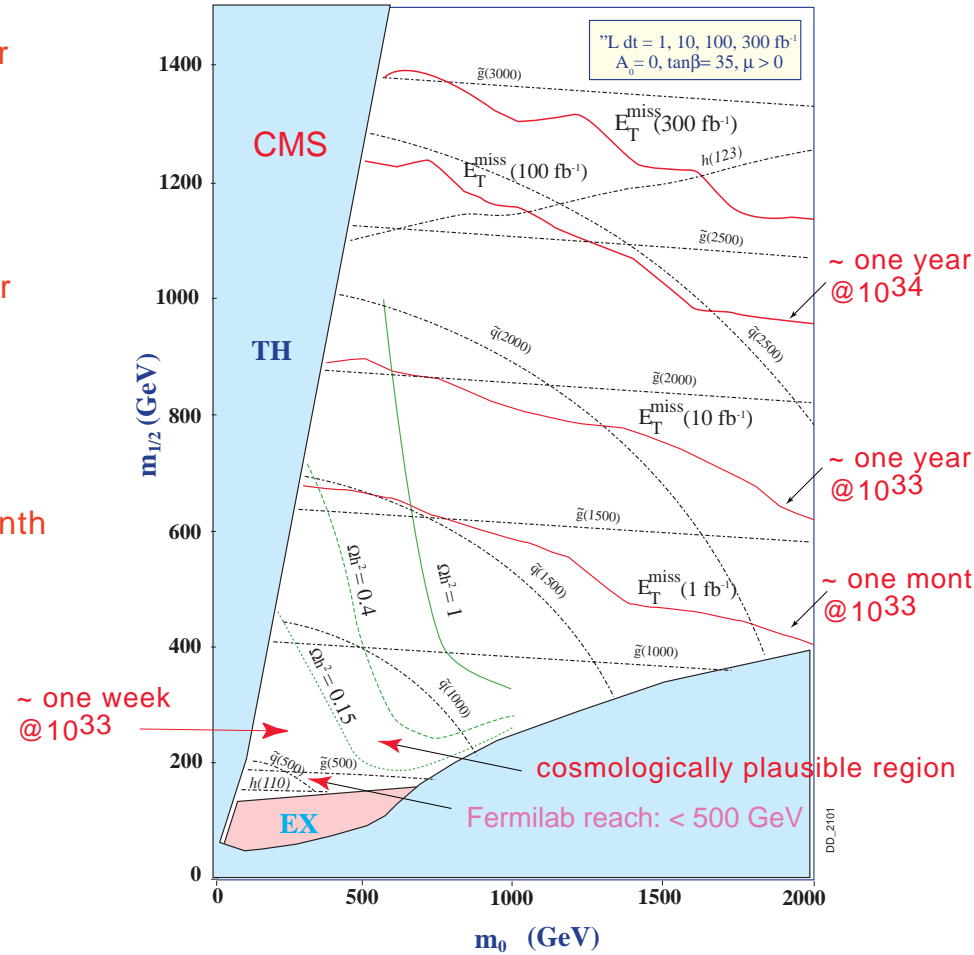


Fig.80